

Spektrální analytické metody

Analytické metody

„bulk“ (průměrná složení) vs lokální analýza

Destruktivní

Semidestruktivní

Nedestruktivní

Atomová spektrometrie

Molekulová spektrometrie

Kvalitativní

Semikvantitativní

Kvantitativní

Kvantová teorie

M. Planck: Kvantová teorie

$$E = h \cdot \nu$$

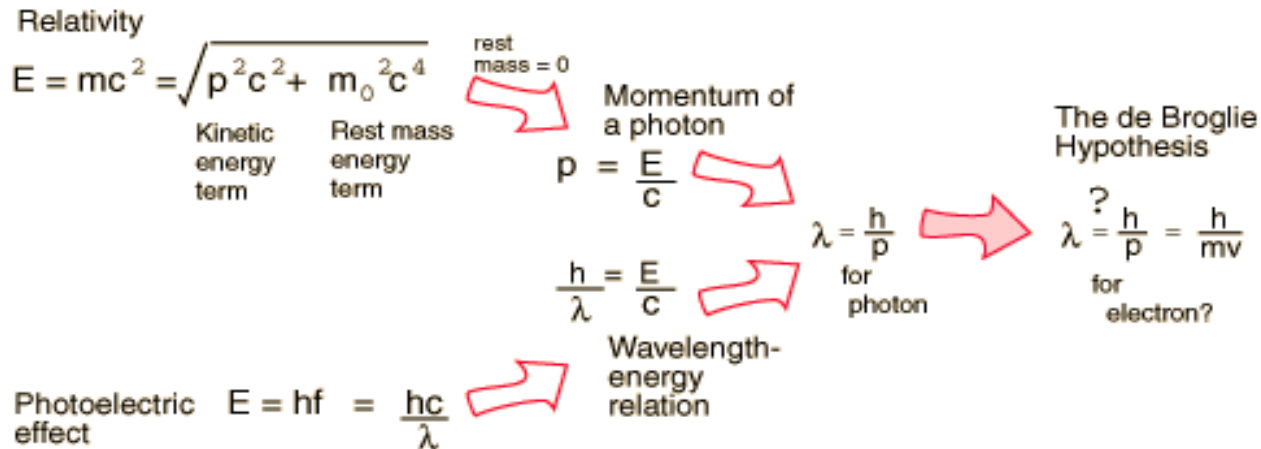
A. Einstein: Fotoelektrický jev

N. Bohr: Kvantový model atomu

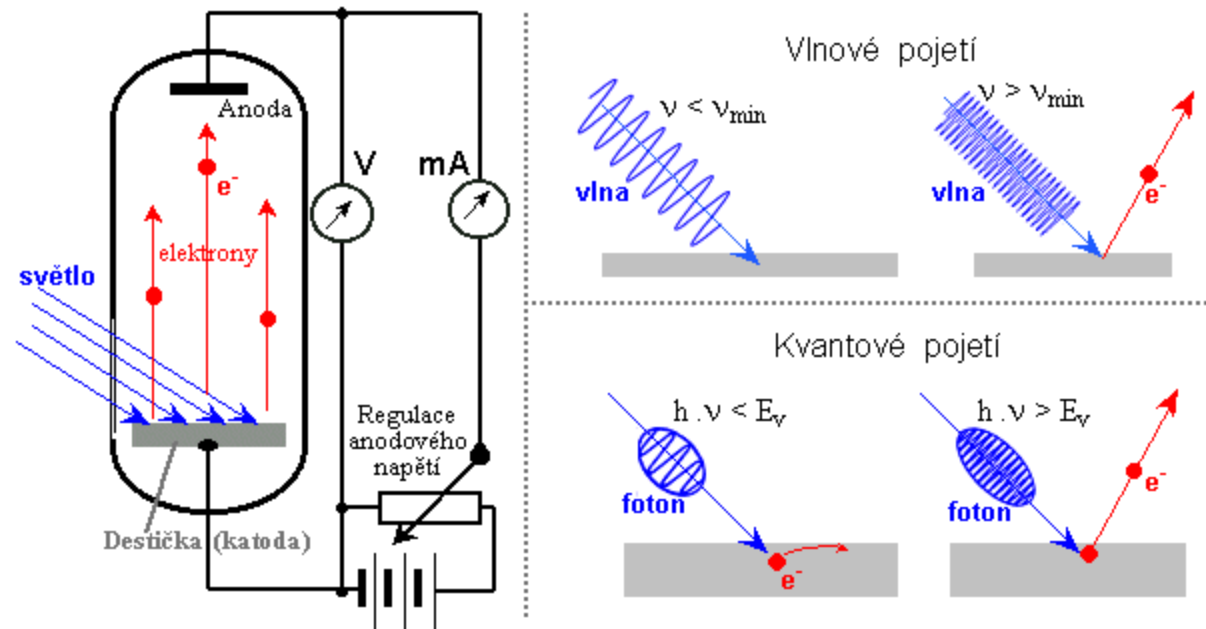
L. De Broglie: Dualita hmota-záření

A. Einstein: Speciální teorie relativity

$$E = m \cdot c^2$$



Vlnění
Částice

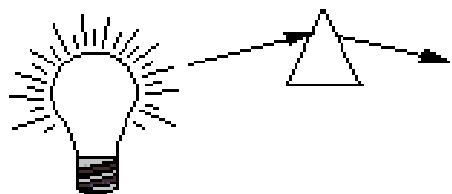


Každá mikročástice o hmotnosti m pohybující se rychlostí v , se může chovat jako vlna o vlnové délce

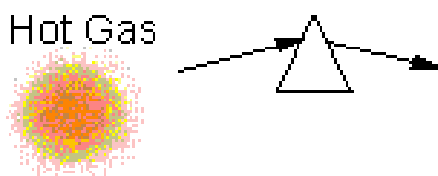
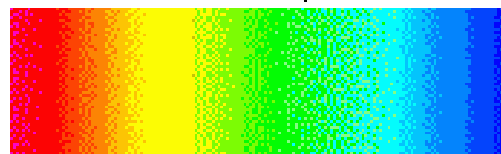
$$\lambda = \frac{h}{p} = \frac{h}{\gamma m v} = \frac{h}{m v} \sqrt{1 - \frac{v^2}{c^2}}$$

De Broglieova-Comptonova vlnová délka

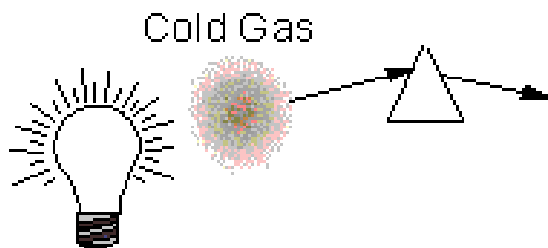
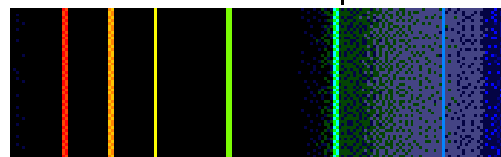
Emisní a absorční spektra



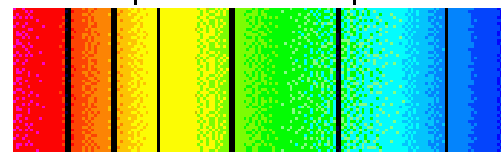
Continuum Spectrum



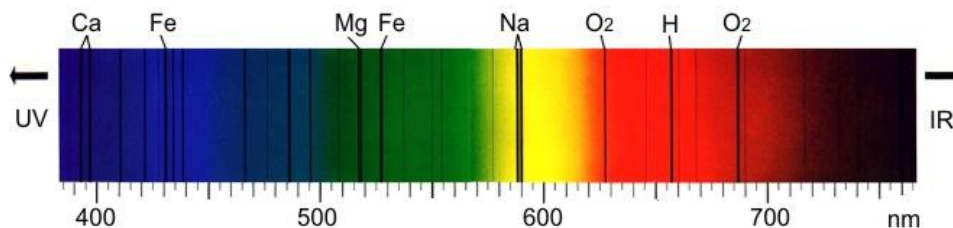
Emission Line Spectrum

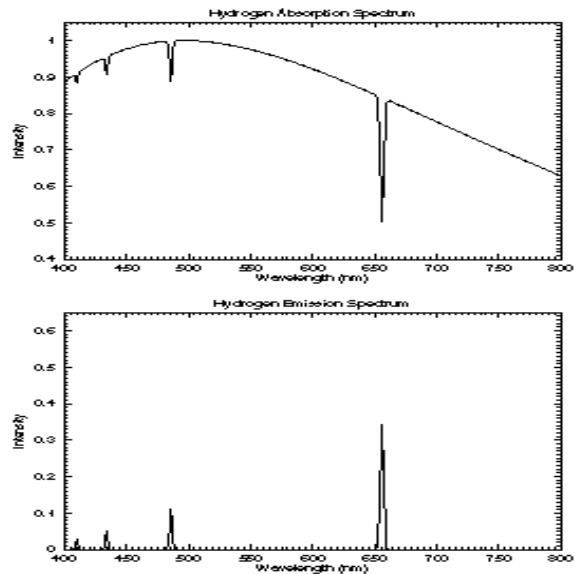
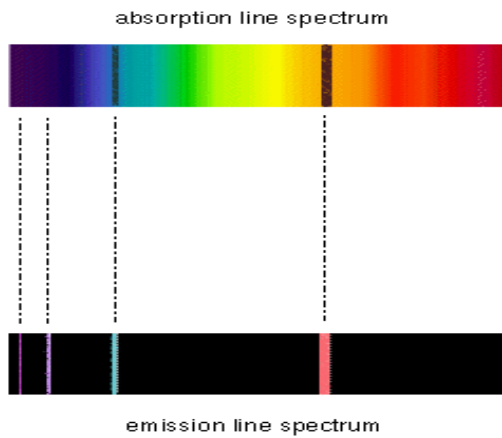
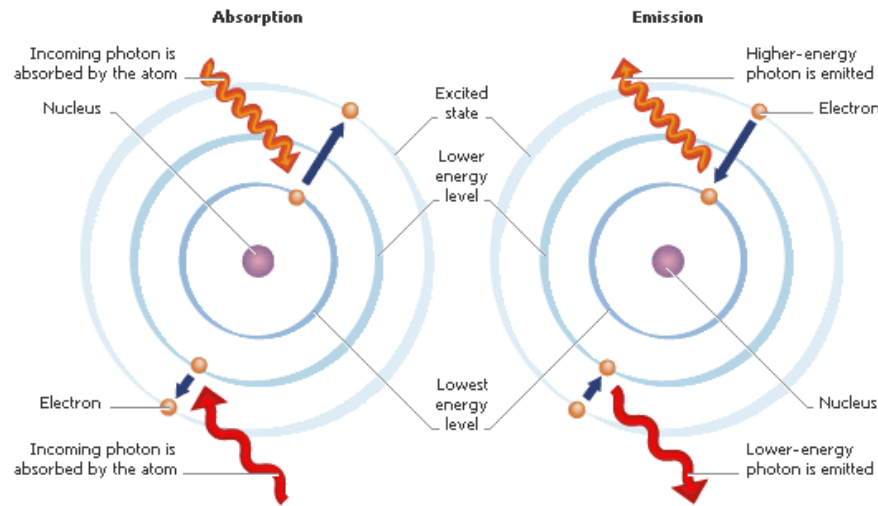


Absorption Line Spectrum



Fraunhoferovy čáry ve slunečním spektru jsou důsledkem absorpce světla atomy různých prvků ve sluneční atmosféře.

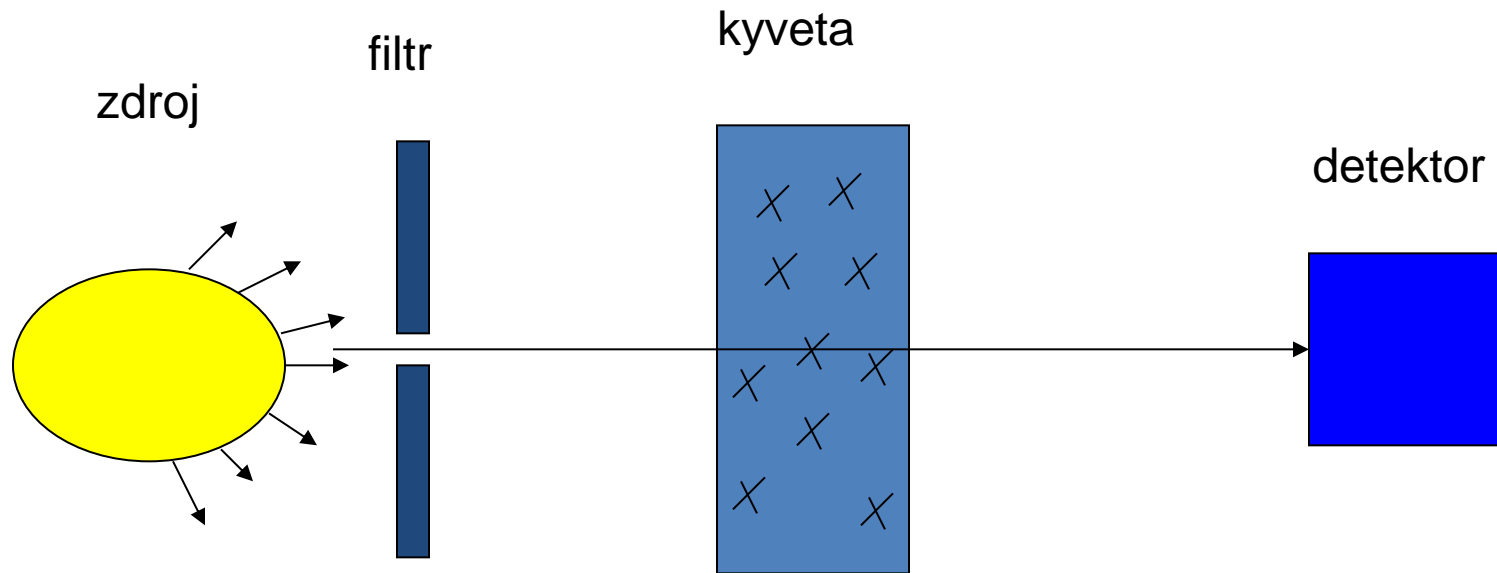




Two ways of showing the same spectra: on the **left** are pictures of the dispersed light and on the **right** are plots of the intensity vs. wavelength. Notice that the pattern of spectral lines in the absorption and emission line spectra are the **same** since the gas is the same.

Lambert – Beerův zákon

Zákon platí pro monochromatické světlo



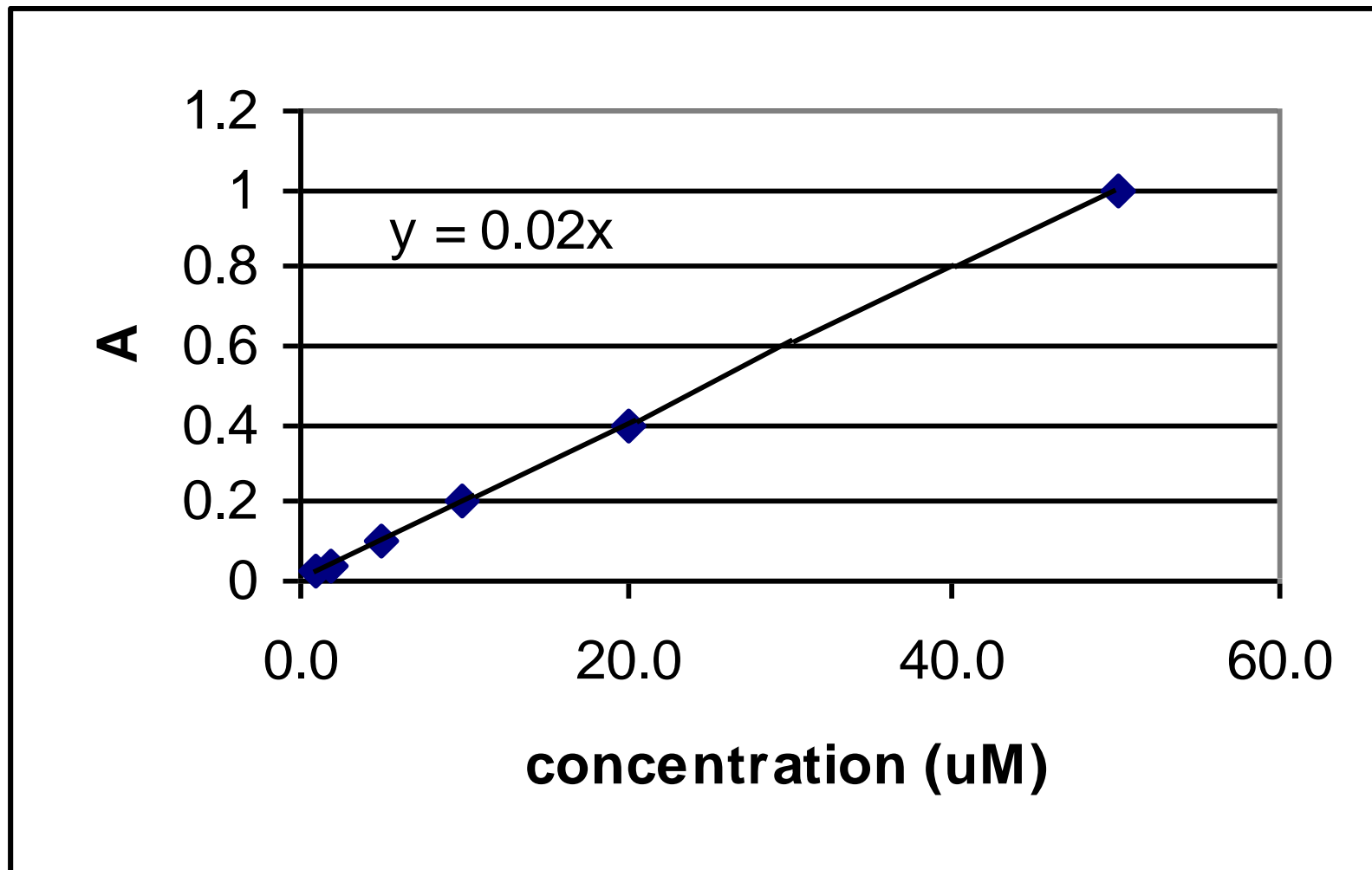
$$\text{Absorbance: } A = -\log T = \log(P_0/P) = ebc$$

$$\text{Transmittance: } T = P_{\text{solution}}/P_{\text{solvent}} = P/P_0$$

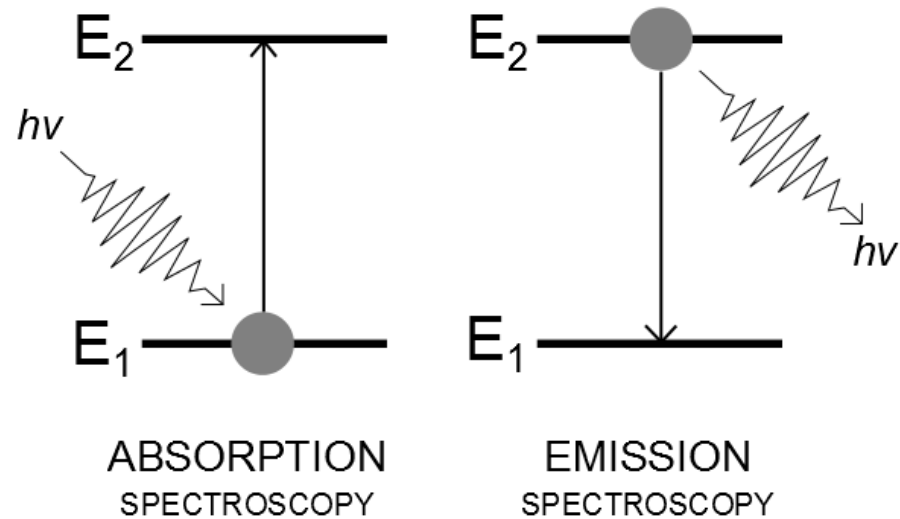
b = tloušťka kyvety, c = koncentrace roztoku, e = absorpční koeficient

Grafické vyjádření Lambert-Beerova zákona

= lineární funkce



Atomová spektrometrie



Atomová absorpční spektrometrie

Roztoková analýza

destruktivní

V plameni

V kyvetě

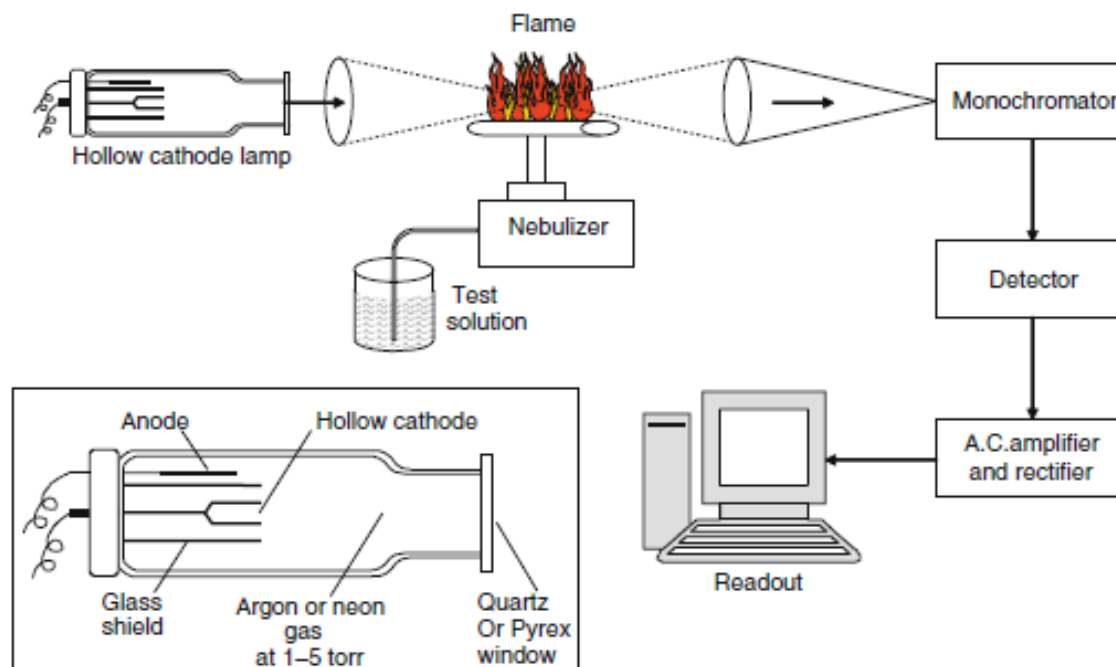


Fig. 34.1 Atomic absorption with hollow cathode lamp (From SKOOG. Principles of Instrumental Analysis, 5E. © 1998 Brooks/Cole, a part of Cengage Learning, Inc. Reproduced by permission. www.cengage.com/permissions)

Spektrografie

Semikvantitativní

Semidestruktivní

Jiskra

El. oblouk

Emisní spektra se zachycují na fotografickou desku

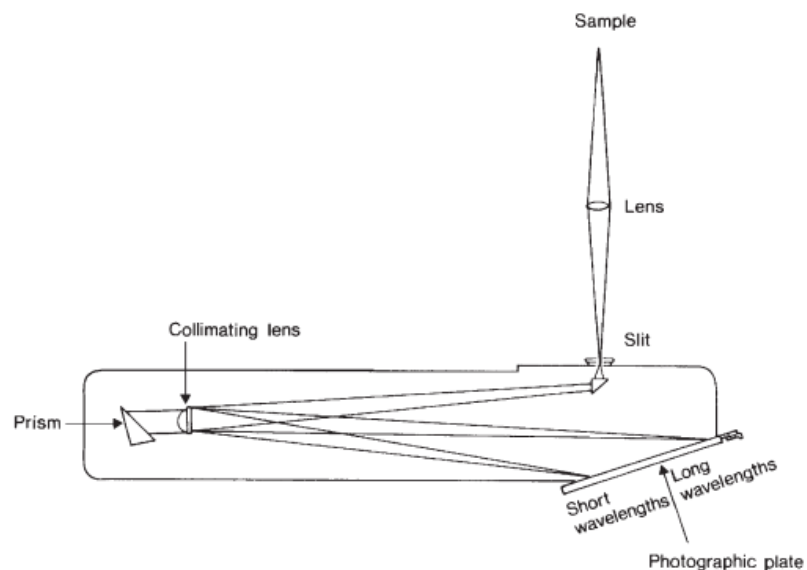
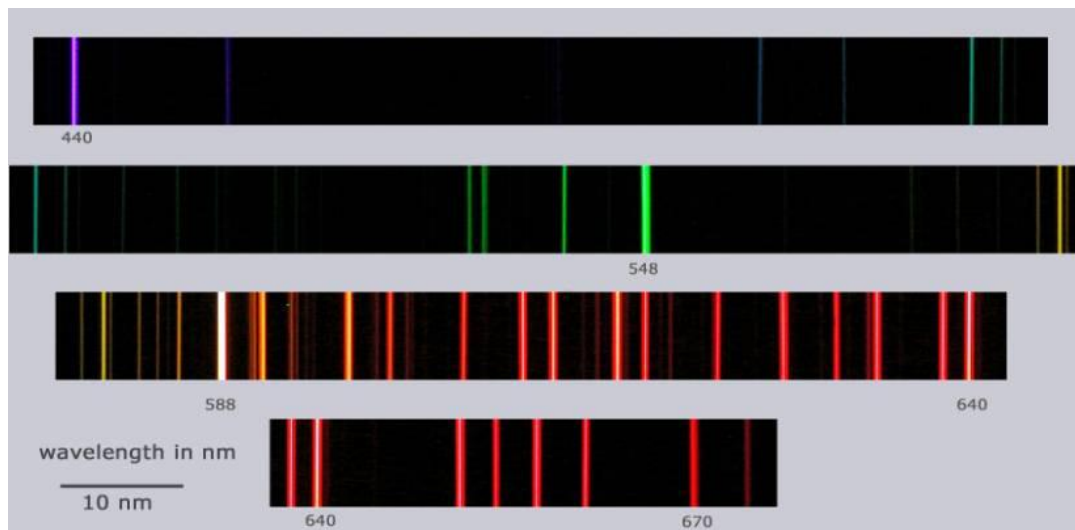
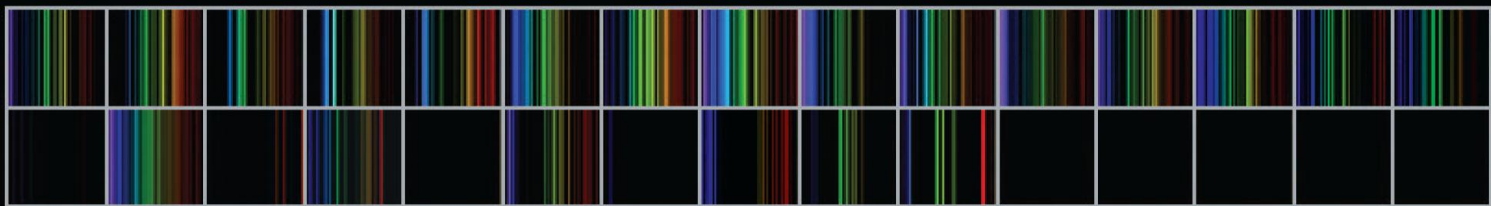
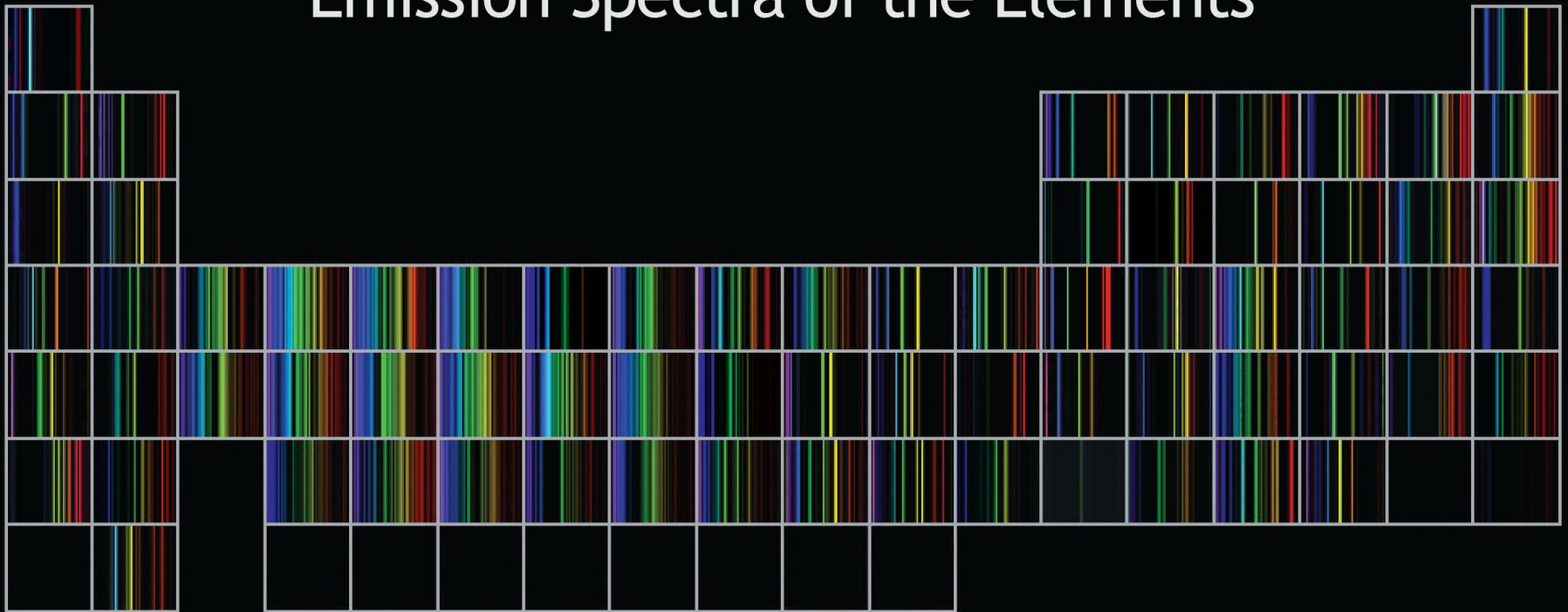


Figure 2.2 Schematic drawing of an optical emission spectrograph. Light from the sample is focused onto the input slit of the spectrograph and is then dispersed via a prism (or diffraction grating) and recorded on a photographic plate. (Adapted from Britton and Richards, 1969; Fig. 108, by permission of Thames and Hudson Ltd.)



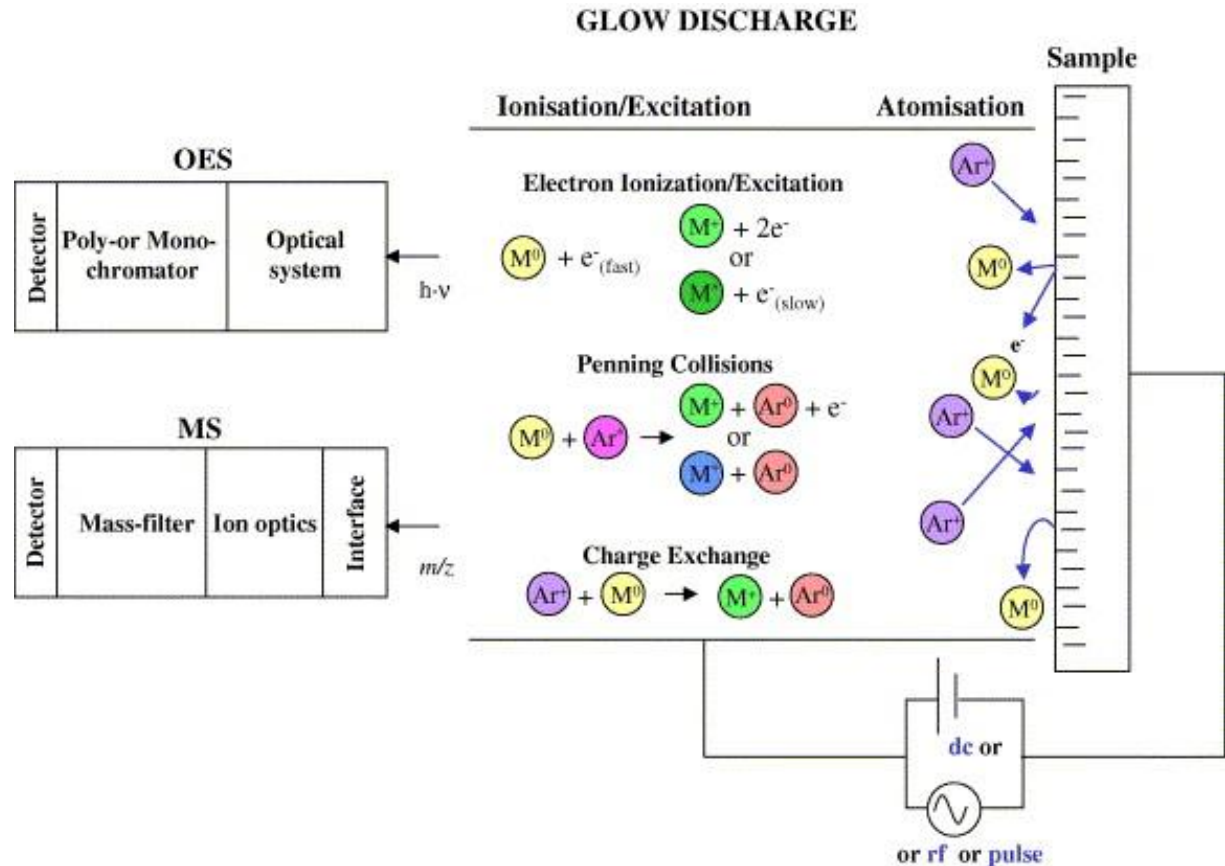
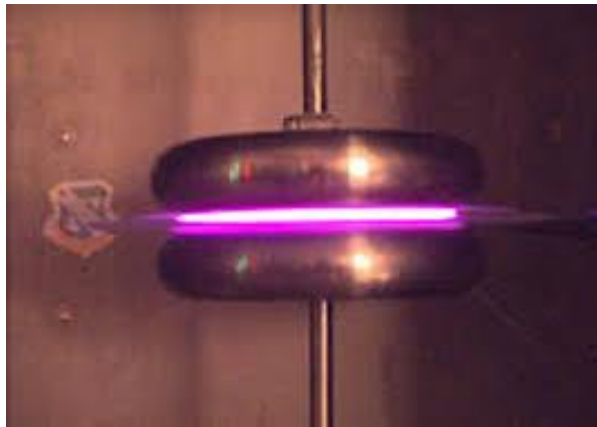
Emission Spectra of the Elements



OES/MS s doutnavým výbojem (GD-OES)

Analýza povrchu

Nedestruktivní



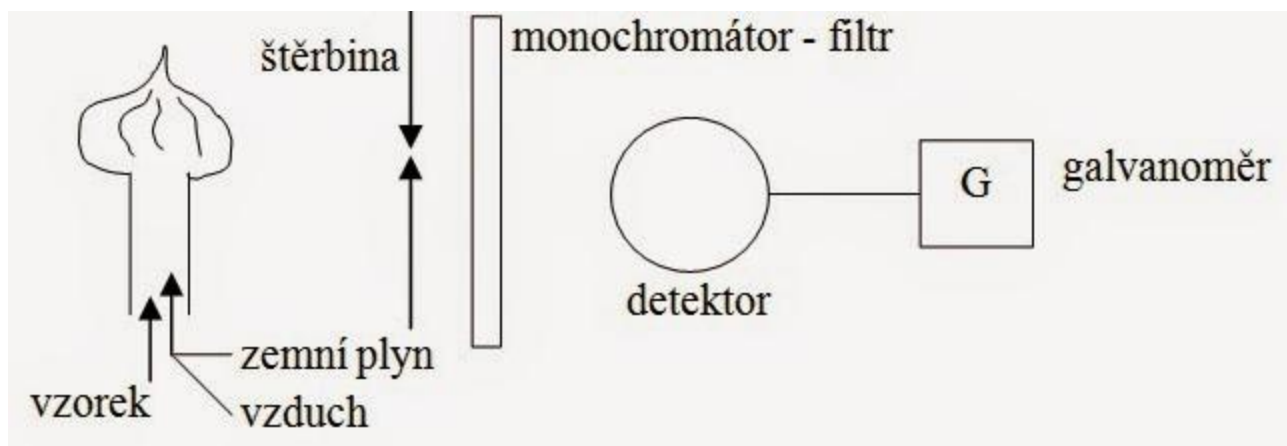
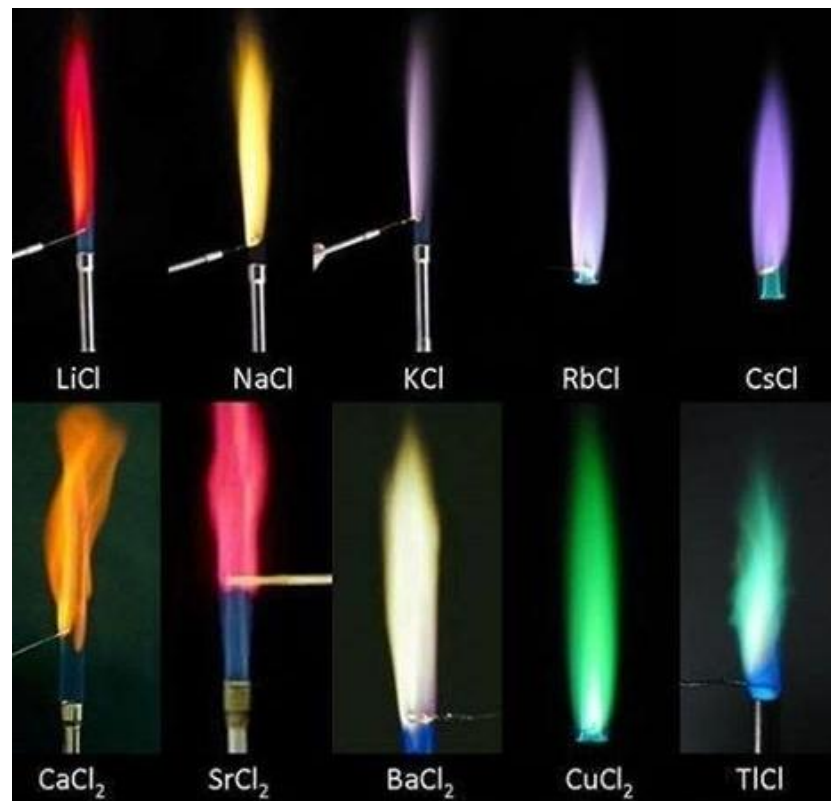
Plamenový test

Plamenová fotometrie

Roztoková analýza

destruktivní

Stanovení snadno
ionizovatelných prvků
Na, Li, K, Mg a Ca



Atomová emisní spektrometrie s indukčně vázaným plazmatem (ICP-OES)

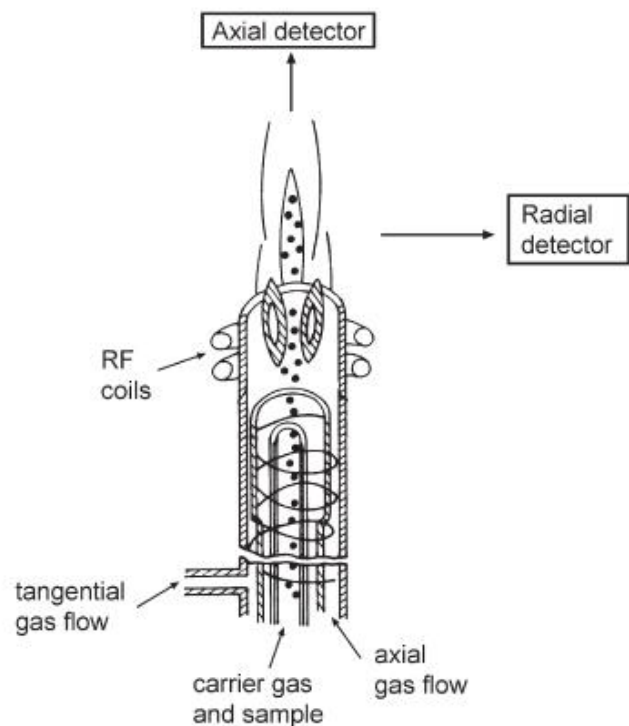


Figure 2.4 Schematic diagram of an ICP torch. The sample is carried into the torch by the carrier argon gas, and is ignited by radio-frequency heating from the RF coils. The tangential argon flow lifts the flame from the burner, preventing melting. The position of the detector in axial or radial mode is shown. (From Pollard *et al.*, 2007; Fig. 3-3, by permission of Cambridge University Press.)

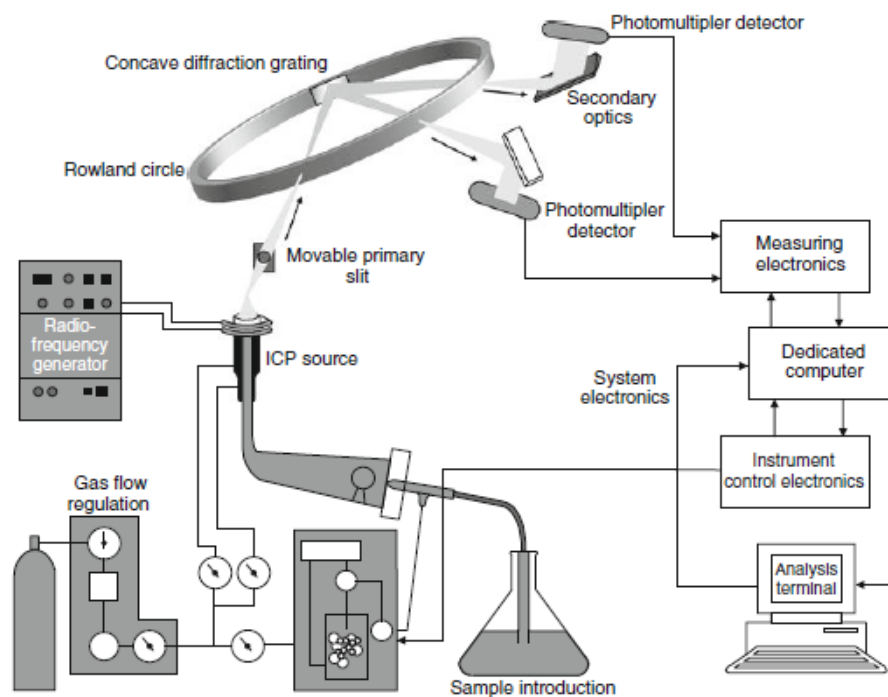
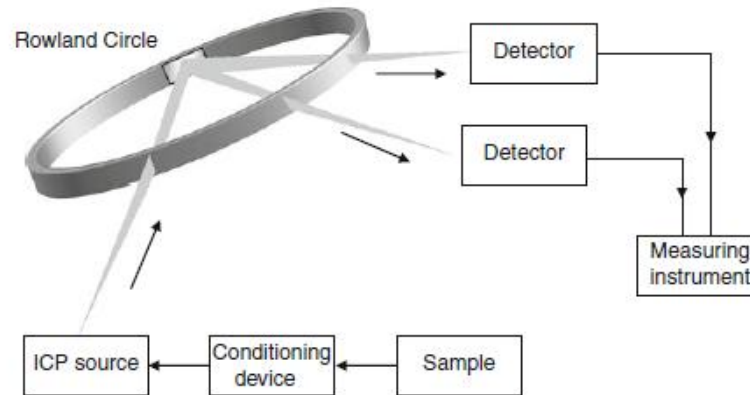


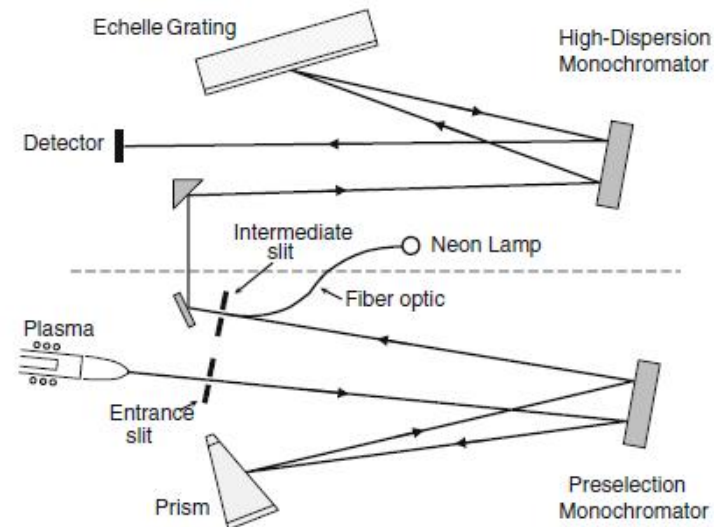
Fig. 34.2 Inductively coupled plasma polychromator (From SKOOG. *Principles of Instrumental Analysis*, 5E. © 1998 Brooks/Cole, a part of Cengage Learning, Inc. Reproduced by permission. www.cengage.com/permissions)

Roztoková analýza

Destruktivní



(a) Simultaneous Multichannel Detector



(b) Sequential Detector

Fig. 34.4 Simultaneous multichannel (a) and sequential detectors (b) ((a) Adapted from SKOOG. Principles of Instrumental Analysis, 5E. © 1998 Brooks/Cole, a part of Cengage Learning, Inc. Reproduced by permission. www.cengage.com/permissions (b) Image used with permission from PerkinElmer, Inc., Waltham, MA)

Multichannel Spectrometers

Spectrographs

Charge-Coupled Devices – 2 CCD's – one for vis and one for UV.

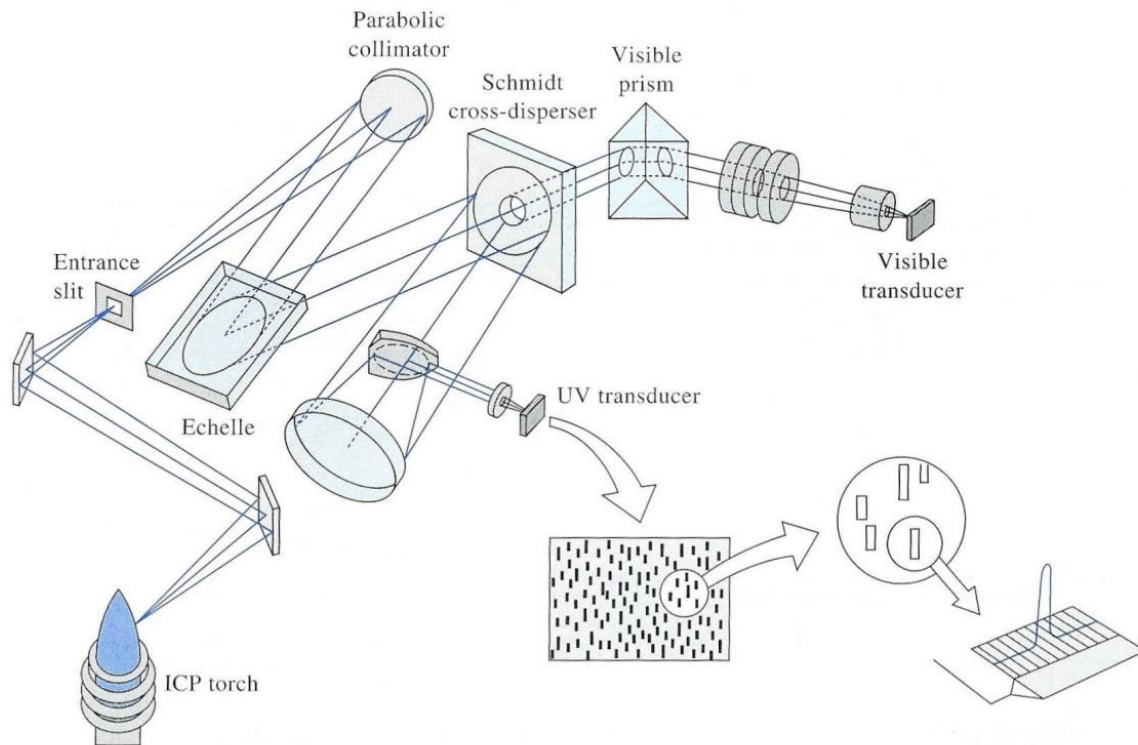
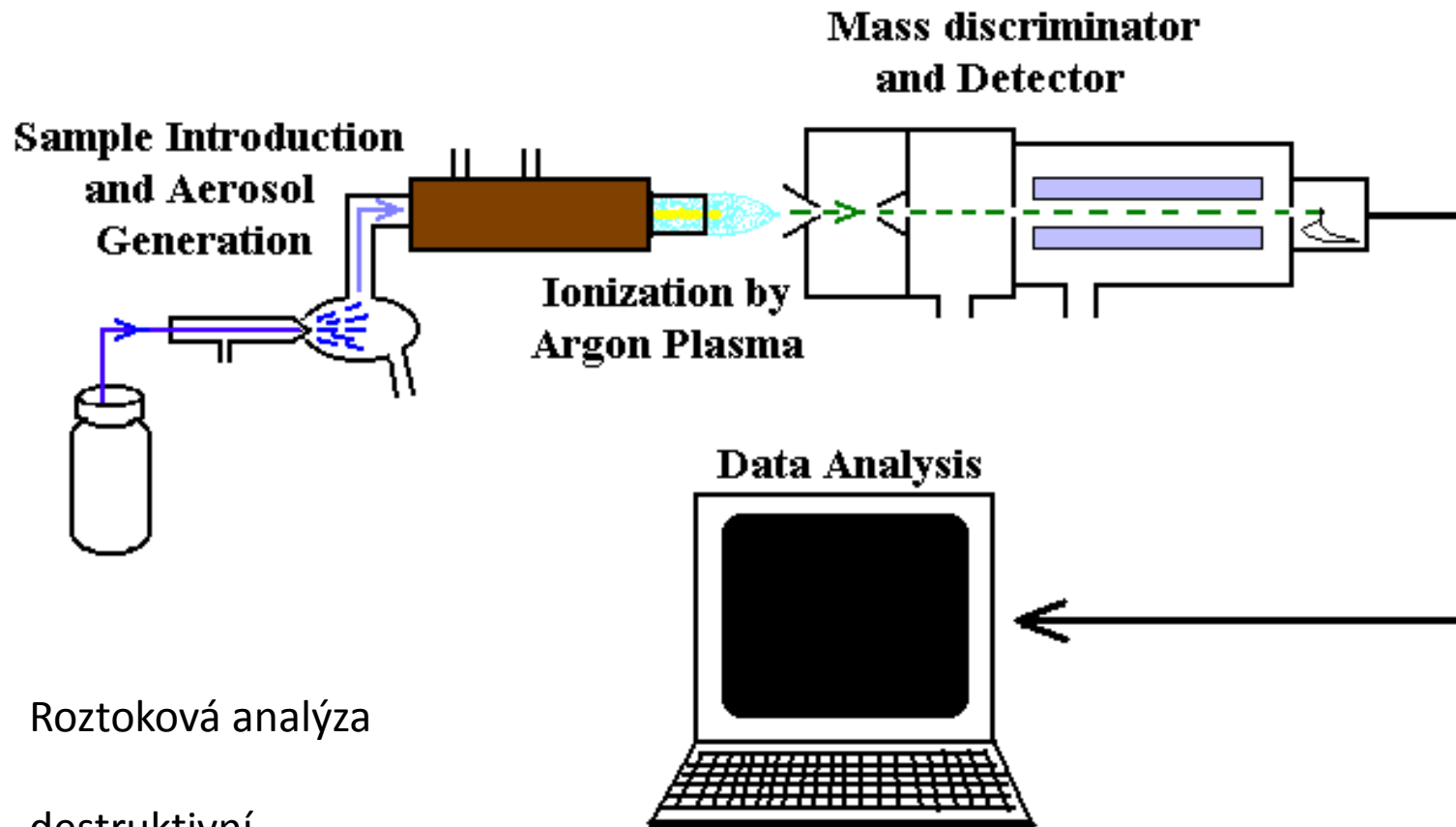


FIGURE 10-11 An echelle spectrometer with segmented array of CCDs. (From T. W. Barnard et al., *Anal. Chem.*, **1993**, 65, 1231. Figure 1, p. 1232. Copyright 1993 American Chemical Society.)

Hmotnostní spektrometrie s indukčně vázaným plazmatem



Roztoková analýza

destruktivní

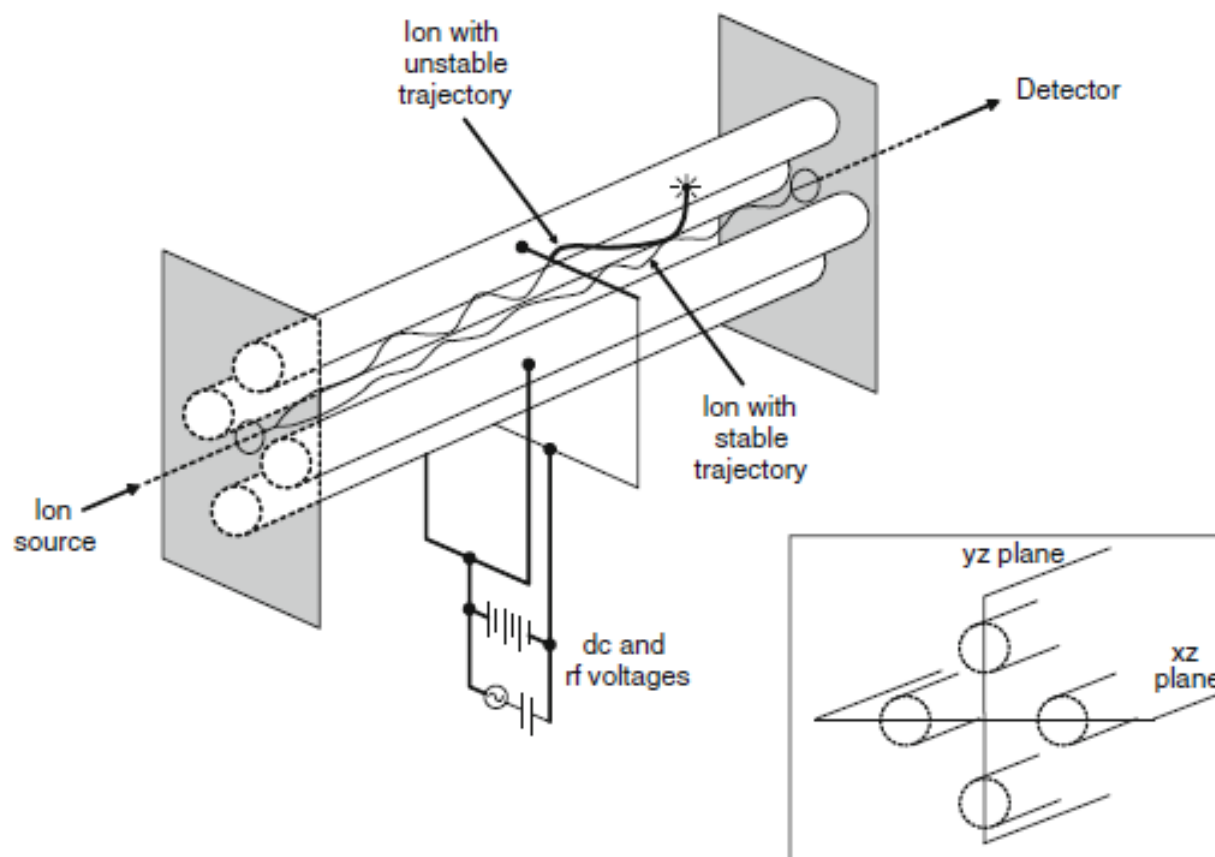


Fig. 31.5 Quadrupole mass spectrometer with inset of xz and yz planes (From SKOOG. Principles of Instrumental Analysis, 5E. © 1998 Brooks/Cole, a part of Cengage Learning, Inc. Reproduced by permission. www.cengage.com/permissions)

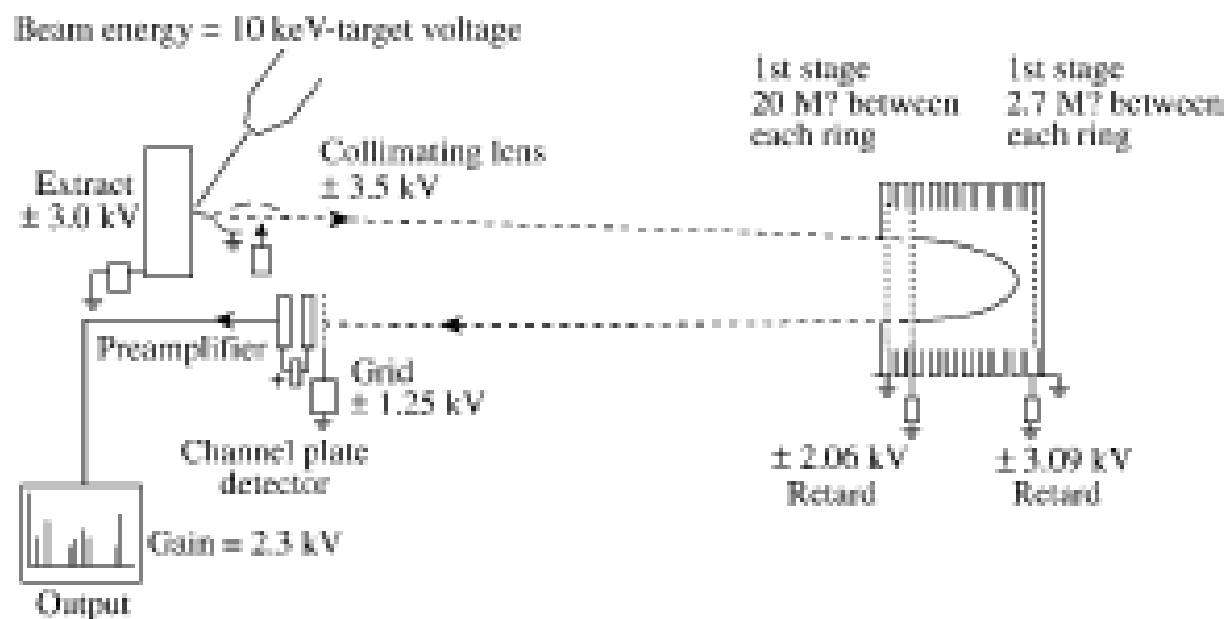


Figure 8.12 Time-of-flight mass analyzer. The secondary ion beam is reflected by a mirror to correct the flight time of ions with identical m/z . (Reproduced with permission from J.C. Vickerman, *Surface Analysis: The Principal Techniques*, John Wiley & Sons Ltd, Chichester. © 1997 J.C. Vickerman.)

LA-ICP-MS

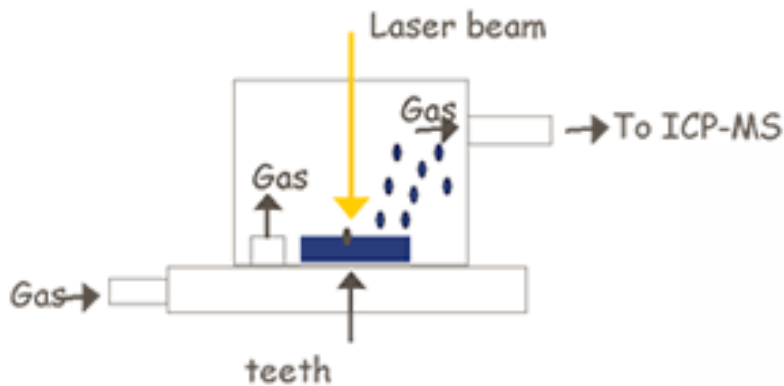
Pevné látky vzorkovány laserovou ablací

LA-ICP-MS method

Laser beam → surface of teeth

Small amount of mass → vaporized

Vaporized particles → ICP-MS



Semidestruktivní metoda

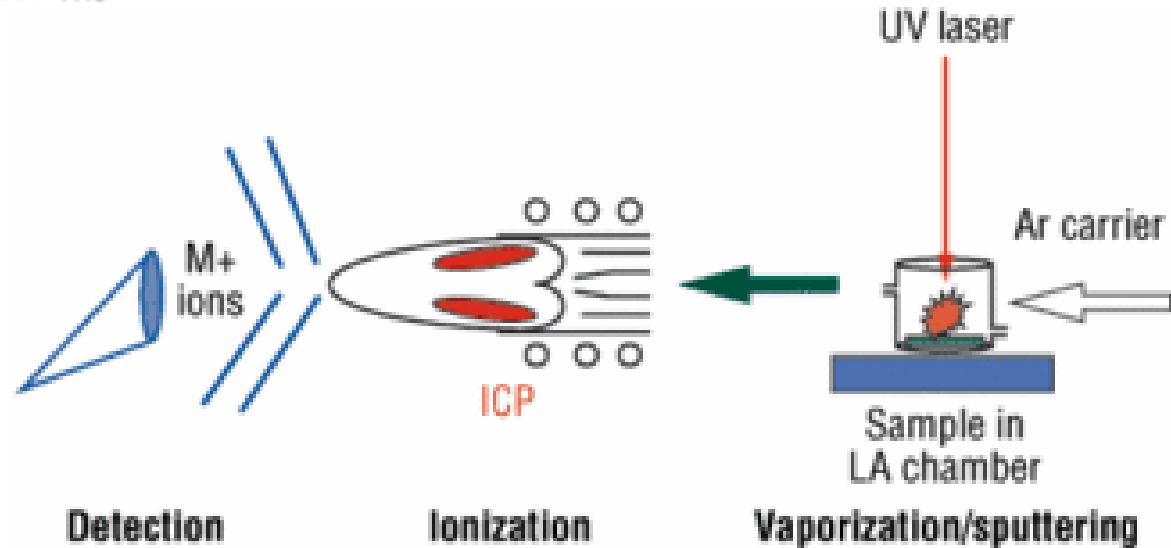
Nd:YAG

Excimer

Kvadrupólový

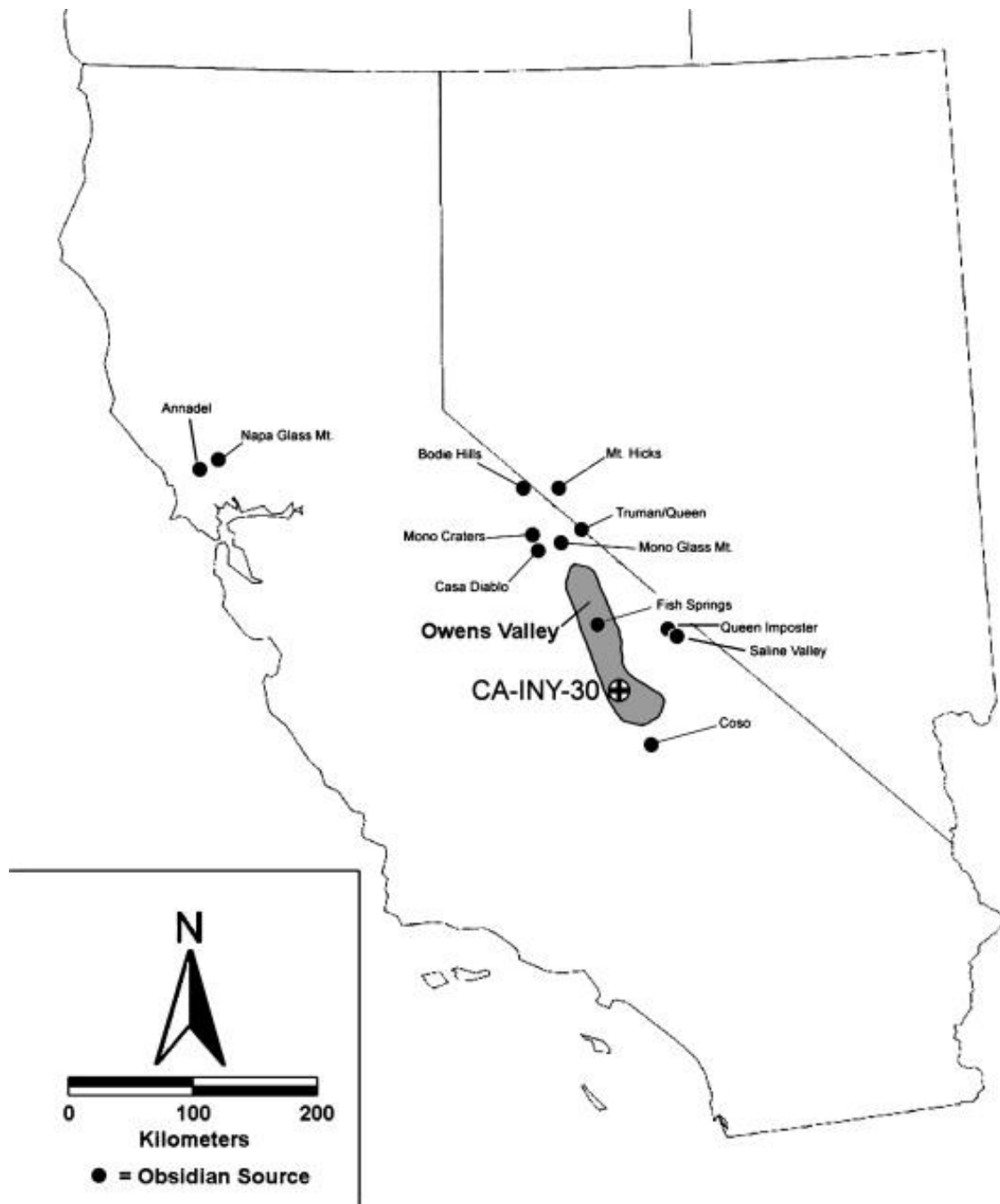
TOF

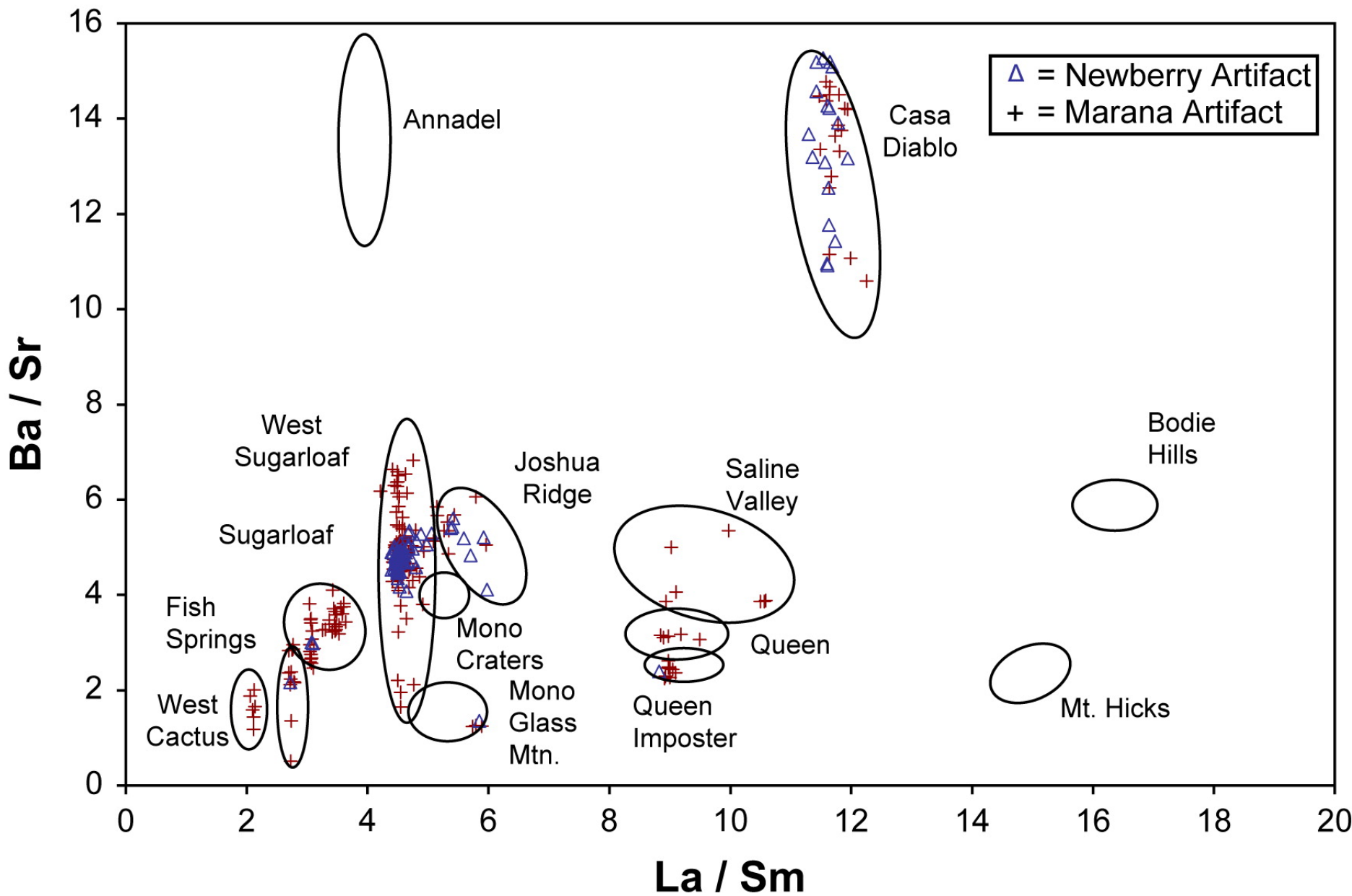
Sektorový (MC)



Provenience obsidiánu

Owens Valley,
vých. Kalifornie





Provenience železa

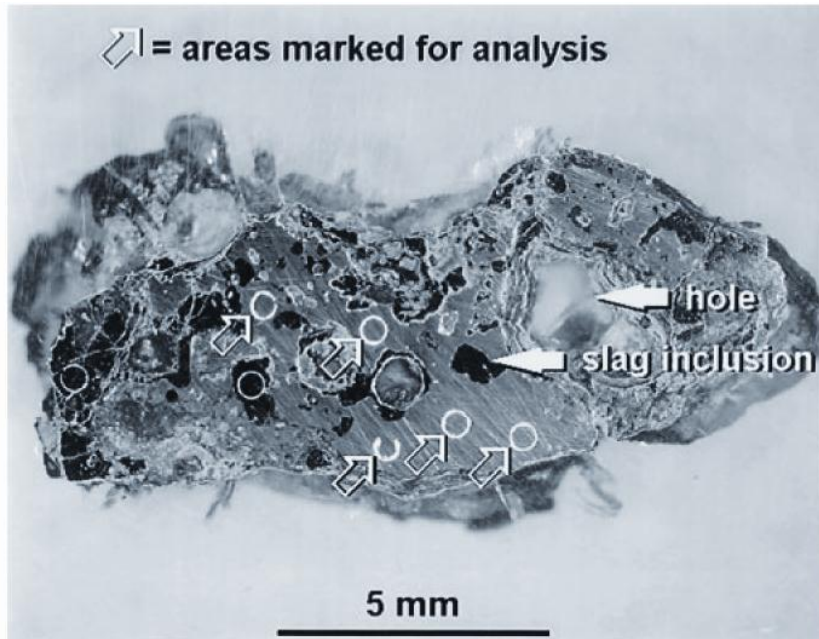


Fig.1 Optical microscopy view of a cross-section of an iron bloom fragment embedded in a synthetic resin

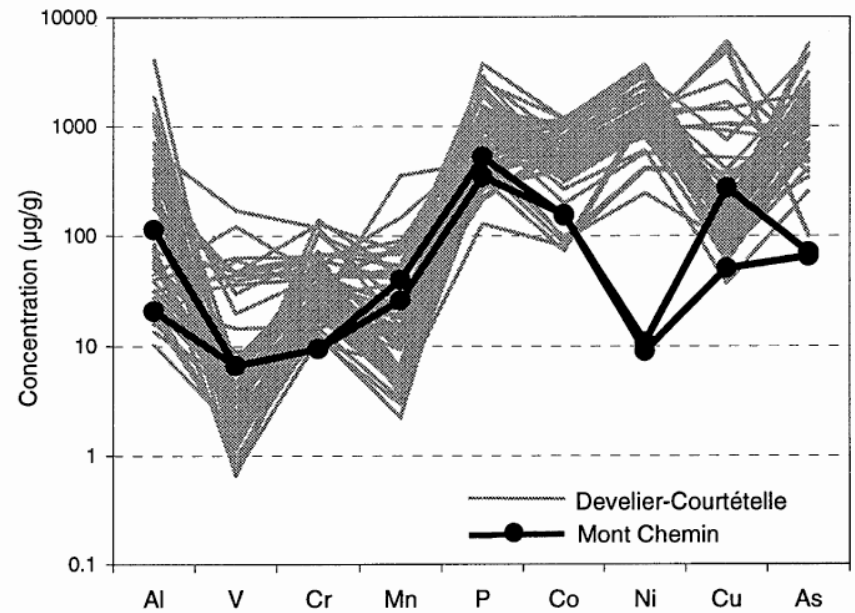
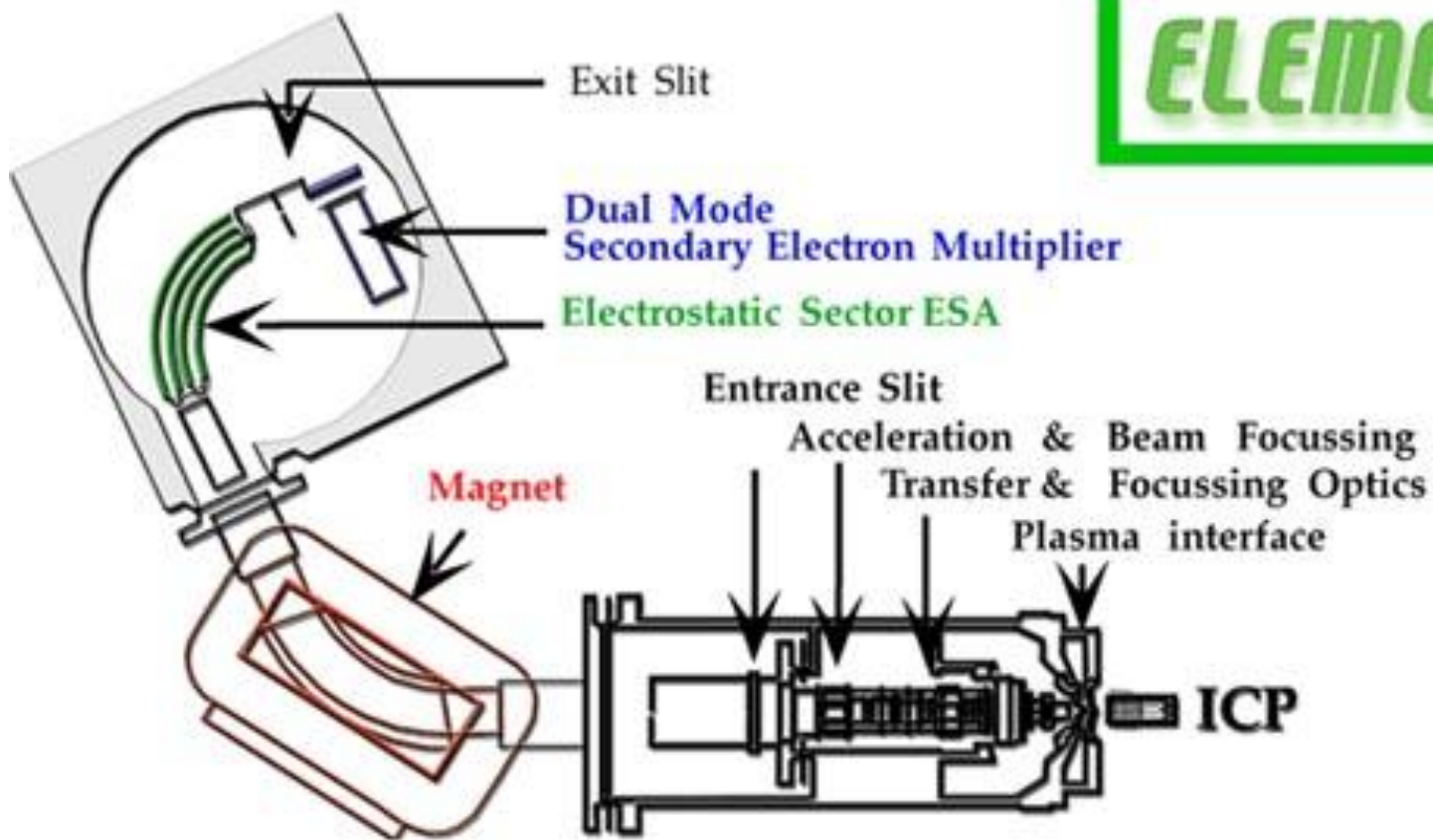


Fig.9 Concentration profile for an iron bloom sample from Mont Chemin (Switzerland), compared to the concentration profiles in the Develier-Courtételle samples, showing low values for Ni in the Mont-Chemin sample

MC LA-ICP-MS

Analýza izotopových poměrů



Izotopy

^a The detection limits are based on a 98% confidence level (3 standard deviations).

^b Identifying a single part per trillion of an element in a solution is analogous to locating a single white raisin in a house (2,700 sq ft) full of regular raisins.

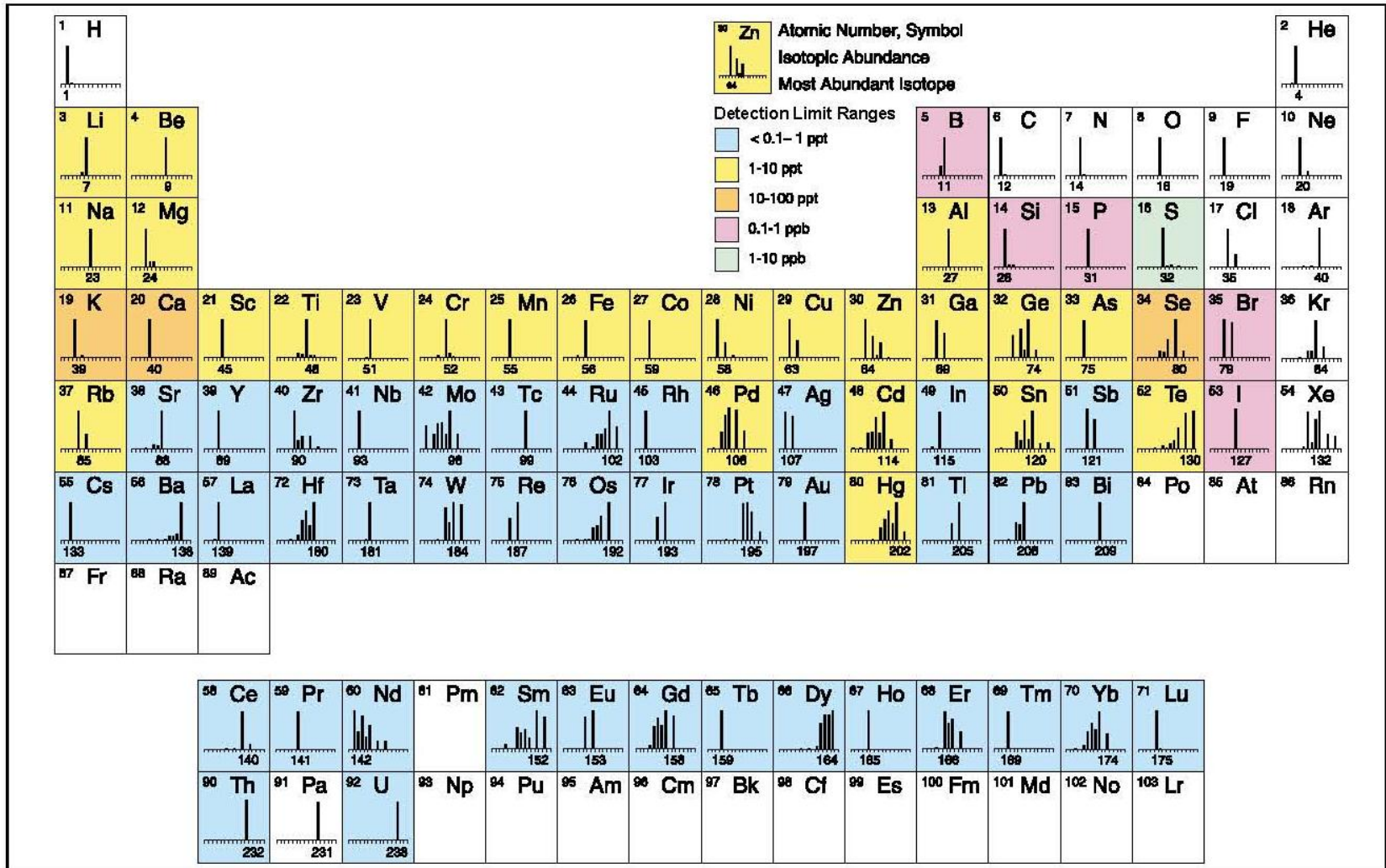


Figure 1. Elements determined by ICP-MS and approximate detection capability.



Analýza izotopových poměrů

Sklo „Art nouveau“

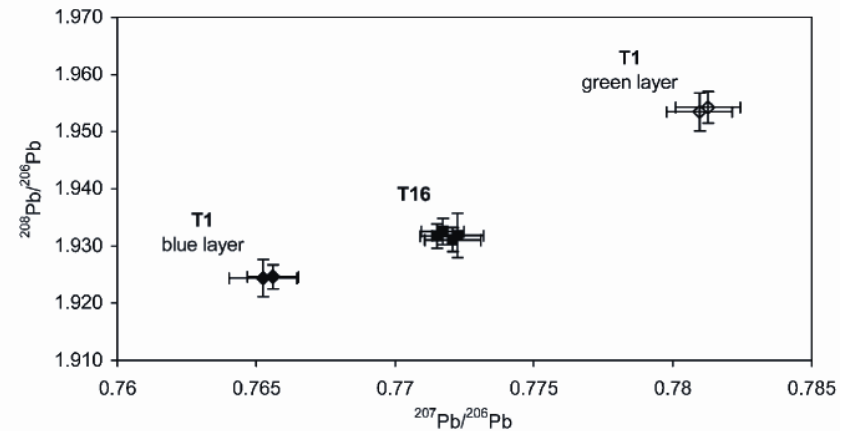


Fig. 2 Lead isotope ratio distribution of the two iridescent Art Nouveau glasses. Glass T1 consists of two layers of approximately equal thickness (coloured green and blue, respectively). Error bars represent total combined uncertainties ($k = 1$).

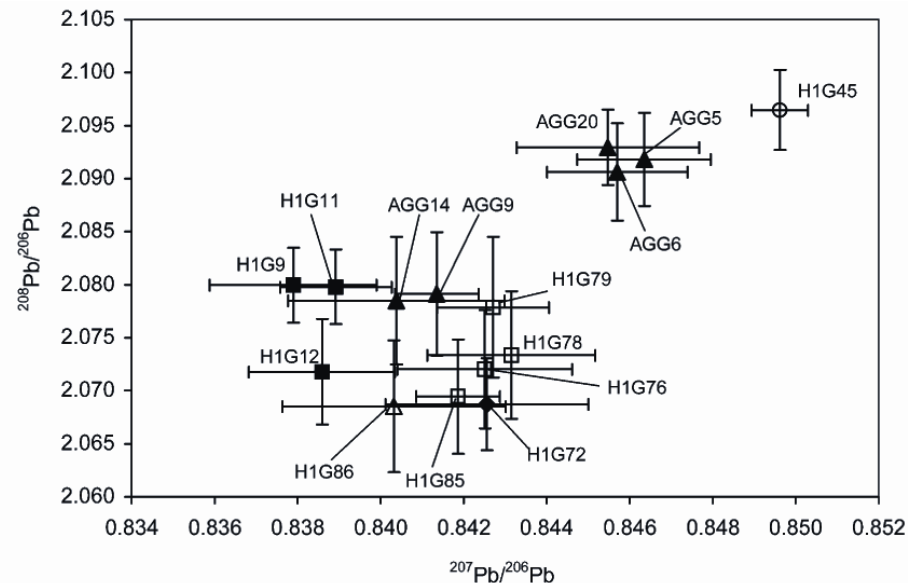


Fig. 3 Lead isotope ratios of Ephesos glass samples after external mass bias correction *via* the NIST SRM 610 glass reference material. Error bars represent total combined uncertainties ($k = 1$). For sample description see Table 1.

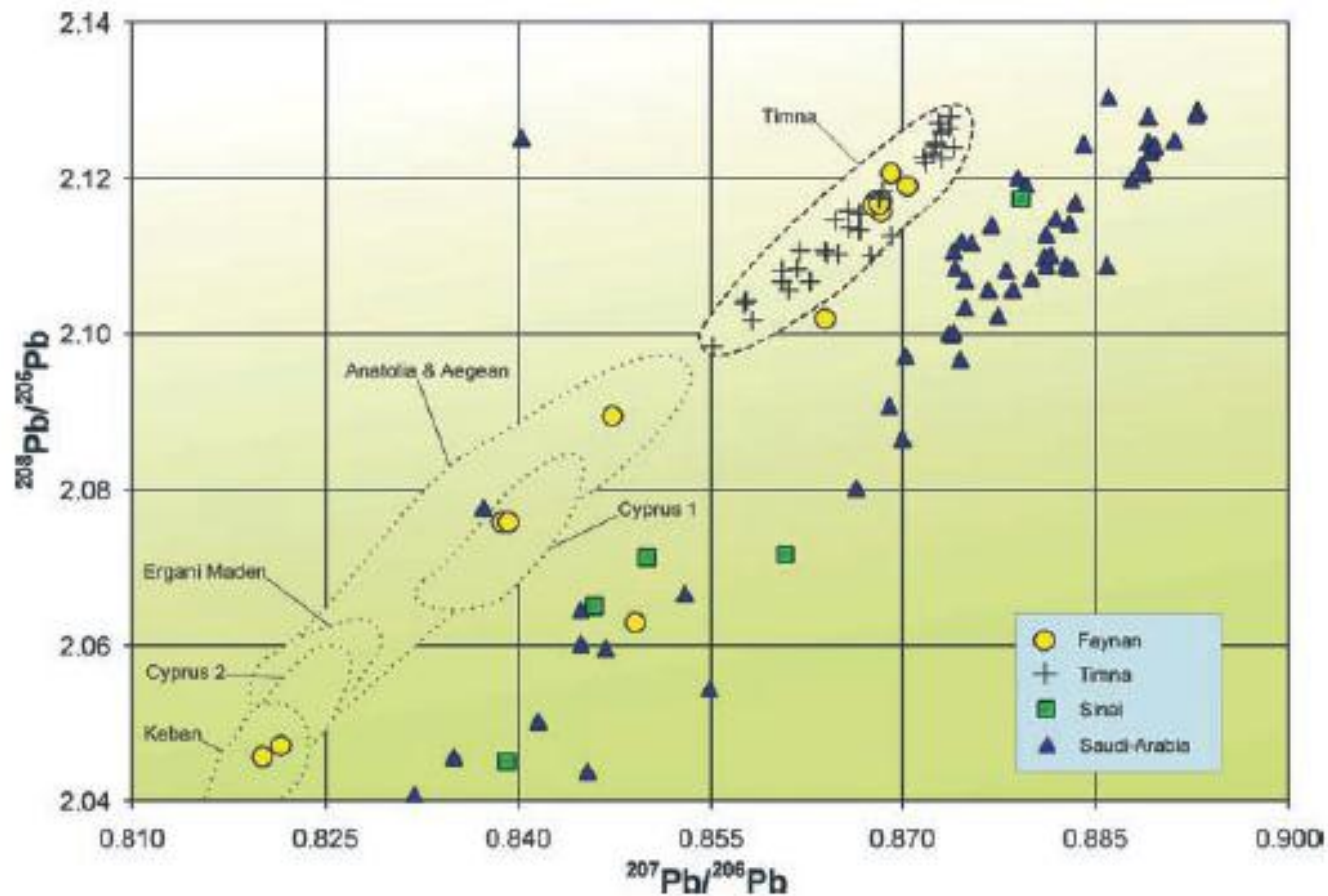
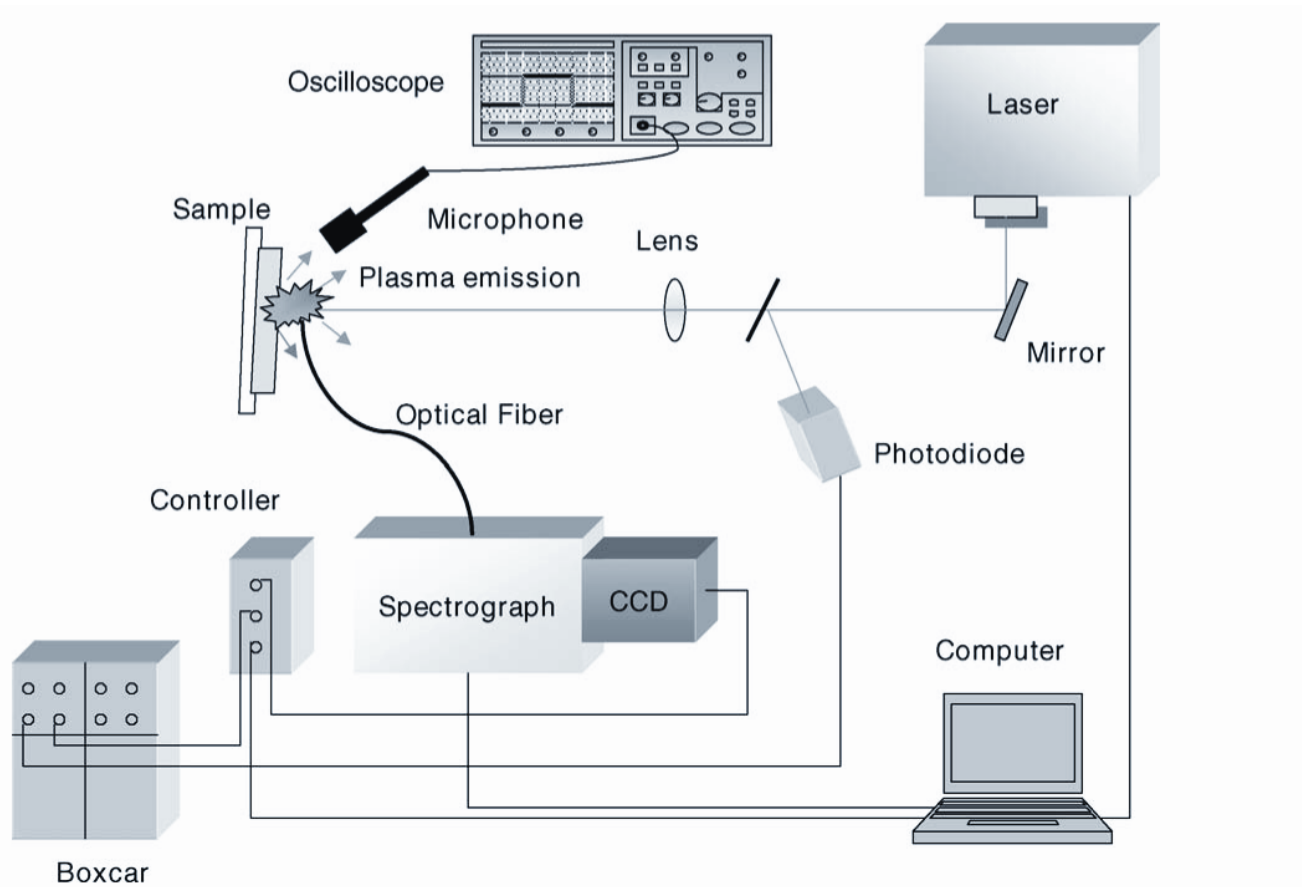


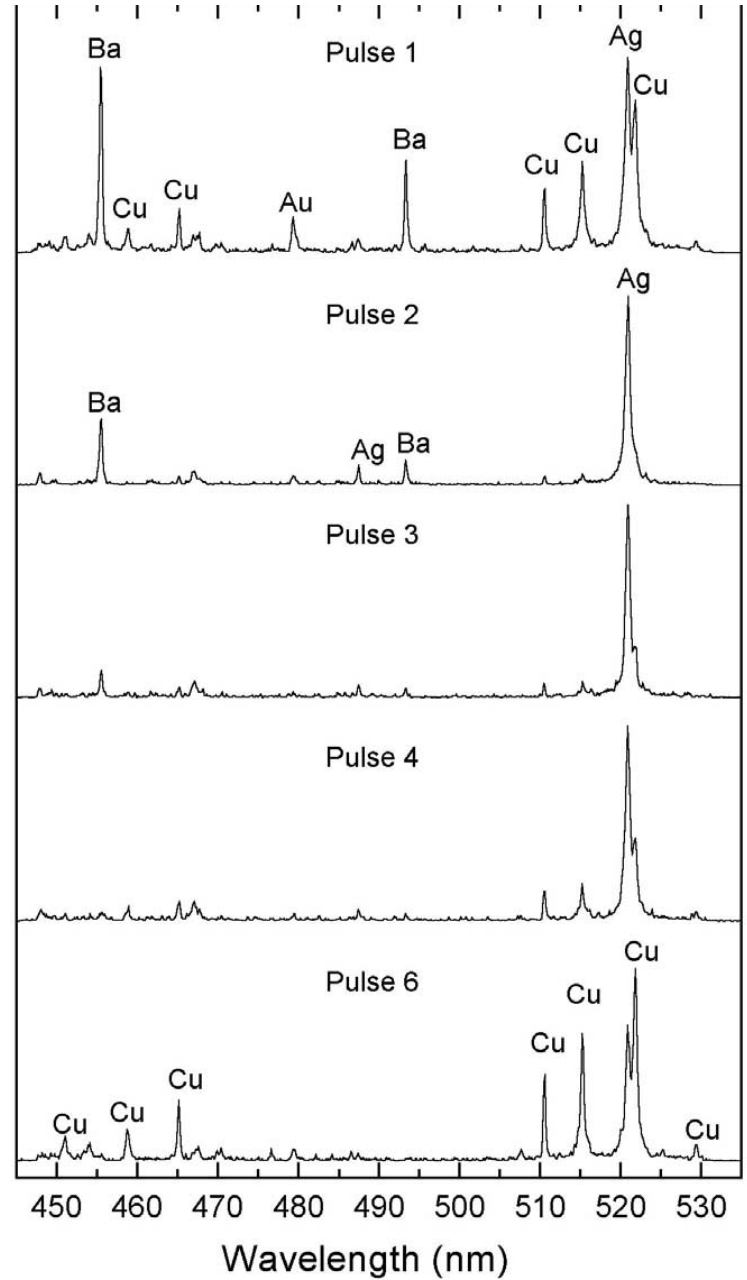
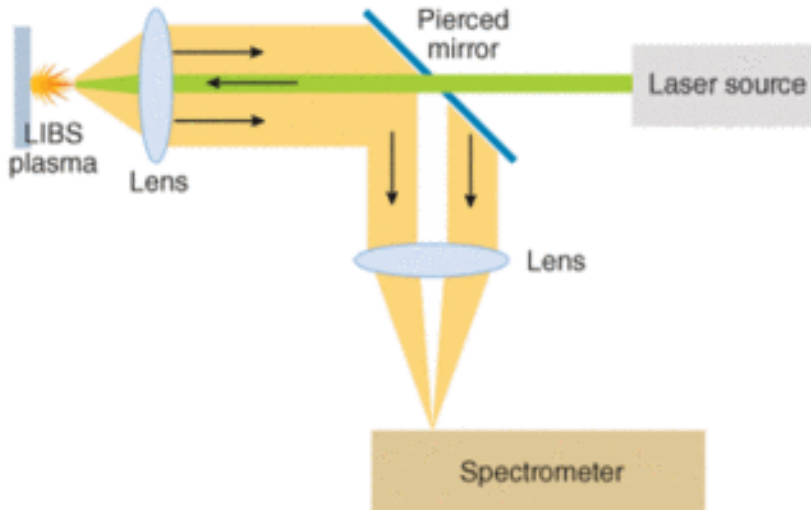
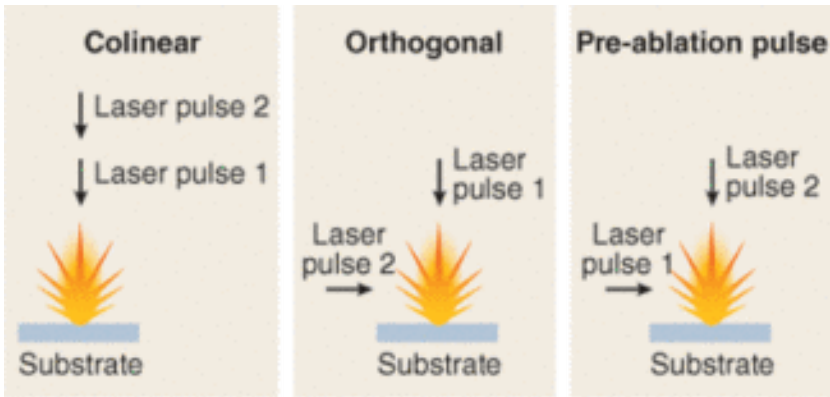
Fig. 4.14. Comparison of lead isotope abundance ratios of Arabah copper ores with ores from around the Eastern Mediterranean and the Arabian Shield. Evidence of ancient mining and smelting is known from Anatolia, the Aegean and from Cyprus (Stos-Gale 1993; Pemicka 1995) but is missing in detail from the Arabian Shield. The graph shows that the main copper mineralizations in the Arabah are among the oldest geological ages. Notice that the “Faynan/Timna field” contains only the data from the DLS and the Amir/Avrona Formation! Similarly old copper ores also occur in Saudi Arabia (Stacey et al. 1980; Bokhari and Kramers 1982; Brill and Barnes 1988) and on the Sinai Peninsula (Hauptmann et al. 1999; Segal et al. 2000)

Laser Induced Breakdown Spectroscopy

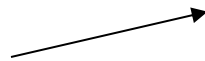


Schematic diagram of the experimental set-up used for the LIBS experiments and for the photoacoustic measurements.

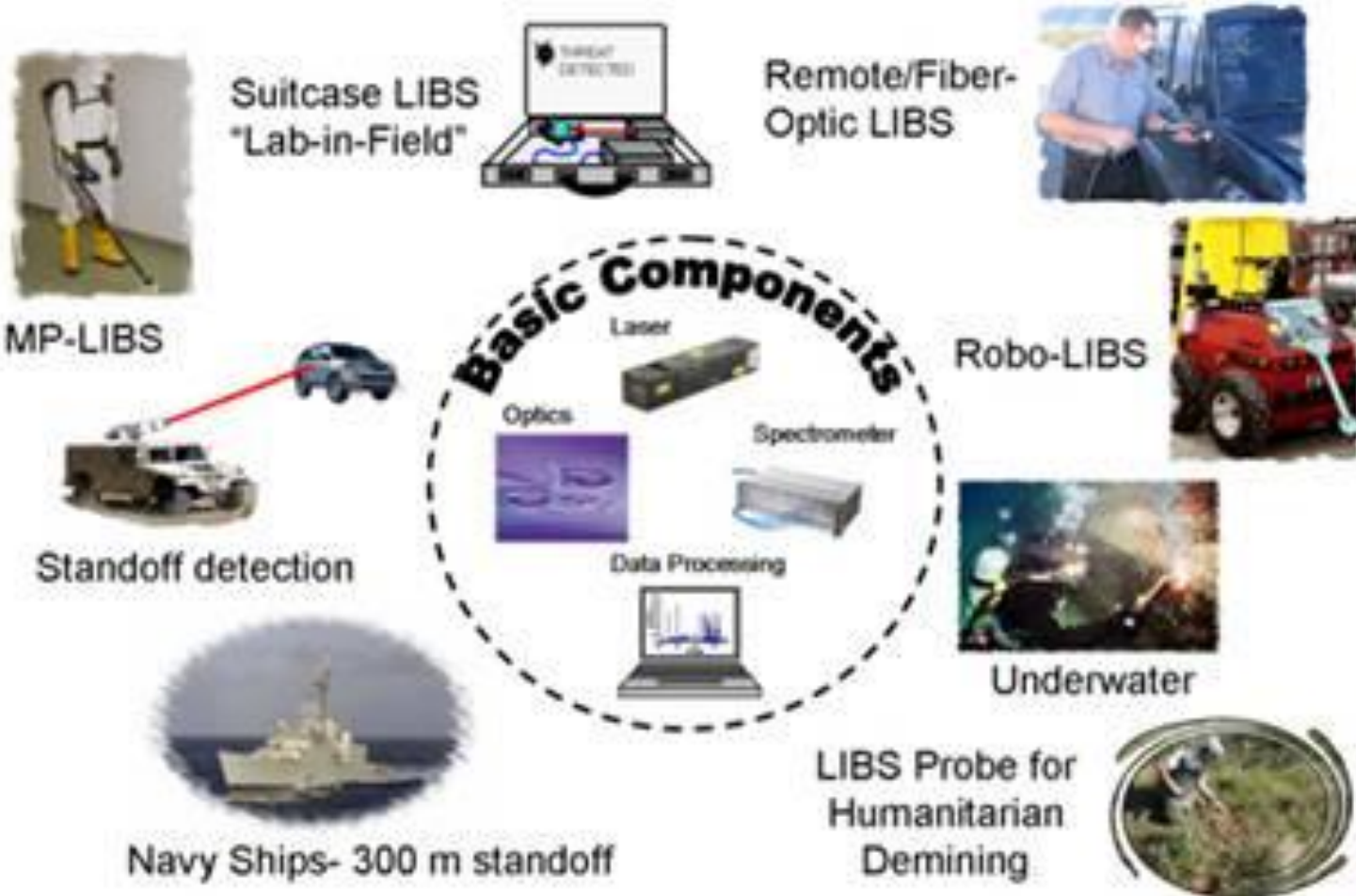
LIBS



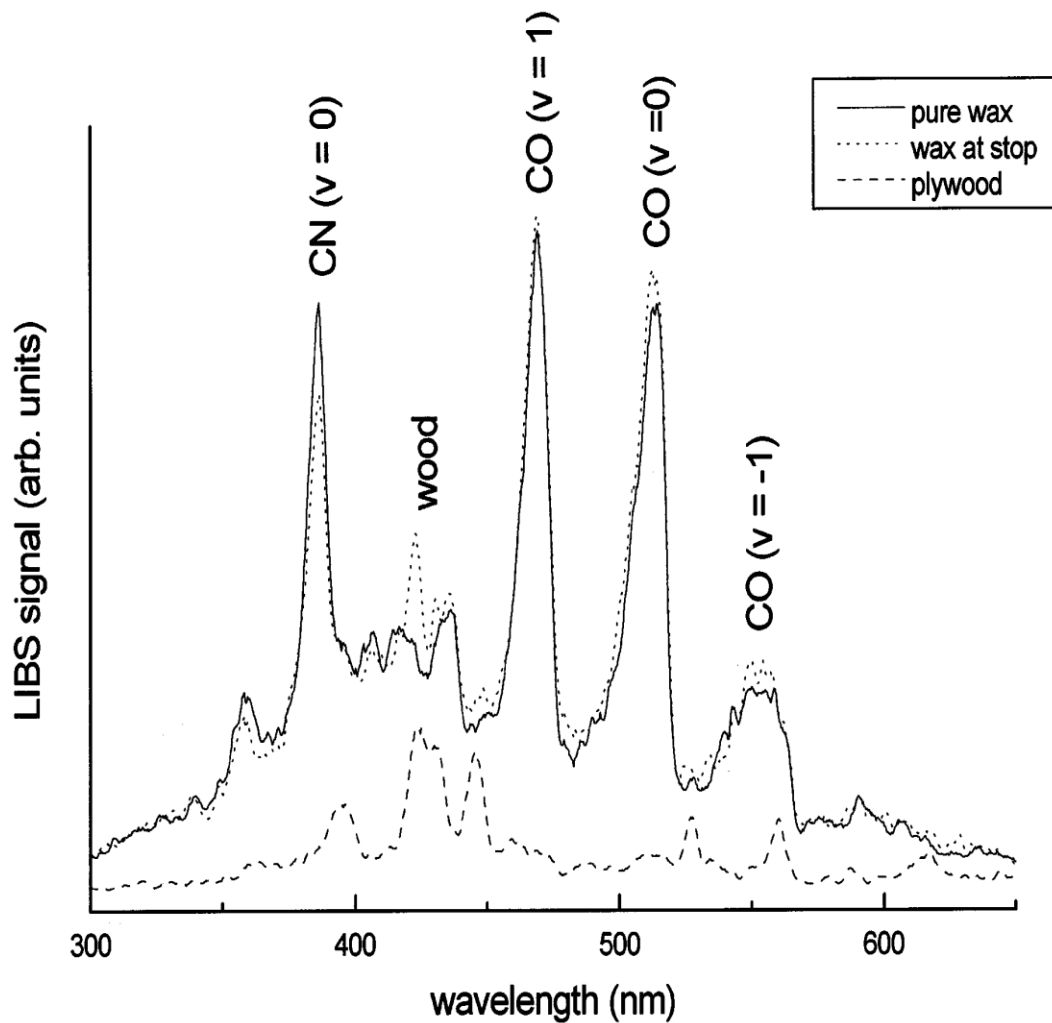
Daguerrotypie, 19. stol.



LIBS



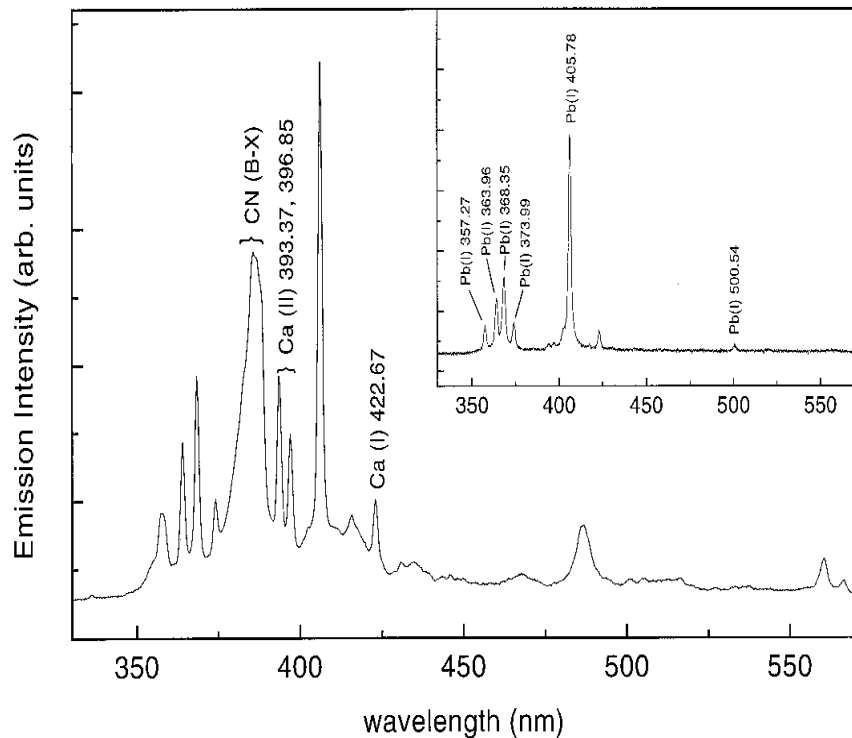
Monitoring odstraňování starých nátěrů



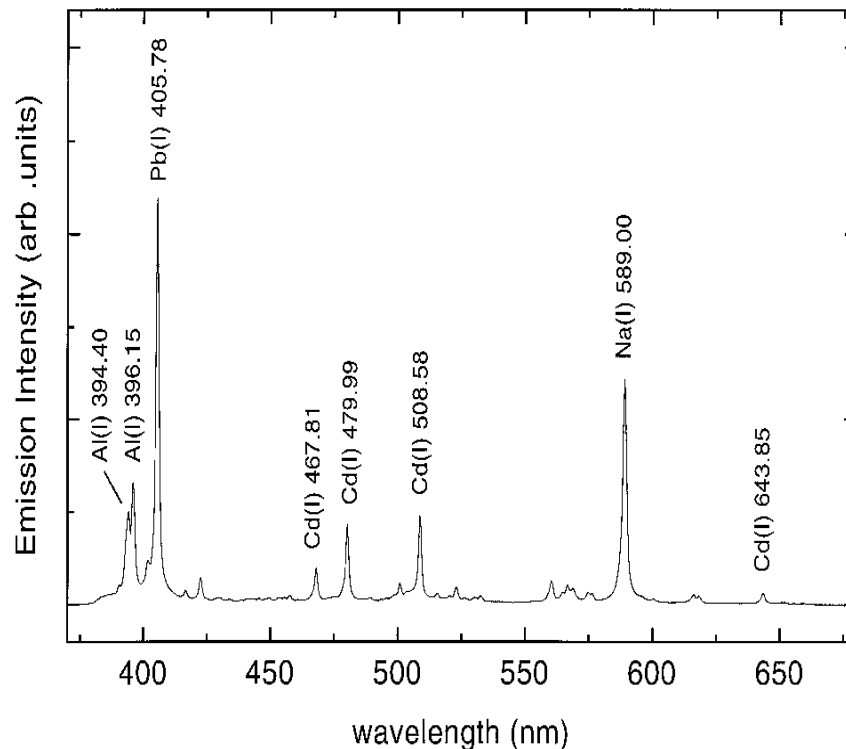
Odstraňování vosku z pláten nebo dřeva (překližka) je časově náročné. Proces lze snadno automatizovat použitím laseru a detekce LIBS.

LIBS spektra vosku vykazují zřetelné pásy CO a CN. Po dosažení spodní vrstvy se objevuje pík 423 nm a čištění je ukončeno.

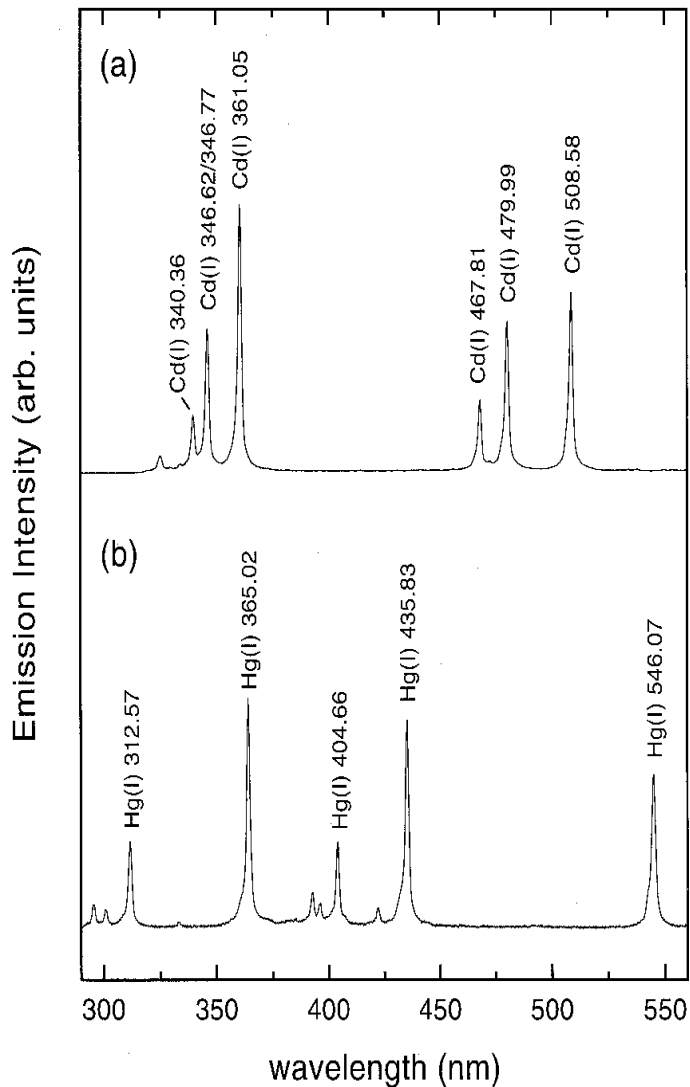
Pigmenty



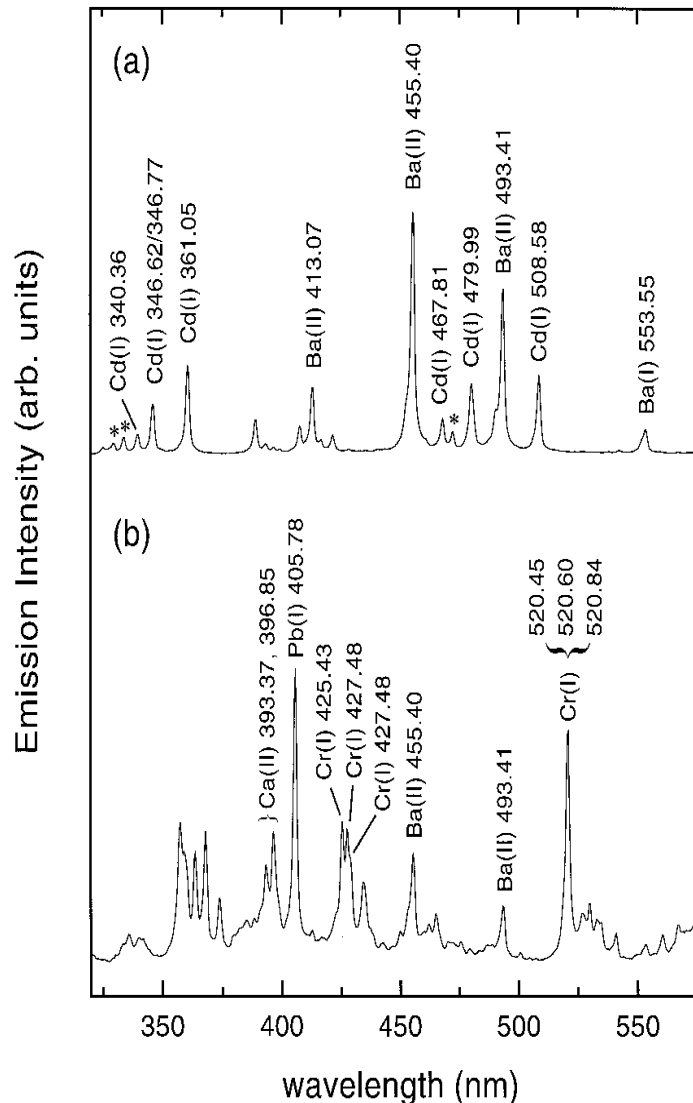
LIBS spektrum olovnaté olejové barvy (olovnatá běloba / Iněný olej). Na vnitřním obrázku spektrum olovnaté běloby. Vlnová délka laseru 1064 nm.



LIBS spektrum směsi pigmentů: olovnatá běloba, kadmiová červeň a ultramarínová modř. Vlnová délka laseru 266 nm.

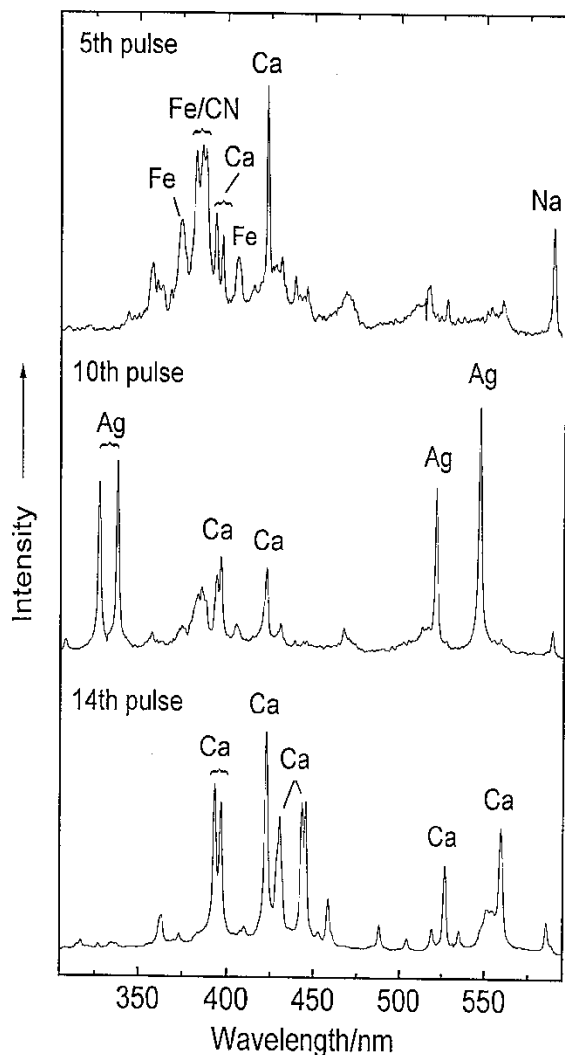


LIBS spektra **(a)** kadmiové červeně (CdSe_{0.9}S_{0.1}) a **(b)** rumělka (HgS). Vlnová délka laseru 1064 nm.



LIBS spektra: **(a)** kadmiová citronová žluť (Cd_{0.9}Zn_{0.1}BaSO₄) a **(b)** chromová žluť (PbCrO₄). Vlnová délka laseru 1064 nm.

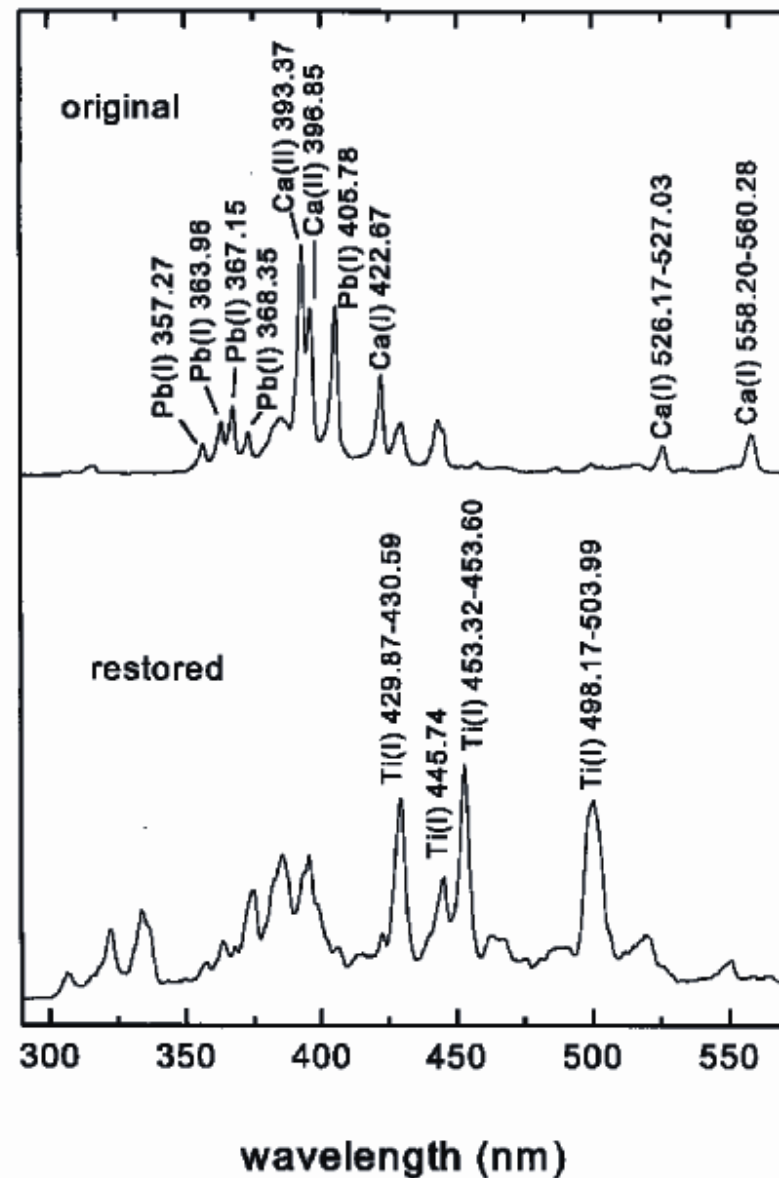
19th c. Russian icon of St. Nicholas.



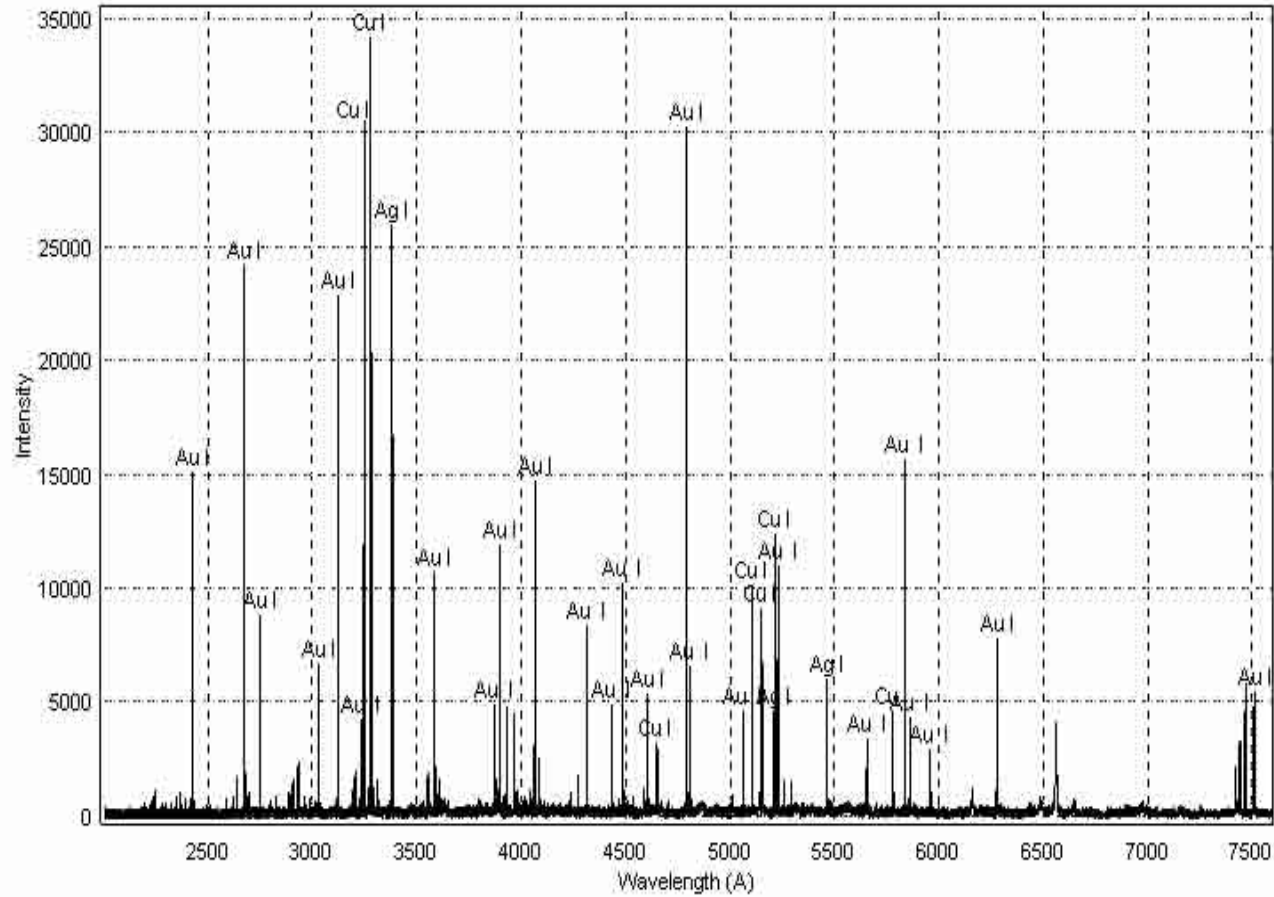
LIBS spektra malby (horní spektrum), stříbrné folie (střední spektrum) a podkladové vrstvy (dolní spektrum). Malba obsahuje pigment obsahující Fe (hnědý, pravděpodobně FeO), podklad je síran vápenatý.

Sledování restaurátorských zásahů

LIBS spektra originální malby a
restaurovaných částí olejomalby.

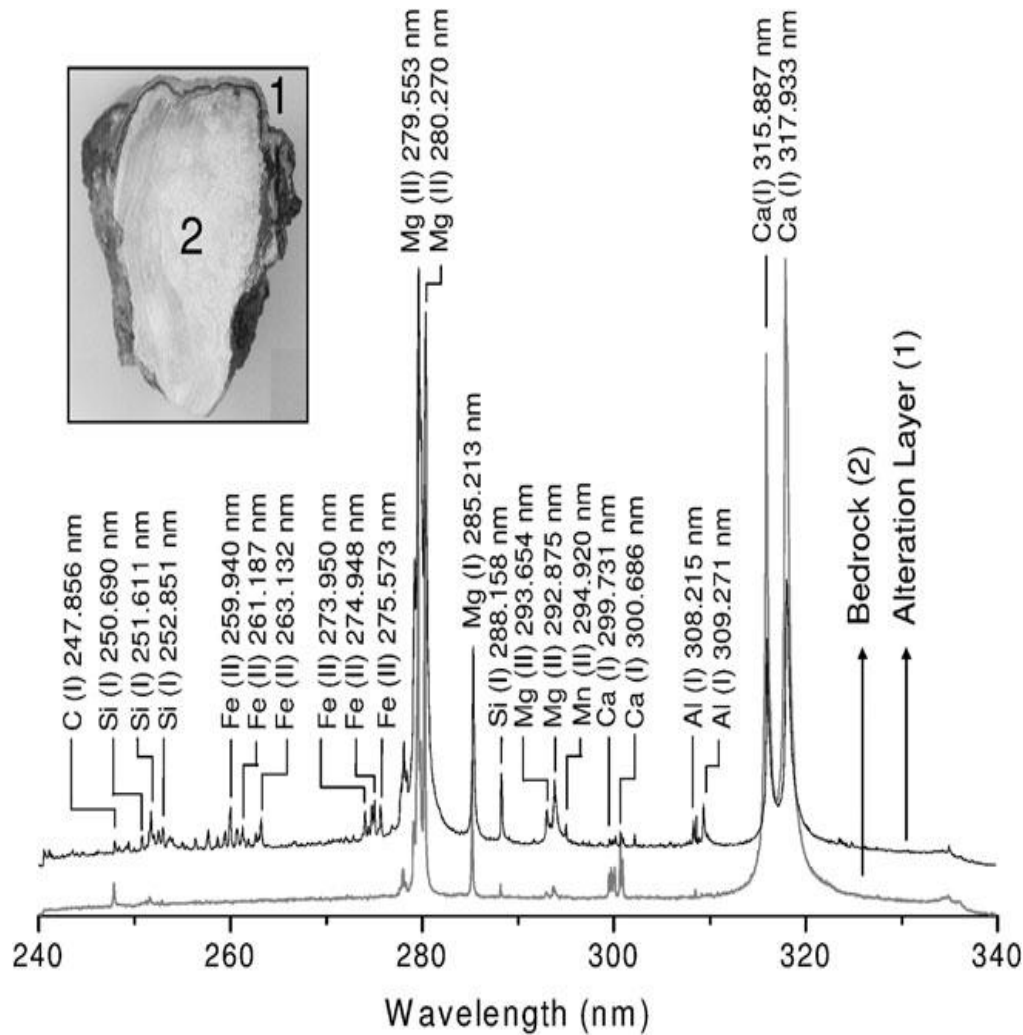


Kovy a slitiny



LIBS analýza slitiny Au.

Čištění kamene



LIBS řezu krápníkem (znečištěný povrch)

Autenticita výrobků z korálu



korál vs. vápenec

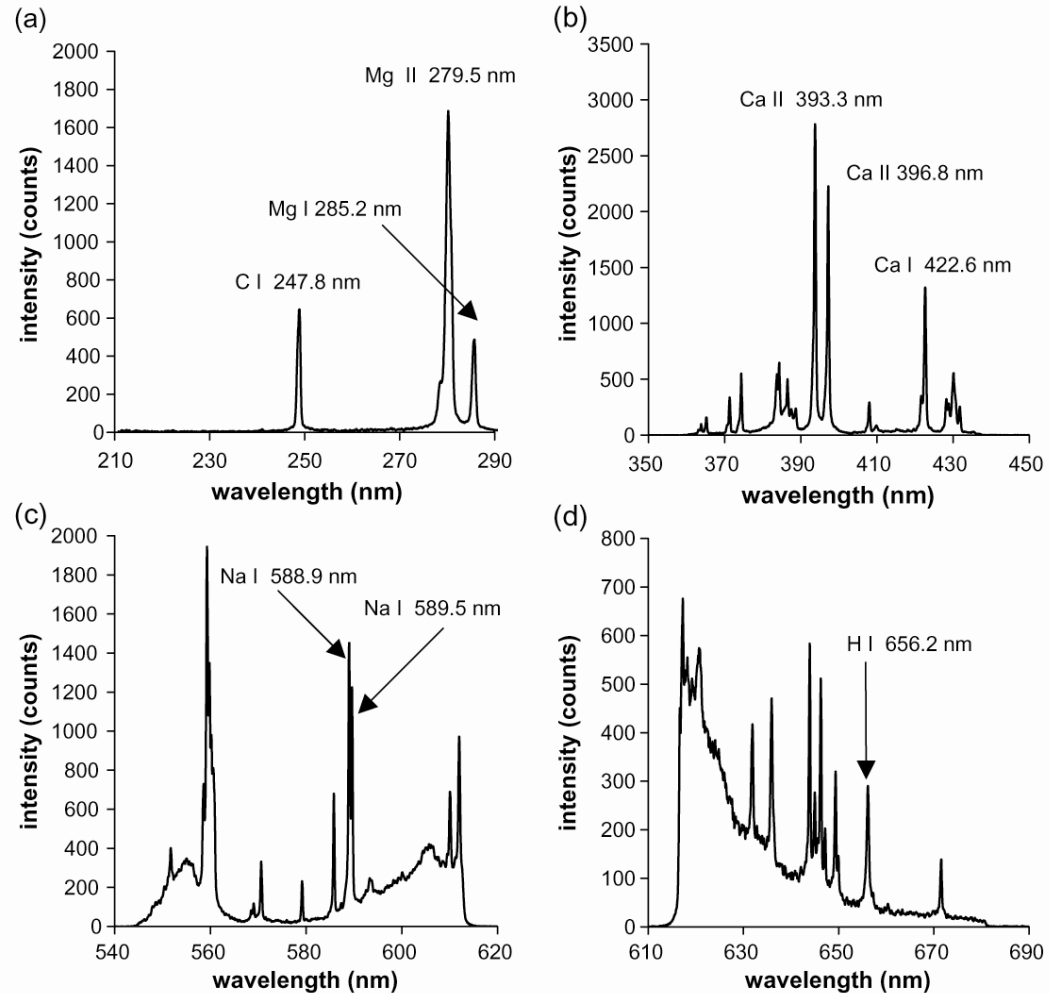
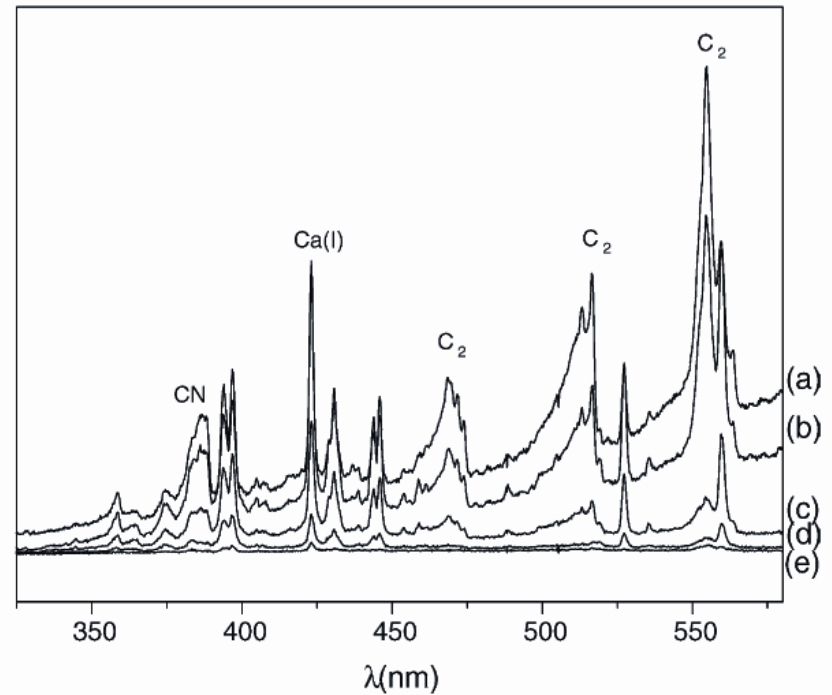
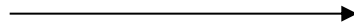


Fig. 5. Emission spectra of a fresh white coral sample in a low pressure plasma of 1.3 kPa in the wavelength region between (a) 220 and 290 nm, (b) 370 and 440 nm, (c) 550 and 620 nm and (d) 620 and 680 nm.

LIBS

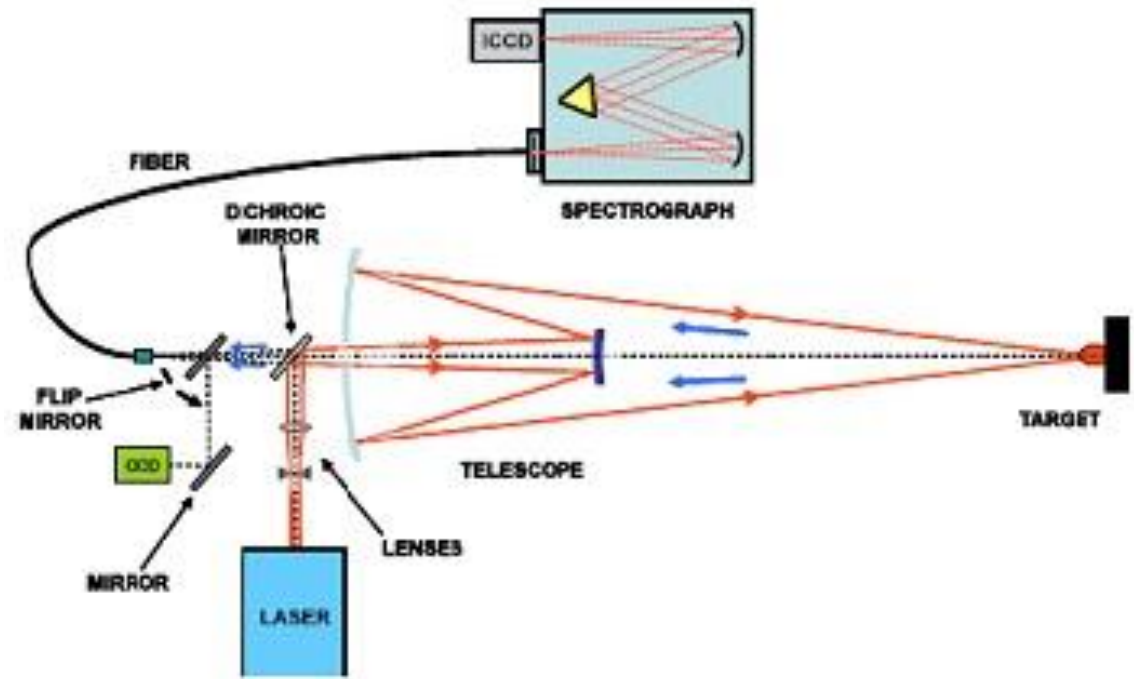
Molekulové pásy



Spojení s Ramanovou spektrometrií

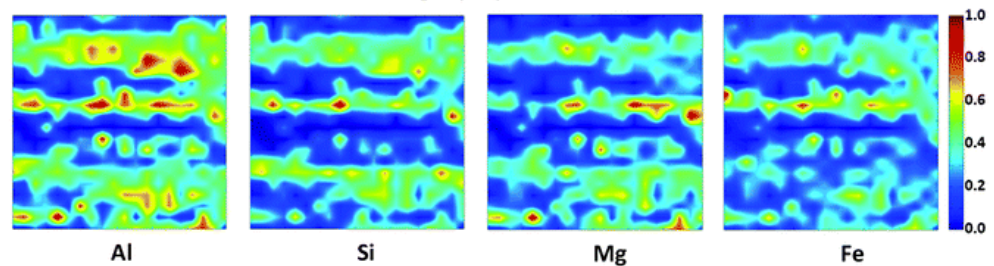
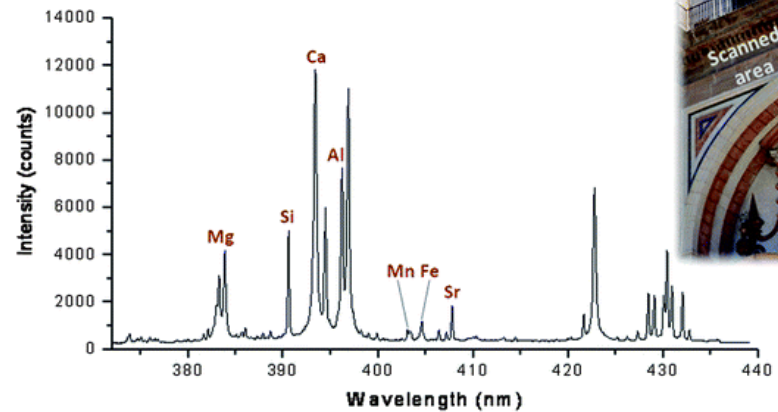
Fig. 6. Evolution of LIBS spectrum with the number of pulses during the removal of black paint on wood: (a) pulse 1, (b) pulse 2, (c) pulse 4, (d) pulse 7 and (e) pulse 9. Irradiation wavelength: 308 nm.

Stand-off LIBS



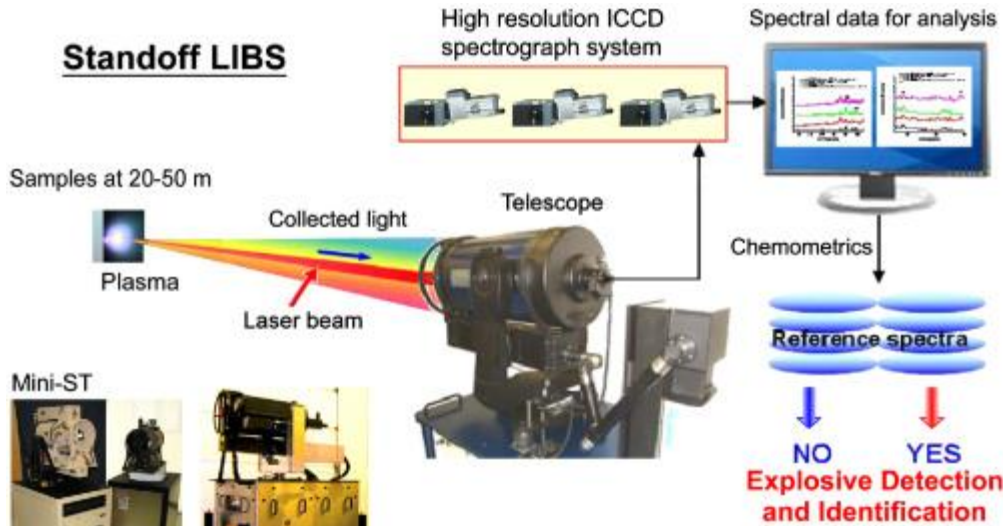
Malaga

Analýza portálu katedrály.



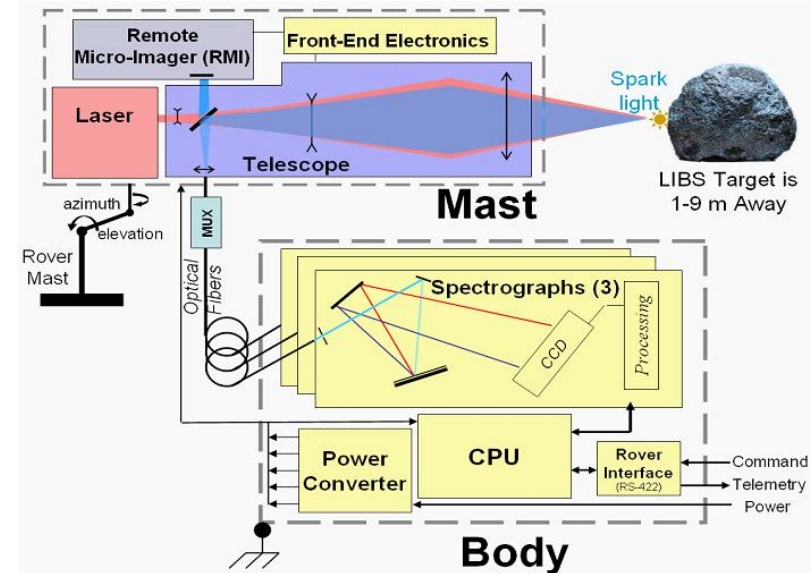
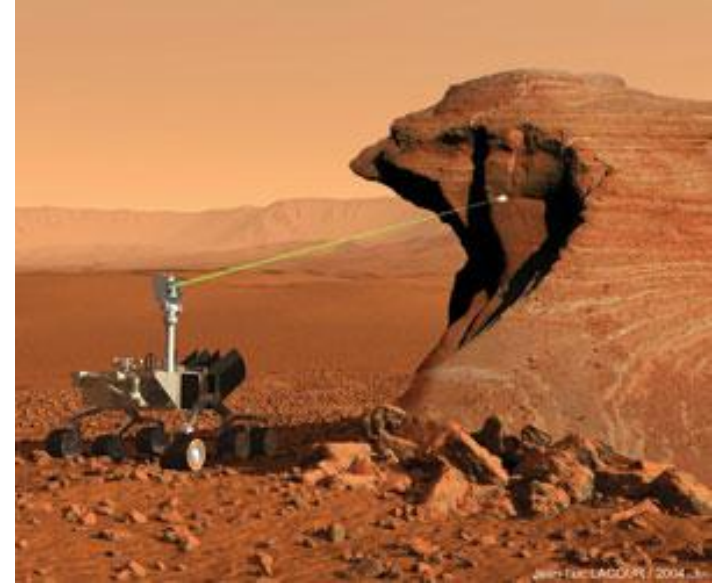
Stand-off LIBS

Standoff LIBS



LIBS data are compared to a library of reference spectra for identification of unknown samples

ChemCam



Spektrometrie laserem indukovaného plazmatu (LIBS)

Terénní a mobilní zařízení



remote LIBS

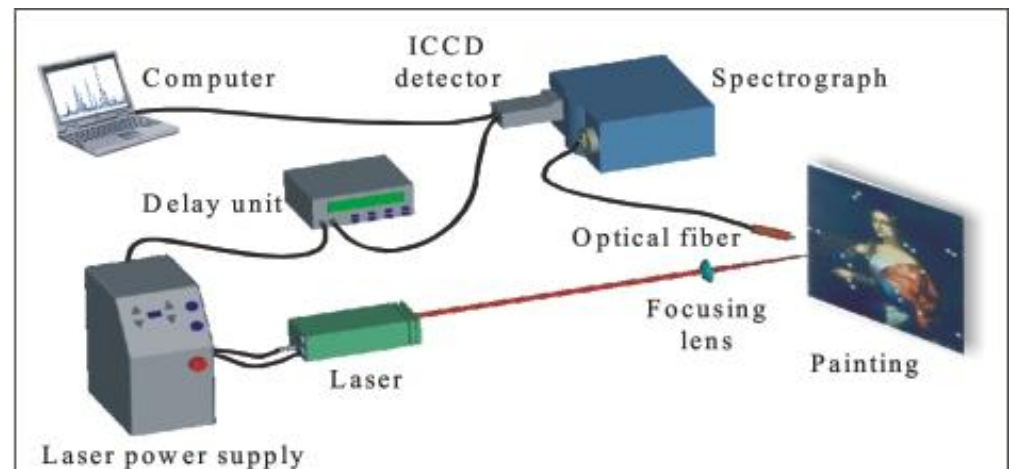
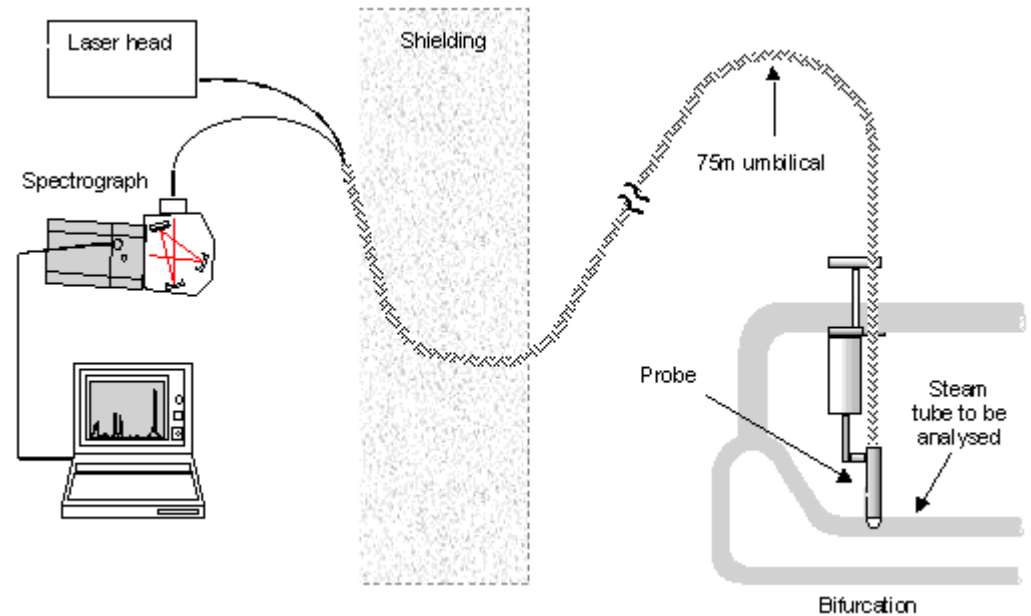
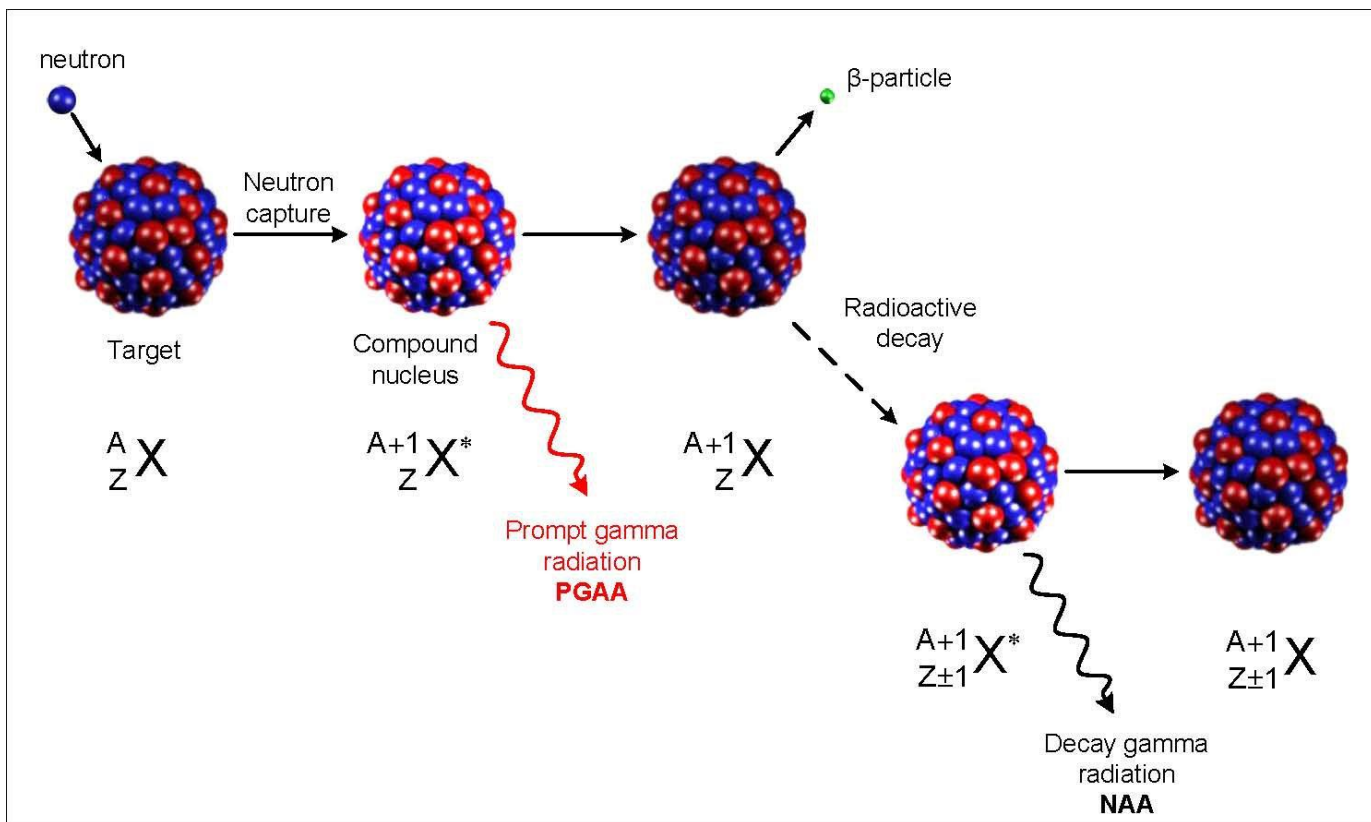


Fig.4.2.2: Typical experimental set-up for LIBS analysis.

© Giakoumaki et al., in: "Handbook on the Use of Lasers in Conservation and Conservation Science", 2008.

Neutronová aktivační analýza



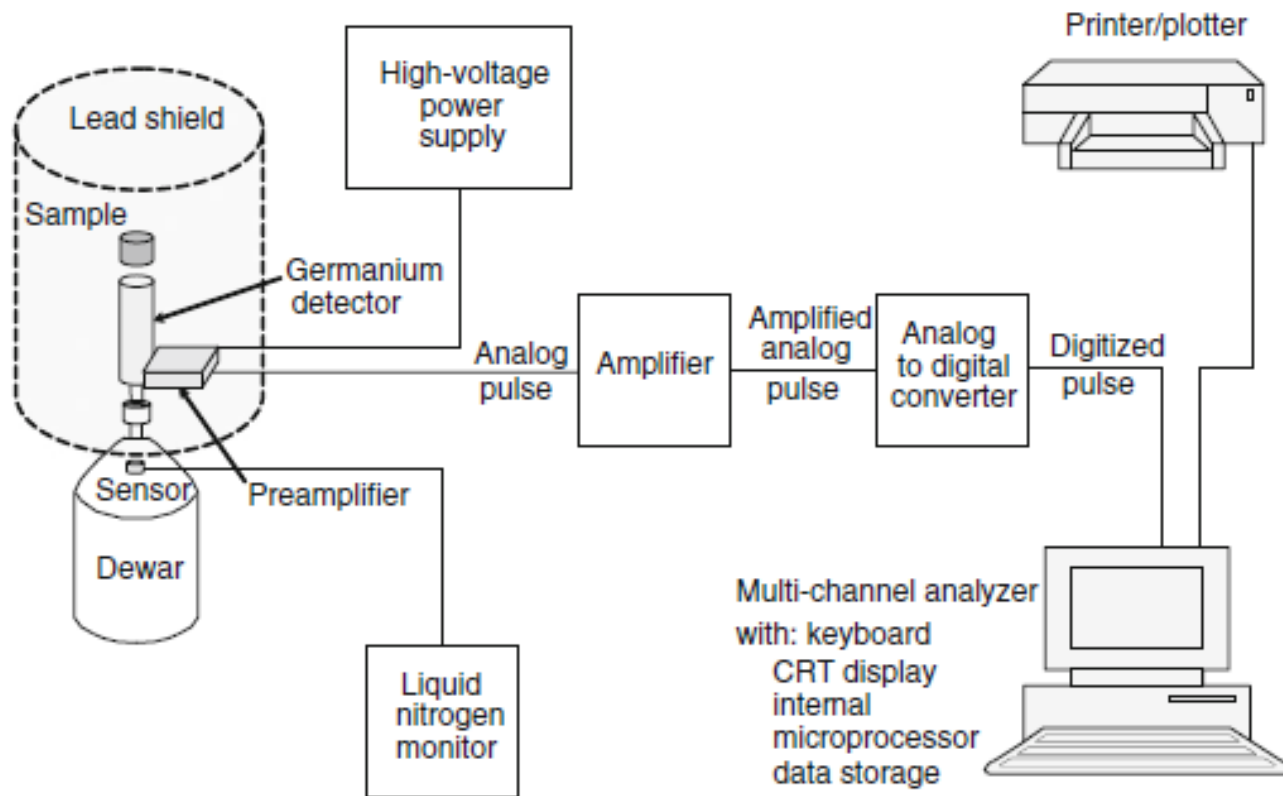


Fig. 32.1 Germanium–lithium detector (From SKOOG. Principles of Instrumental Analysis, 5E. © 1998 Brooks/Cole, a part of Cengage Learning, Inc. Reproduced by permission. www.cengage.com/permissions)

Rentgenová fluorescenční analýza (XRF)

Rentgenová

Radionuklidová

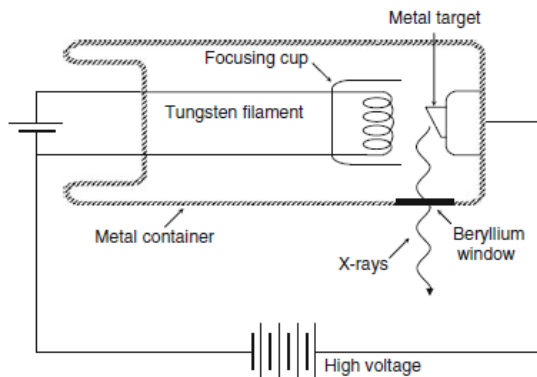
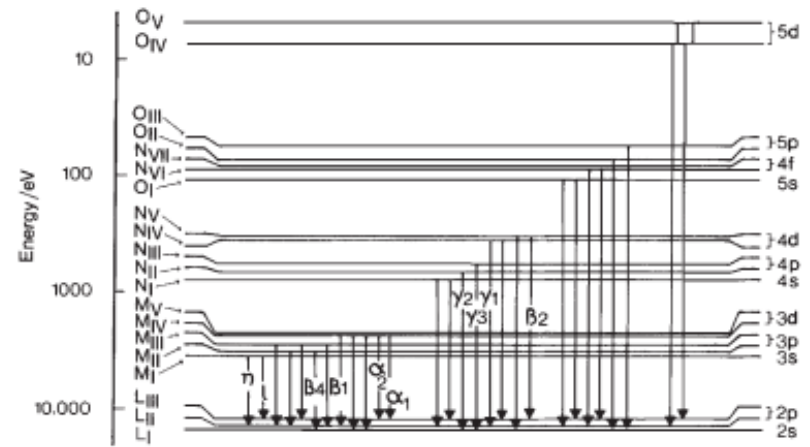
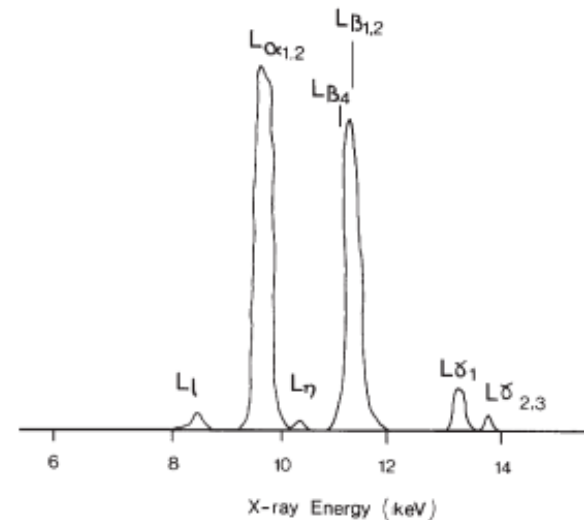


Fig. 37.1 X-ray tube ("Fundamentals of Physics", Second Edition Extended, David Halliday and Robert Resnick, copyright 1981, Reproduced with permission of John Wiley & Sons, Inc.)



a



b

Figure 2.8 Electronic transitions giving rise to the L spectrum of gold. The L spectrum is considerably more complicated with three main lines normally resolved as shown in the accompanying spectrum – L_{α} (arising from two transitions), L_{β} (with up to 17 contributing transitions) and L_{γ} (up to 8 transitions), plus a number of 'forbidden' transitions. (After Jenkins, 1974; Fig. 2-11. © John Wiley & Sons Limited. Reproduced with permission.)

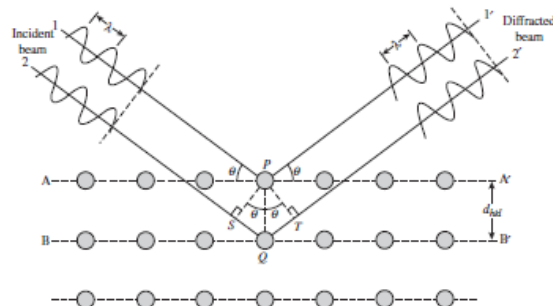


Figure 2.6 Bragg diffraction by crystal planes. The path difference between beams 1 and 2 is $SQ + QT = 2 PQ \sin \theta$. (Reproduced with permission from W.J. Callister Jr., *Materials Science and Engineering: An Introduction*, 7th ed., John Wiley & Sons Inc., New York. © 2006 John Wiley & Sons Inc.)

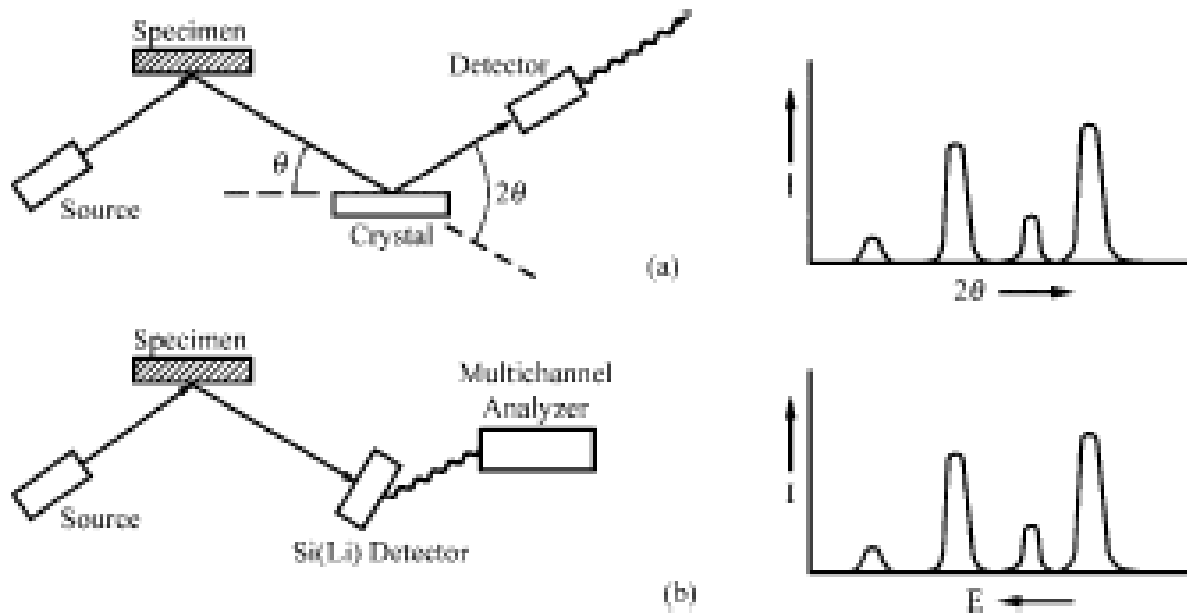
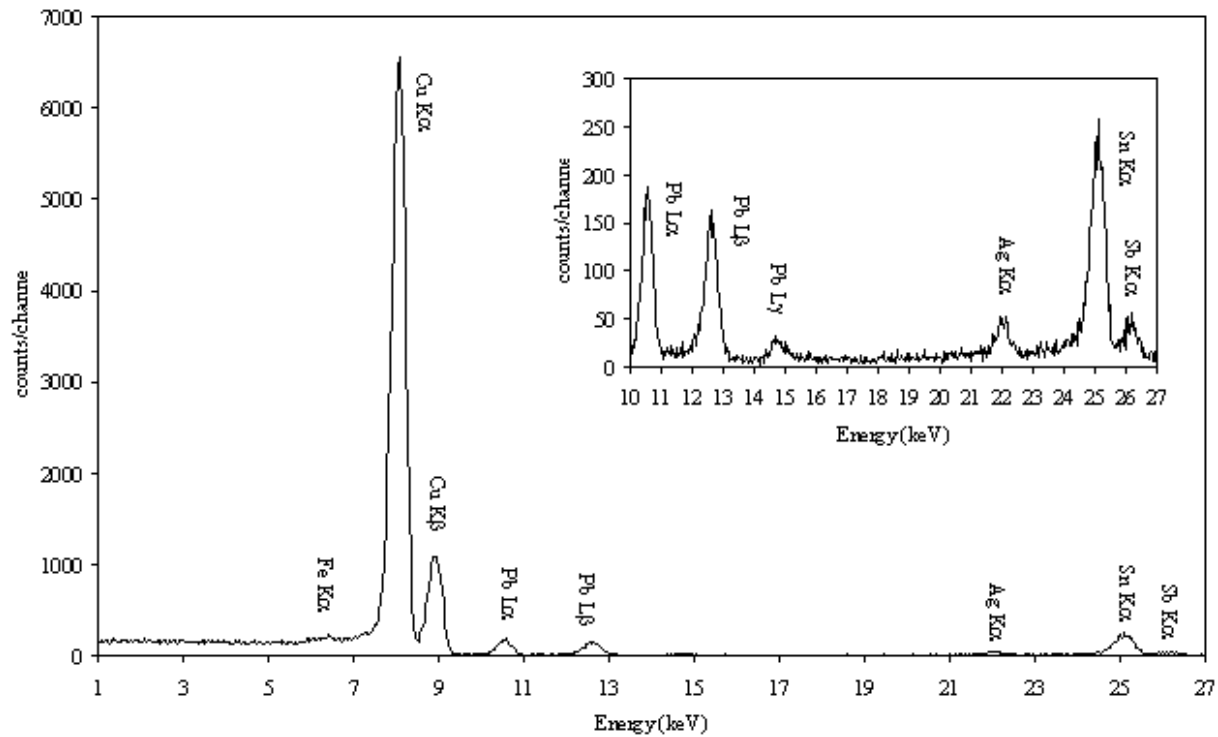
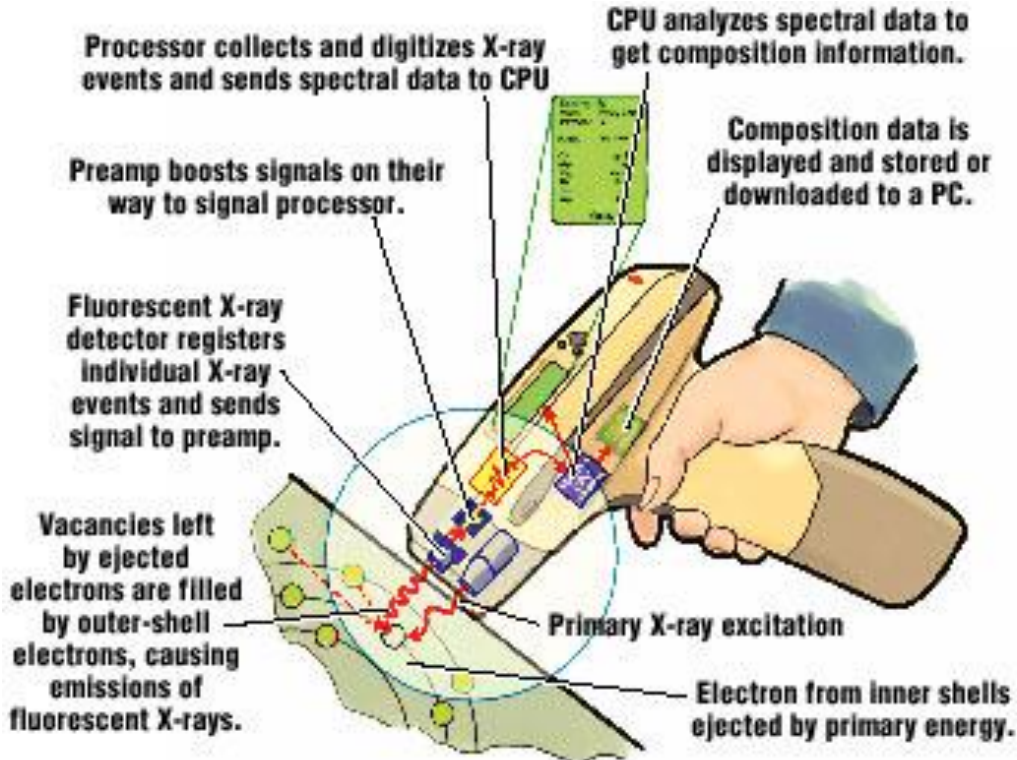


Figure 6.6 Main components and dispersive spectra of: (a) WDS; and (b) EDS.



Benvenuto Cellini's Bronze statue of Perseus during its restoration in June, 1998 at the Uffizi Museum in Florence

Portable X-Ray Fluorescence (PXRF)



Elektronová mikrosonda

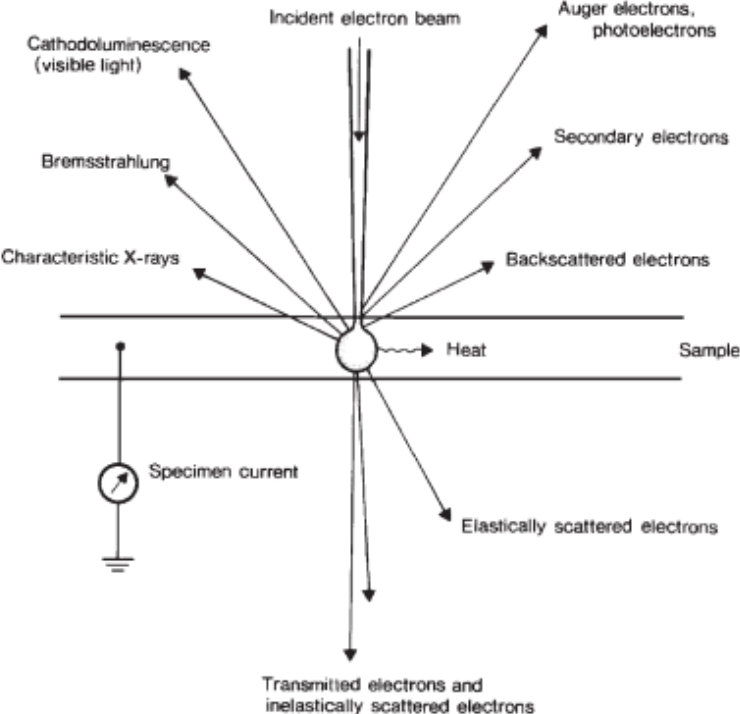


Figure 2.12 Interaction of primary electrons with a thin solid sample, showing the various processes which can take place. (After Woldseth, 1973; Fig. 4-1.)

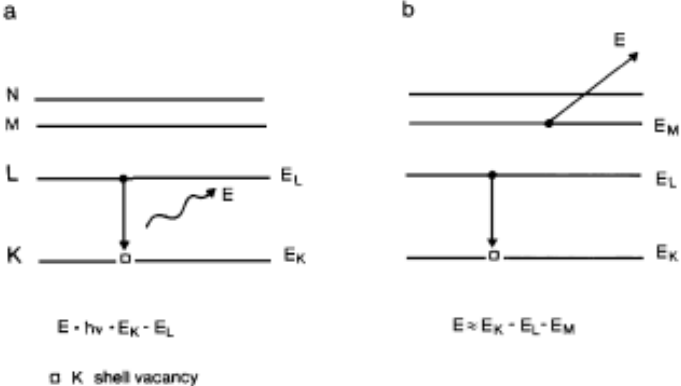


Figure 2.6 The X-ray emission and Auger processes. An inner vacancy in the K shell de-excites via one of two competing processes – (a) X-ray emission, in which an L electron drops down and the excess energy is carried away by an X-ray photon, or (b) the Auger process, in which an L electron drops down, but the excess energy is carried away by a third electron – in this case from the M shell.

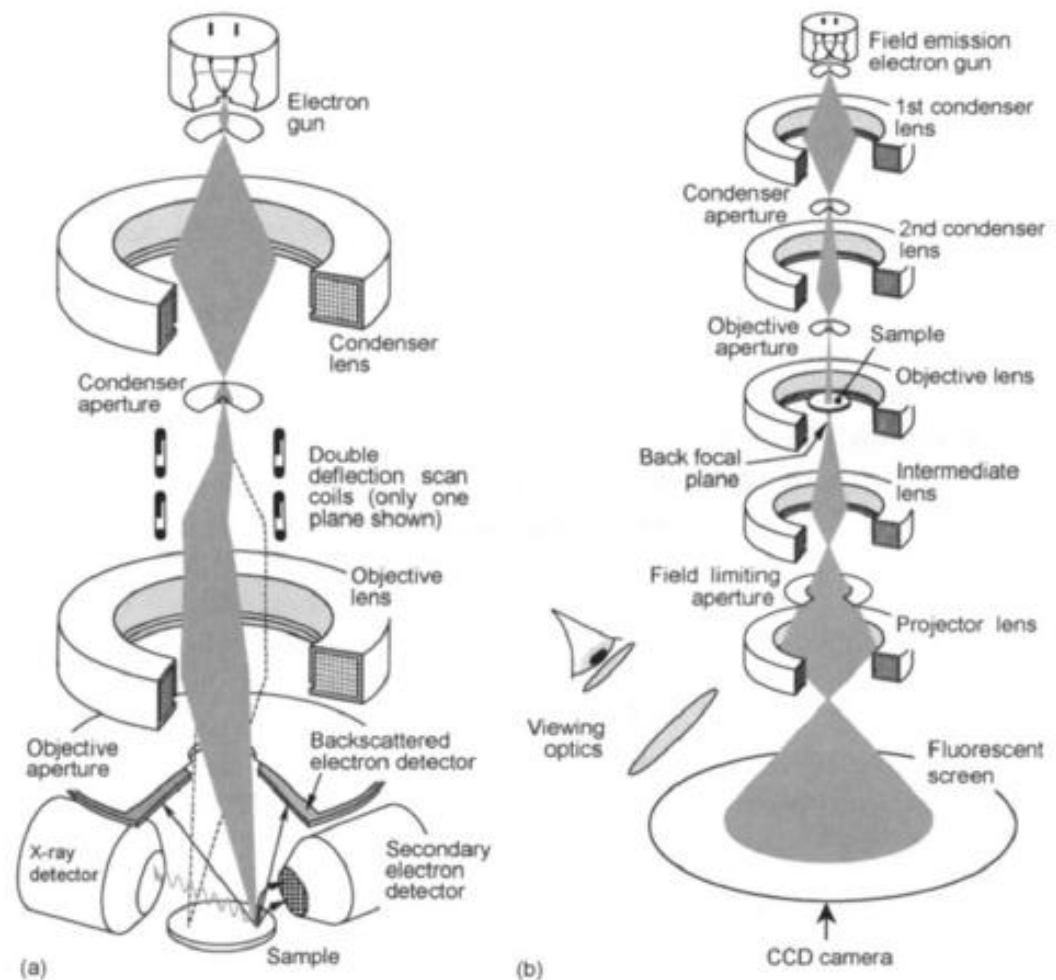


Fig. 3.1. General types of electron microscope. (a) Scanning electron microscope (SEM); (b) transmission electron microscope (TEM).

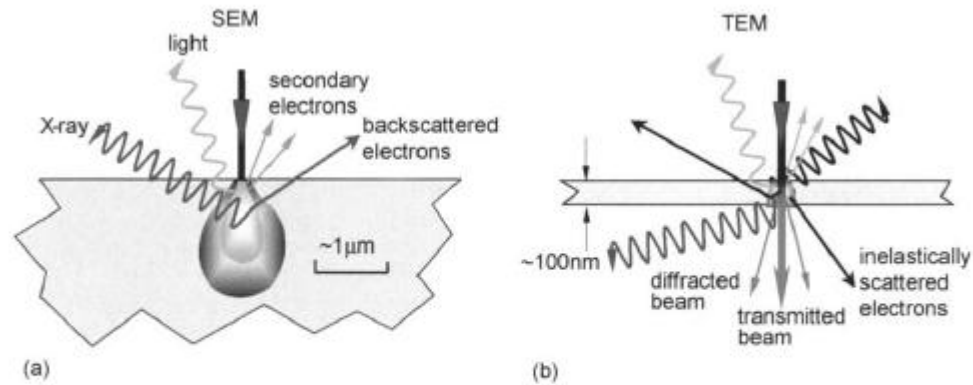


Fig. 3.2. Interaction of electrons with a solid showing effects of interaction volume.
 (a) SEM sample; (b) sample thinned for TEM.

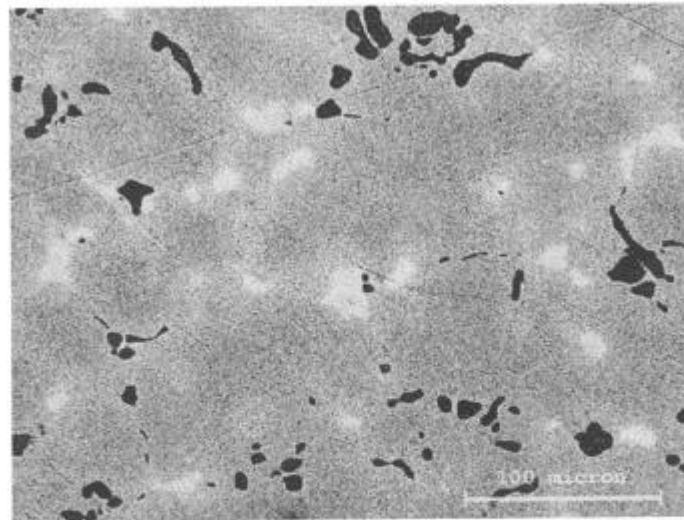


Fig. 3.25. BSE image of a copper-arsenic alloy. The alpha phase is composed of regular grains, containing 3% As. Along the grain boundaries Cu_3As intermetallics, with an As concentration up to 28% (bright phase), are present next to copper sulphide inclusions (dark phase). Magnification 400 [67]. Reproduced with permission from TMS Publications.



Fig. 1. Photograph of the coin of post-Roman Empire examined in this study. Its diameter was approximately 15 mm.

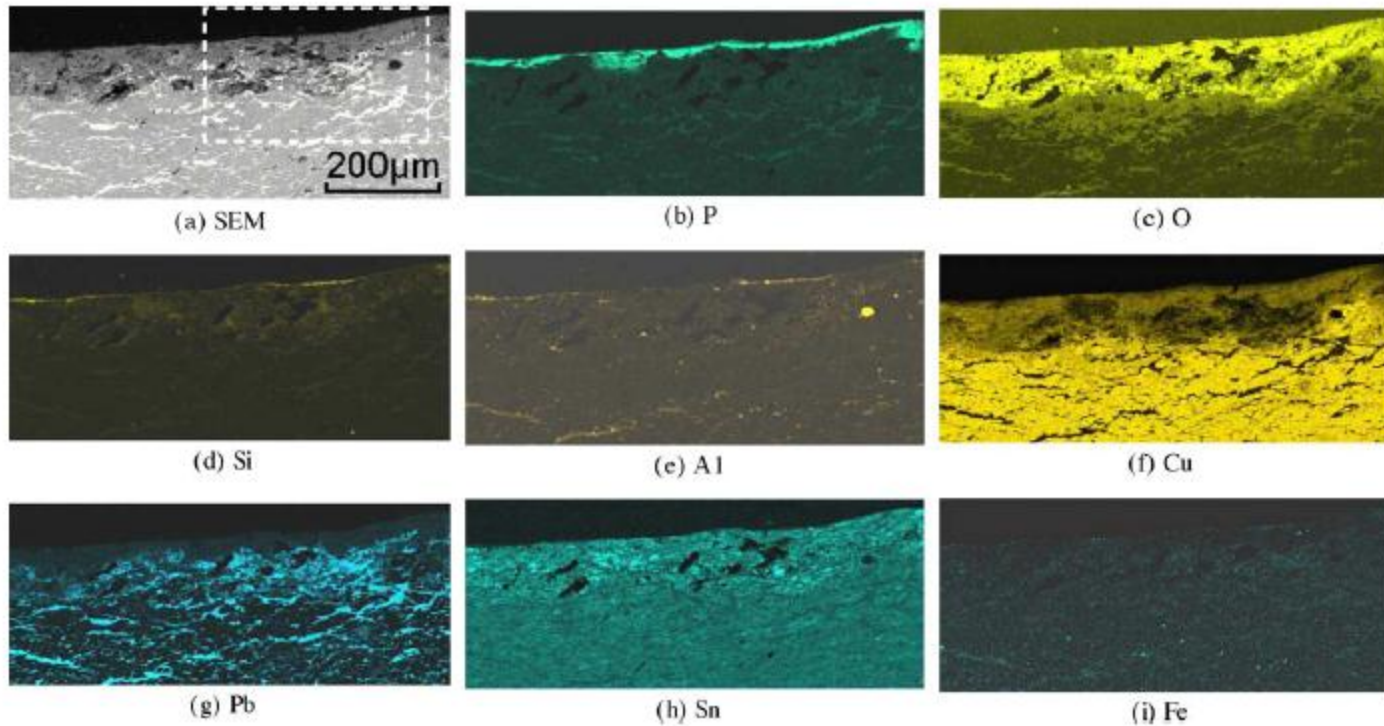
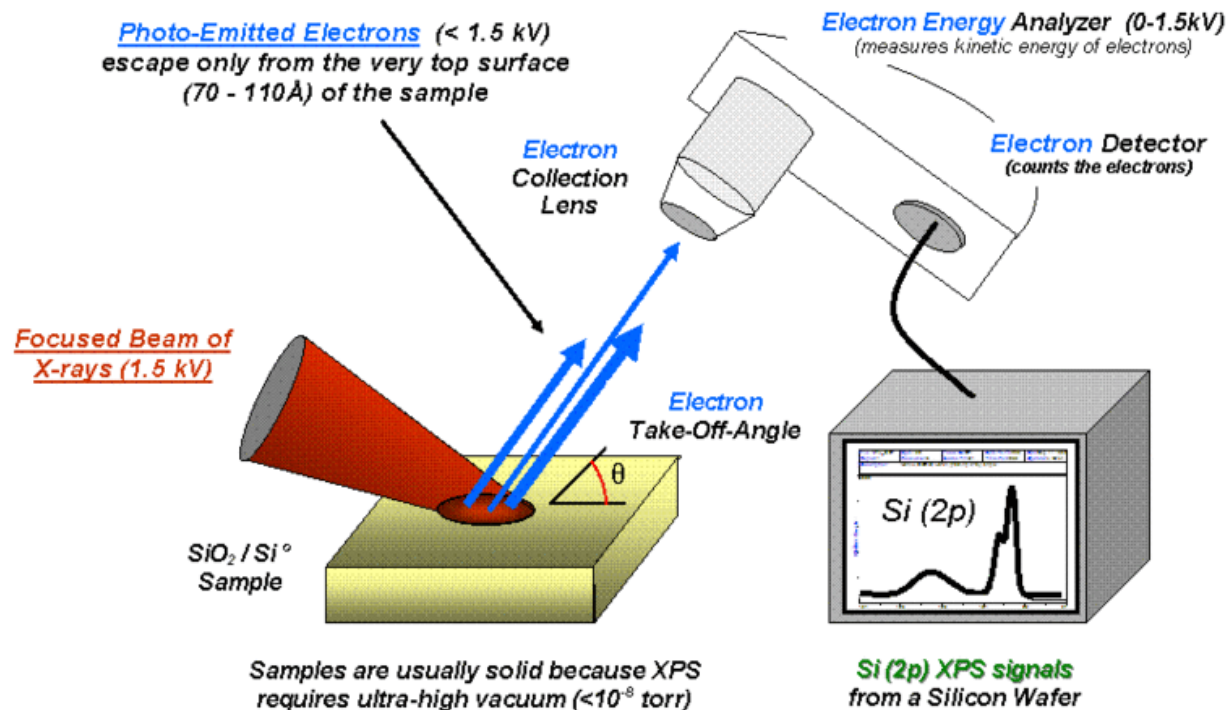


Fig. 2. SEM picture (a) and EDS analyses (b–i) of the cross-section of the post-Roman bronze coin. The dashed rectangle in (a) corresponds to the area where EDS analyses were performed (cf. Fig. 3).

Fotoelektronová spektroskopie (ESCA)



Ultrafialová (UPS) Rentgenová (XPS)

Sledování kinetické energie fotoelektronů,
Ta závisí na energii molekulového orbitalu.

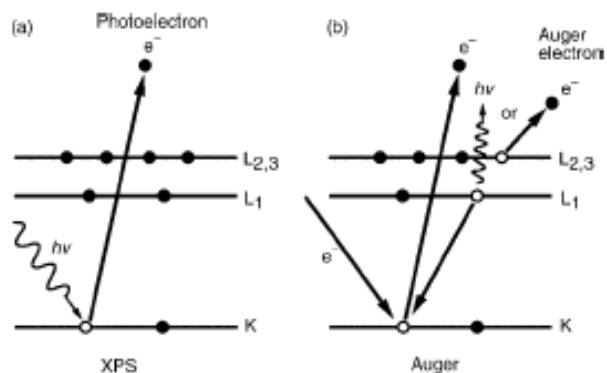


Figure 7.1 Emission processes of characteristic electrons: (a) a 1s photoelectron; and (b) a $KL_1L_{2,3}$ Auger electron

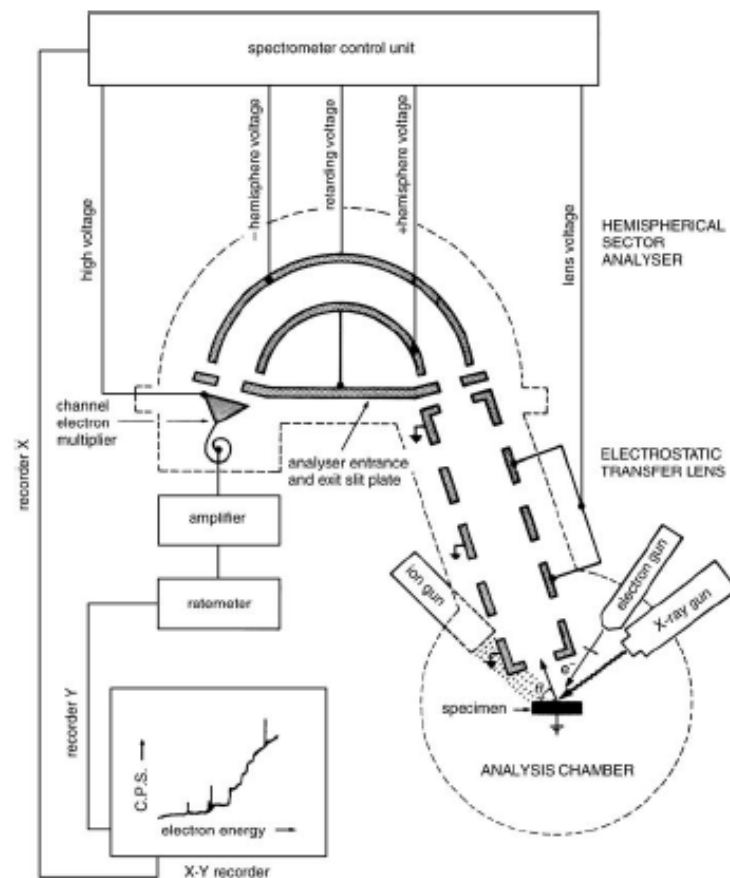
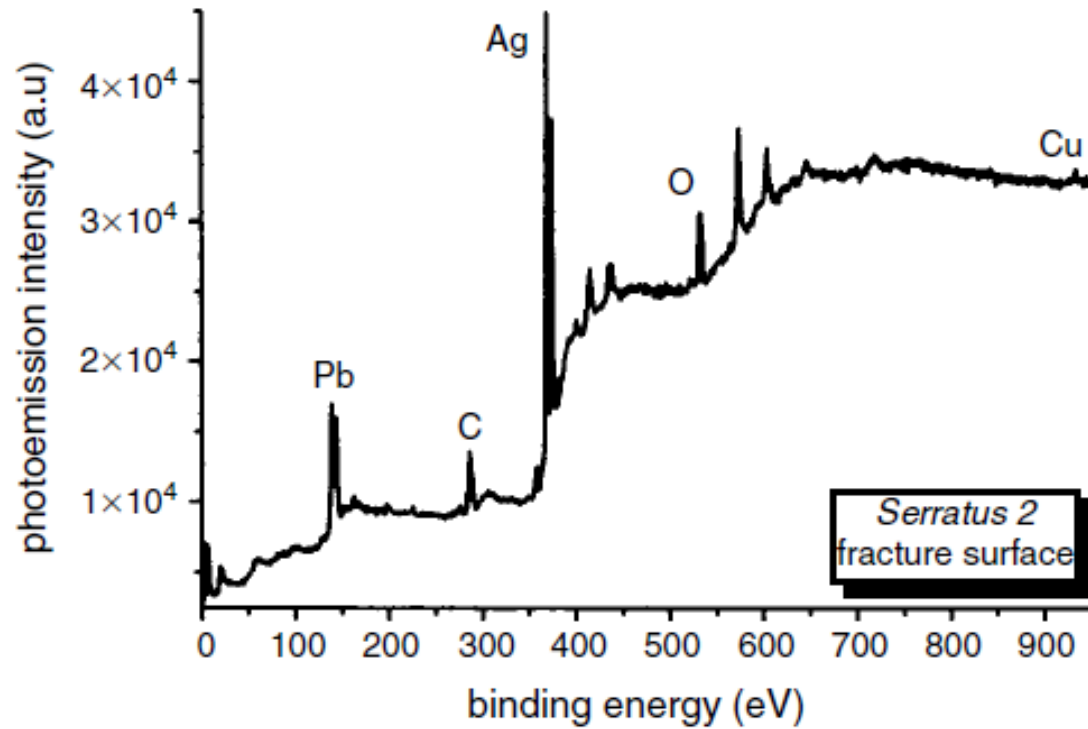


Figure 7.5 Structure of an electron spectrometer. (Reproduced with permission from J.F. Watts, *An Introduction to Surface Analysis by Electron Spectroscopy*, Oxford University Press, Oxford. © 1990 Royal Microscopy Society.)

Serratus – římská republikánská mince



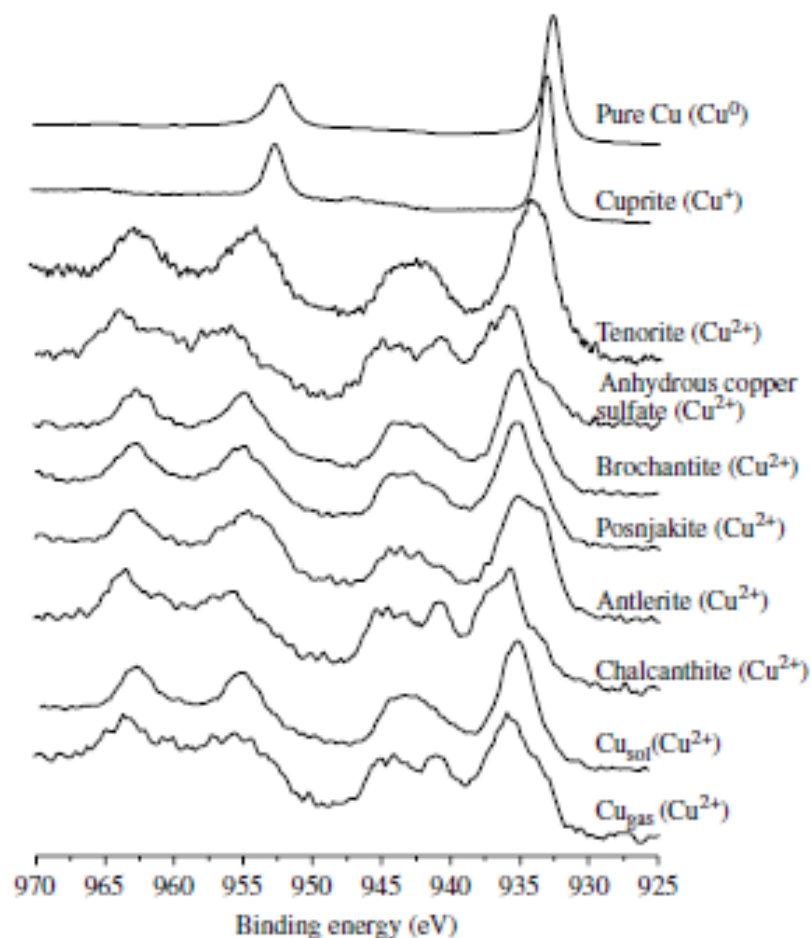


Figure 1. Normalized Cu 2p regions of the different compounds. From top to bottom: copper, cuprite, tenorite, anhydrous copper sulfate, brochantite, posnjakite, antlerite, chalcantite, artificial weathering in solution at 20 °C, artificial weathering in SO_2 atmosphere.

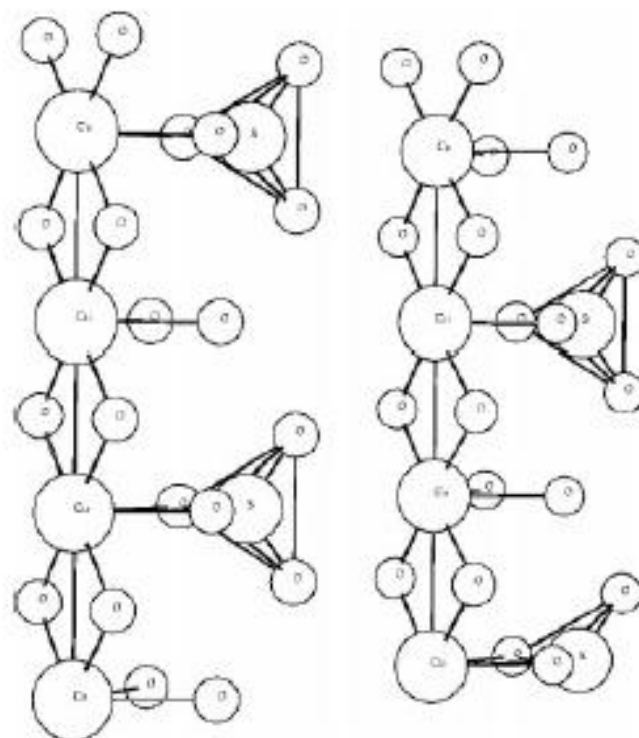


Figure 2. Structure of brochantite, realized with the software XMAKEMOL, using data from Ref. 8.

PIXE a PIGE

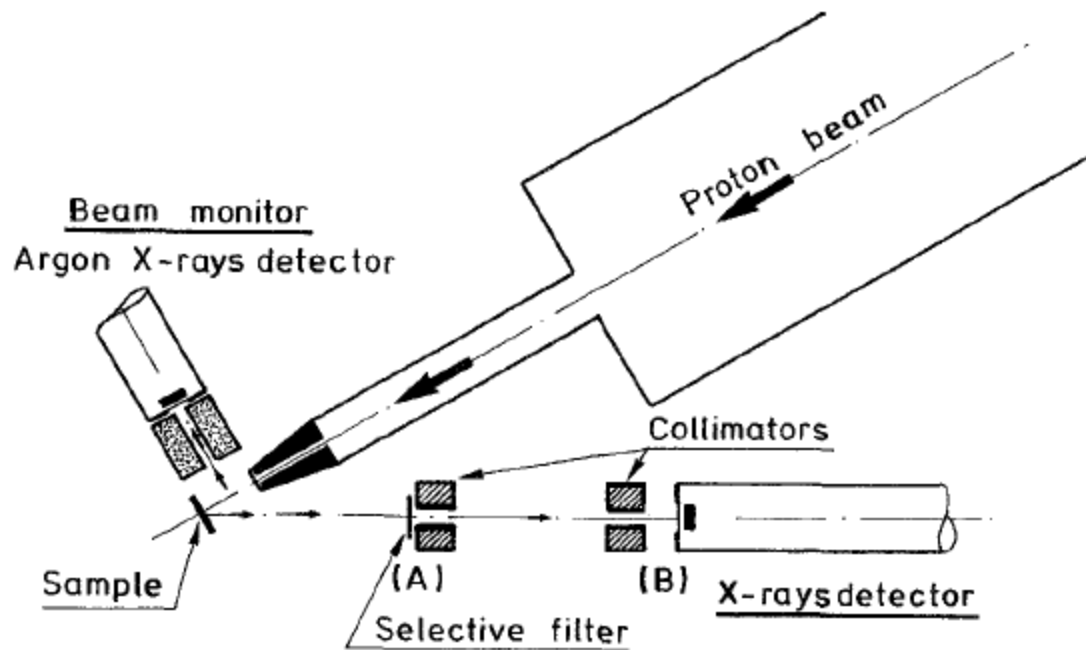


Fig. 11.1. The non-vacuum PIXE set-up used at LARN.

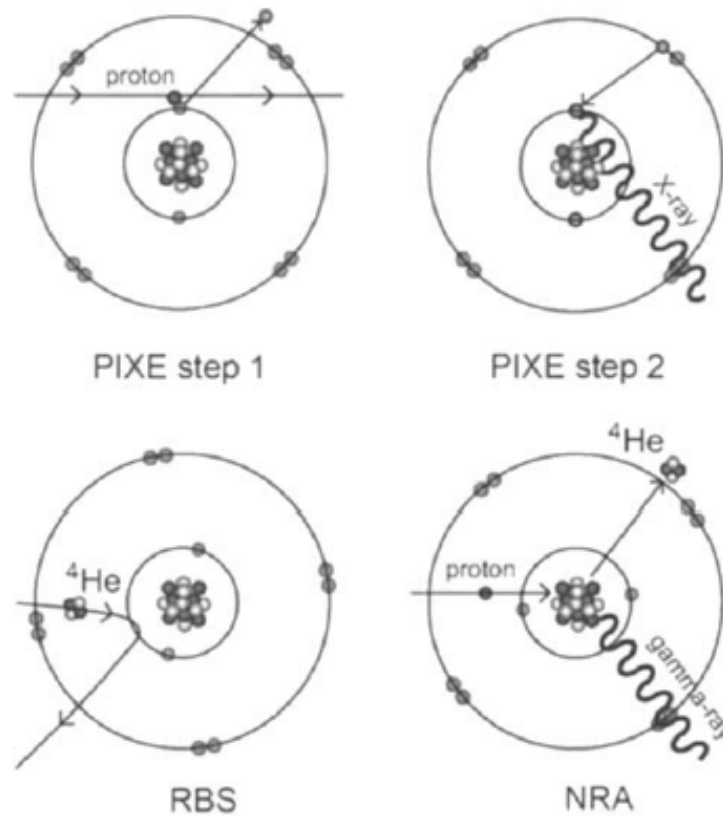


Fig. 5.1. Physical principles of IBA techniques. Particle-induced X-ray emission (PIXE) is a two-step process: an inner-shell electron of the target atom is expelled by the impinging ion, then follows an electronic rearrangement accompanied by X-ray emission. Rutherford backscattering spectrometry (RBS) relies on a purely elastic process based upon the electrostatic repulsion between positively charged projectile and target nuclei. NRA occurs when the projectile and the target nuclei come close enough to undergo a nuclear reaction with emission of characteristic photons or charged particles.

Akrotiri Řecko

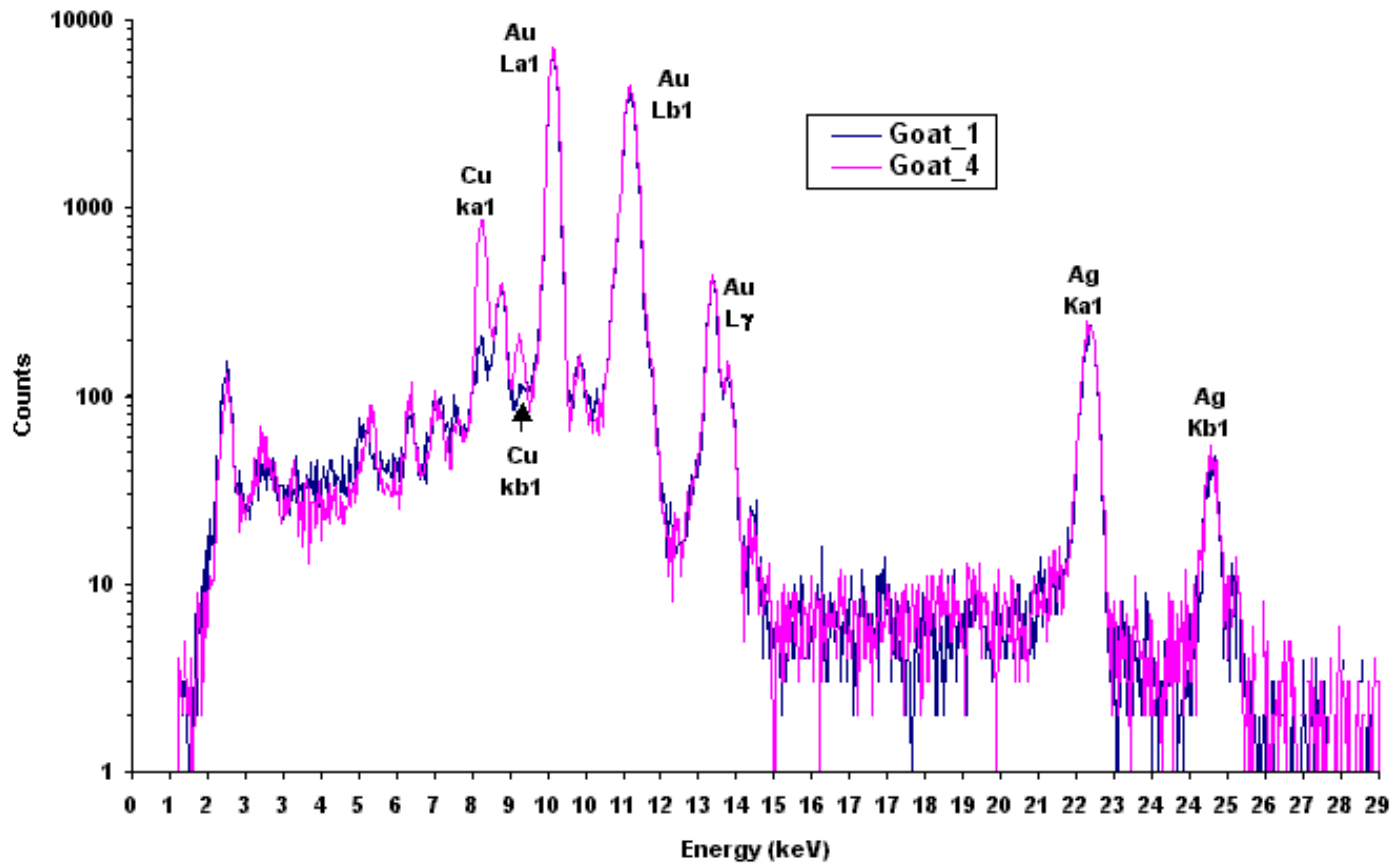




Figure 2 - Koson gold coin (Dacian stater)

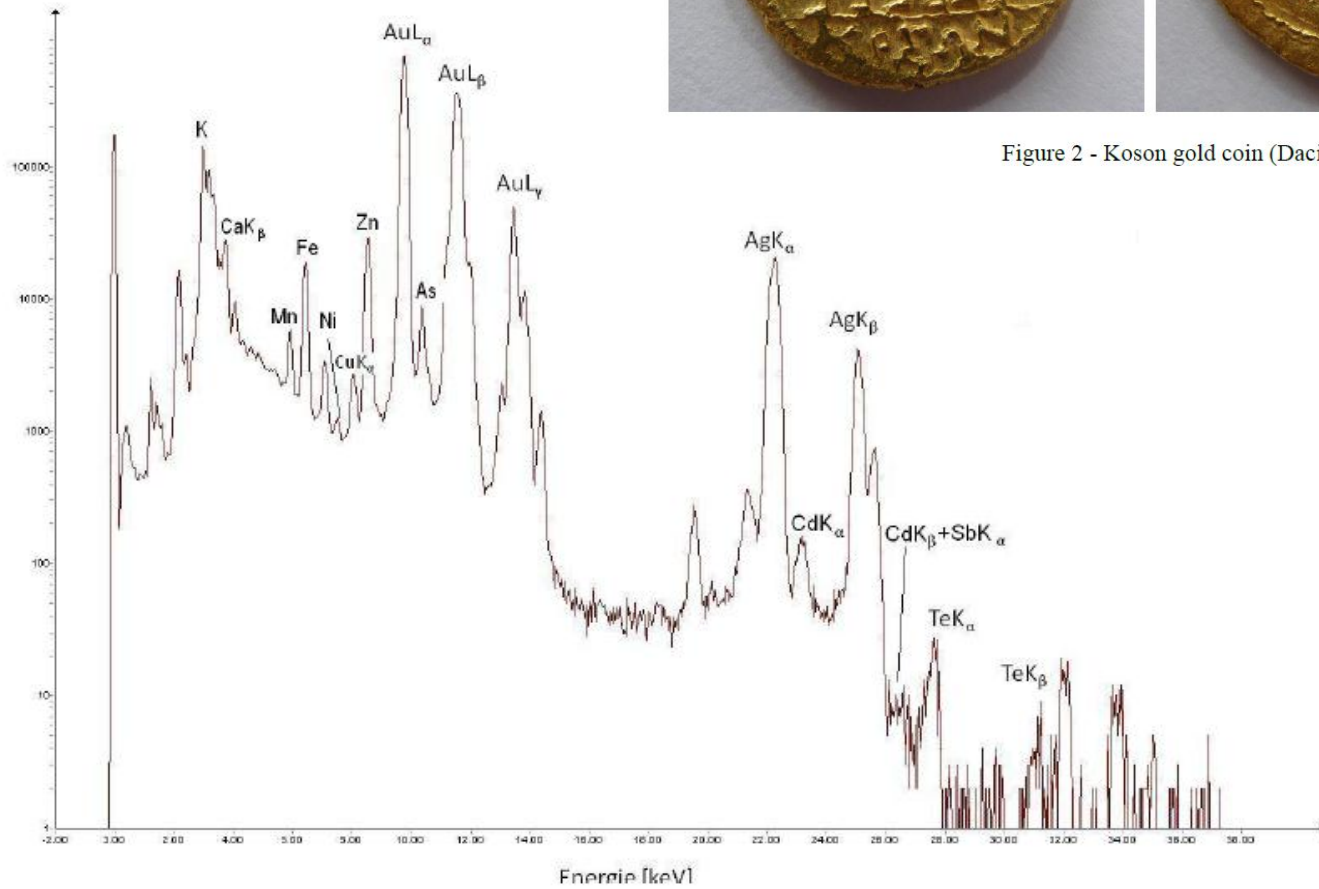


Figure 4 - Micro-PIXE spectrum – native gold sample - Cavnic

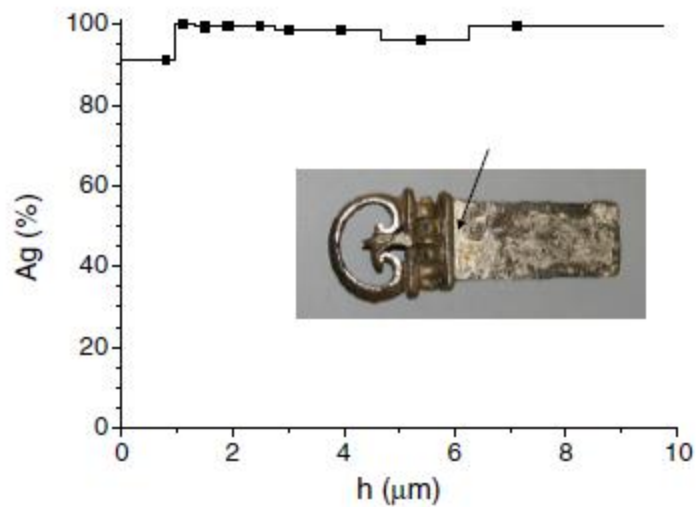


Fig. 4. Silver layer on the Roman belt buckle made of brass.

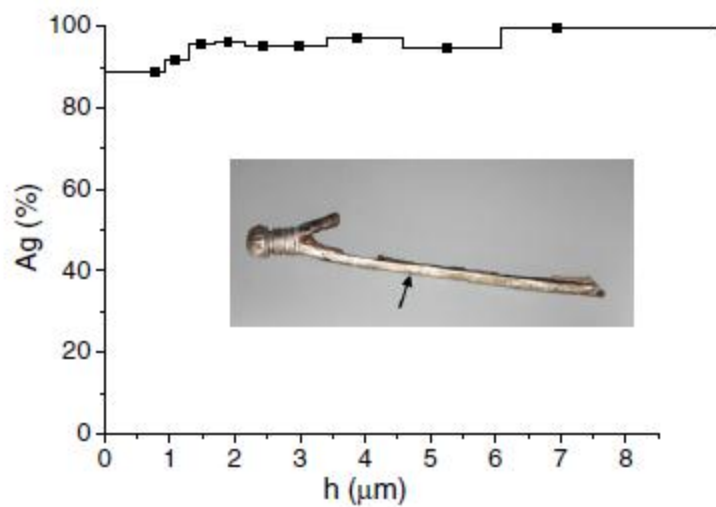


Fig. 5. Silver layer of the iron scabbard border.

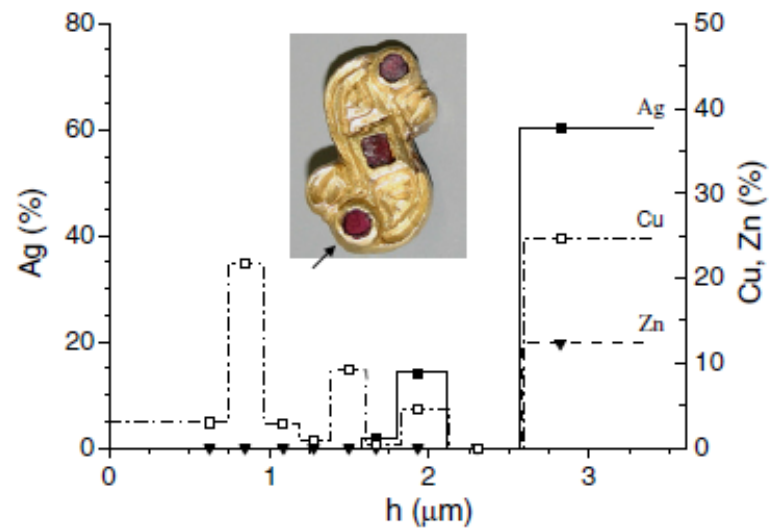
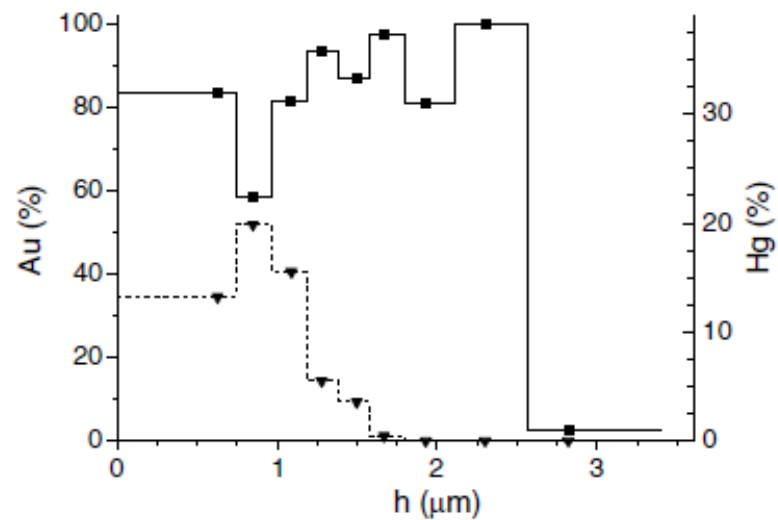


Fig. 6. Gilding layer on the S-type brooch.

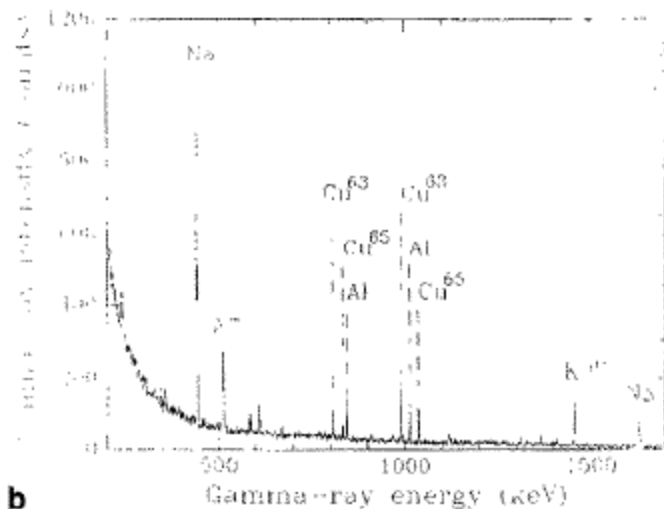
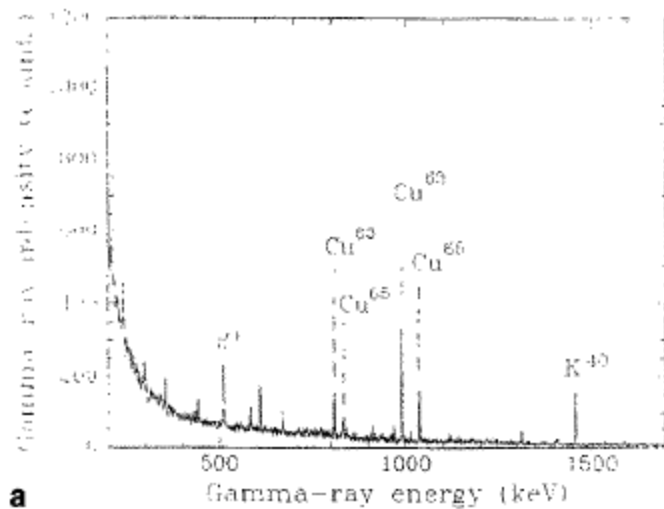


Fig. 6. 2.5 MeV PIGE spectrum of the sheet from Santa Flora (Teruel): (a) bulk and (b) patina. Spectrum (b) was obtained simultaneously with the RBS spectrum of Fig. 4(b).



2. Schematic drawings of the archaeological bronzes: (1) from Castrelin de Paluezas (León), (2) perforated sheet from Castrelin de Paluezas (León), and (3) sheet from Santa Flora (Teruel).

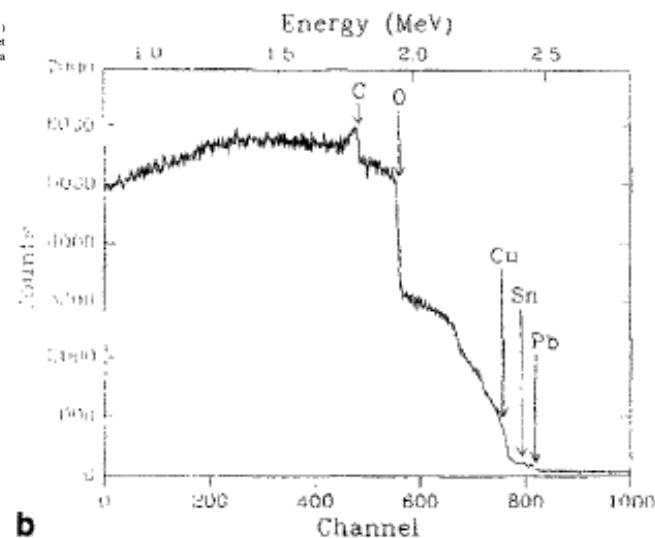
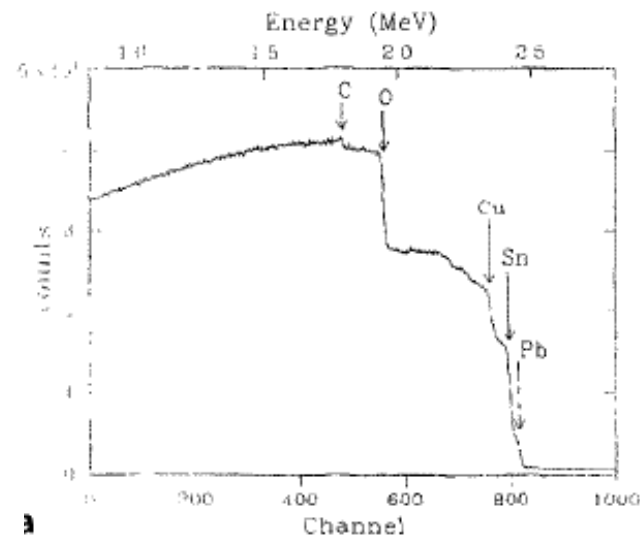


Fig. 4. 2.5 MeV RBS spectrum from a patina covered region of (a) the perforated sheet from Castrelin de San Juan de Paluezas (León), and (b) sheet from Santa Flora (Teruel).

Secondary Ion Mass Spectrometry

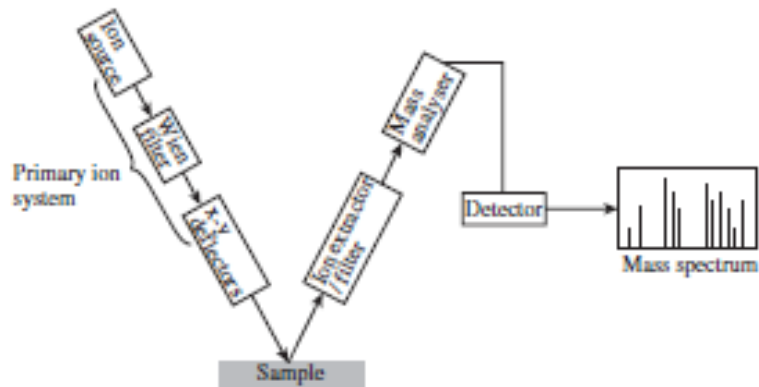


Figure 8.5 SIMS instrumentation.

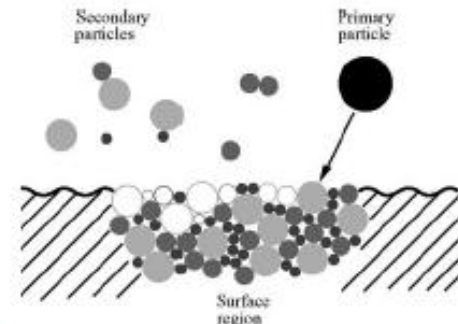


Figure 8.1 Secondary particle generation by an energetic primary particle.

Ar⁺
Xe⁺

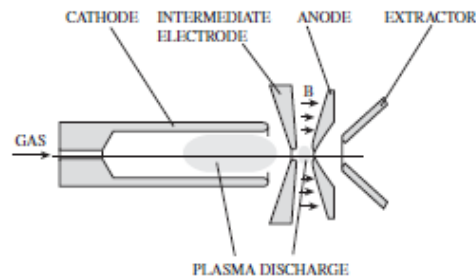


Figure 8.7 Duoplasmatron ion source. The magnetic field marked **B** intensifies the plasma by confining electrons close to the axis. (Reproduced with permission from J.C. Vickerman and D. Briggs, *ToF-SIMS Surface Analysis by Mass Spectrometry*, IM Publications and SurfaceSpectra, Chichester and Manchester. © 2001 IM Publications.)

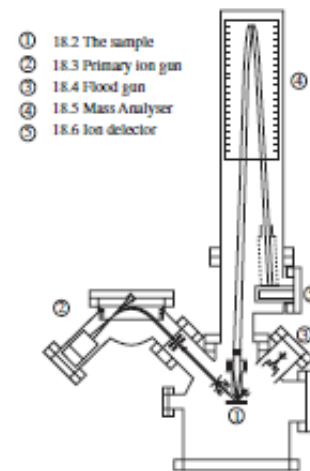


Figure 8.13 Time-of-flight SIMS instrumentation. (Reproduced with permission from J.C. Vickerman and D. Briggs, *ToF-SIMS Surface Analysis by Mass Spectrometry*, IM Publications and SurfaceSpectra, Chichester and Manchester. © 2001 IM Publications.)

Tell Beydar (Izrael)

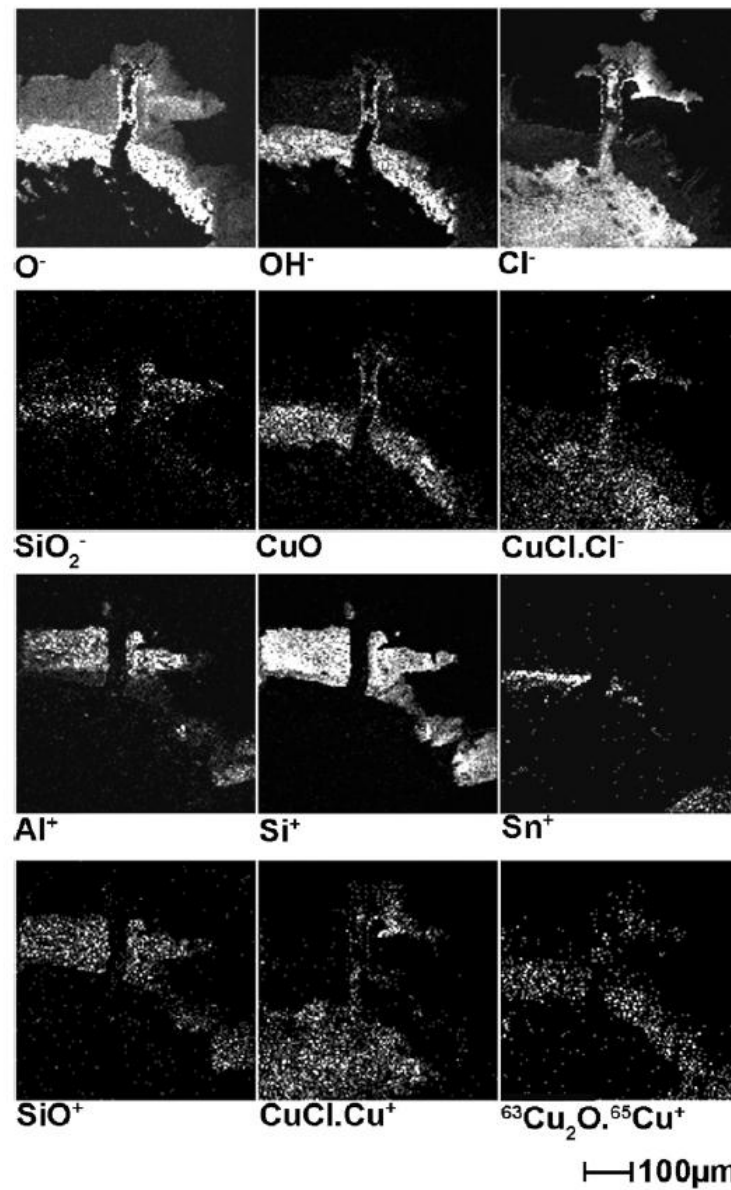
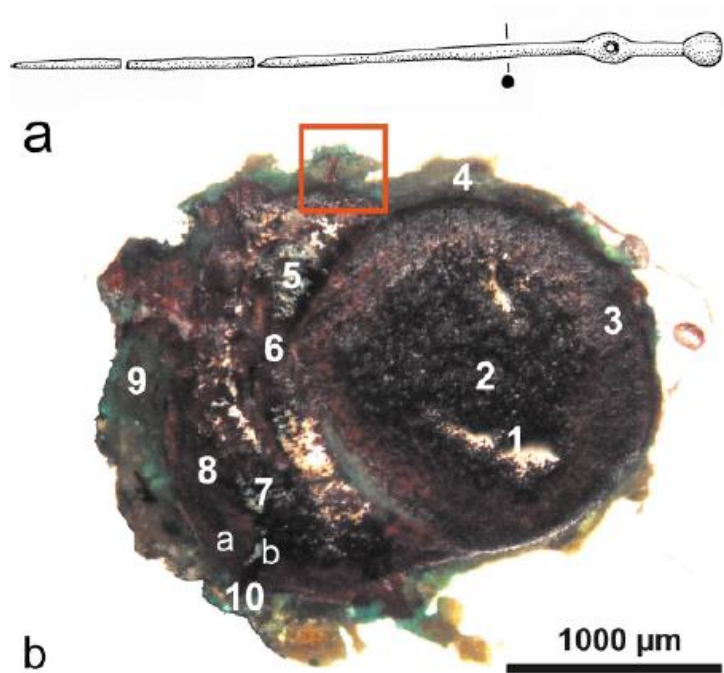
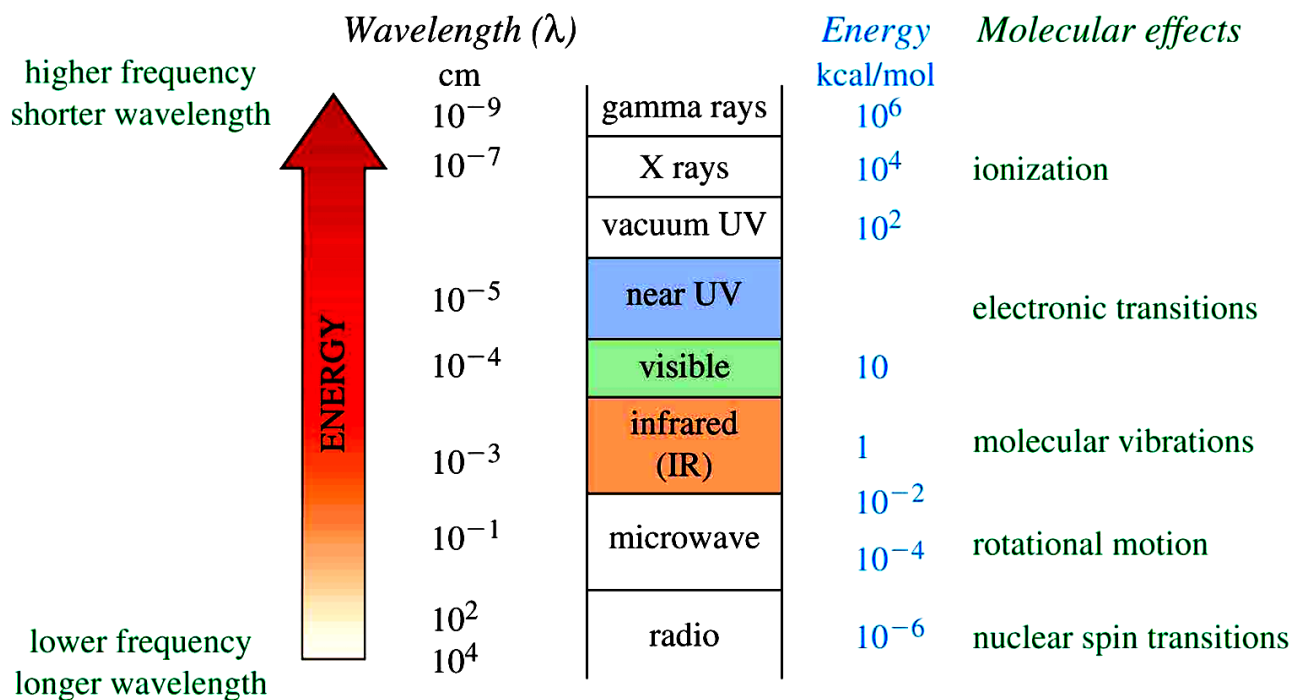
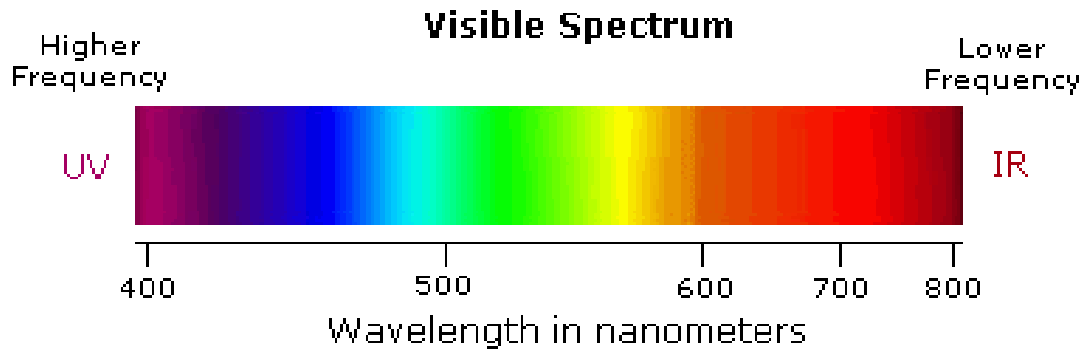


Fig. 3 Ion images of sample B18 obtained with TOF-SIMS. The area of analysis is indicated by the square in Fig. 1b

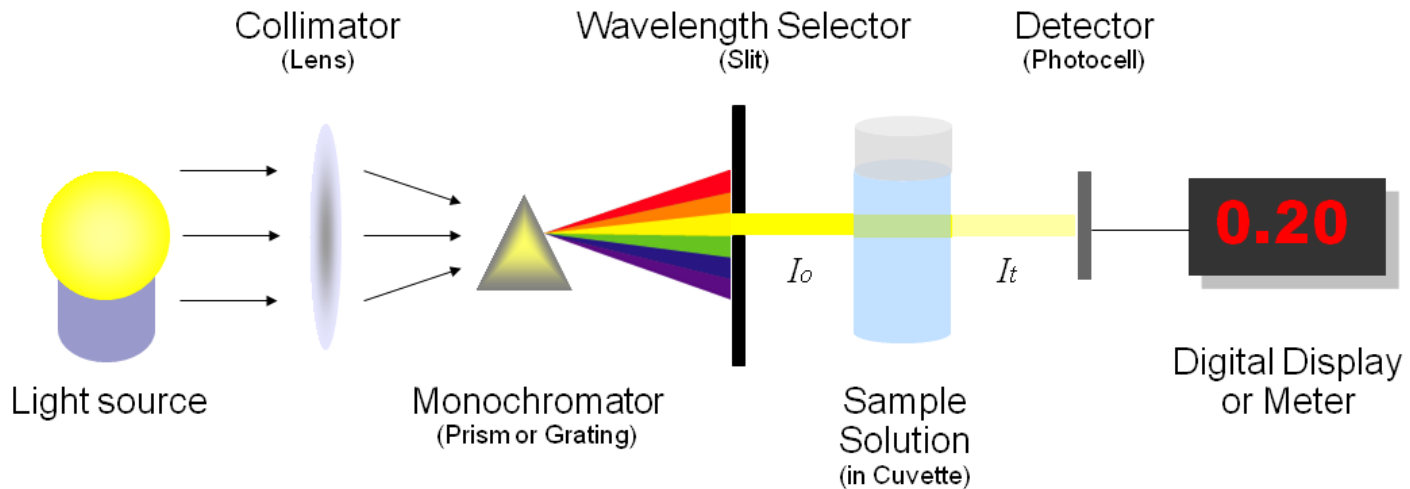
Molekulová spektrometrie



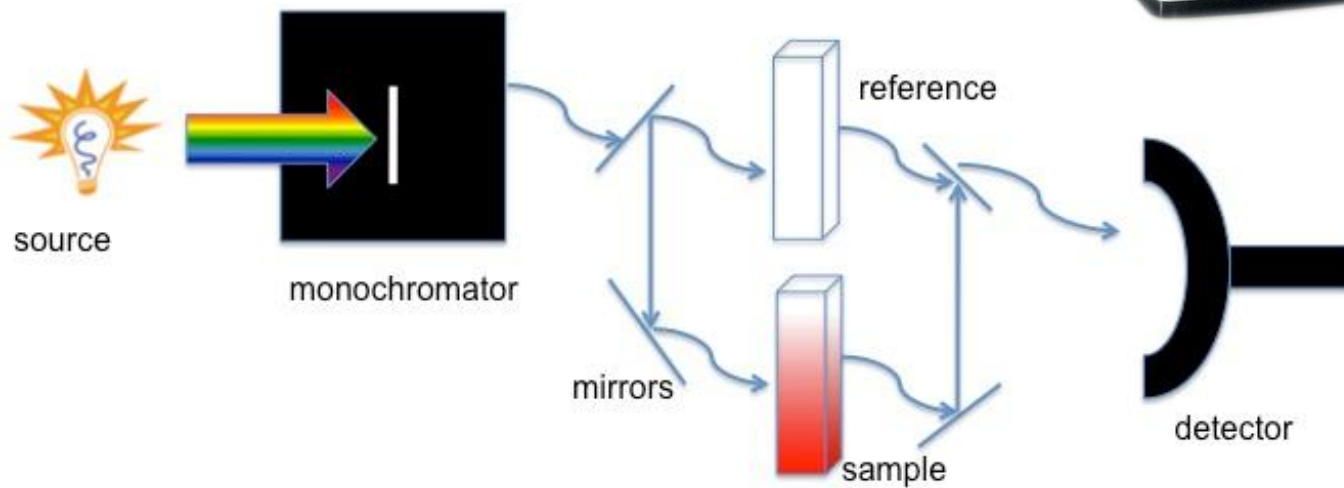
UV-VIS spektrometrie



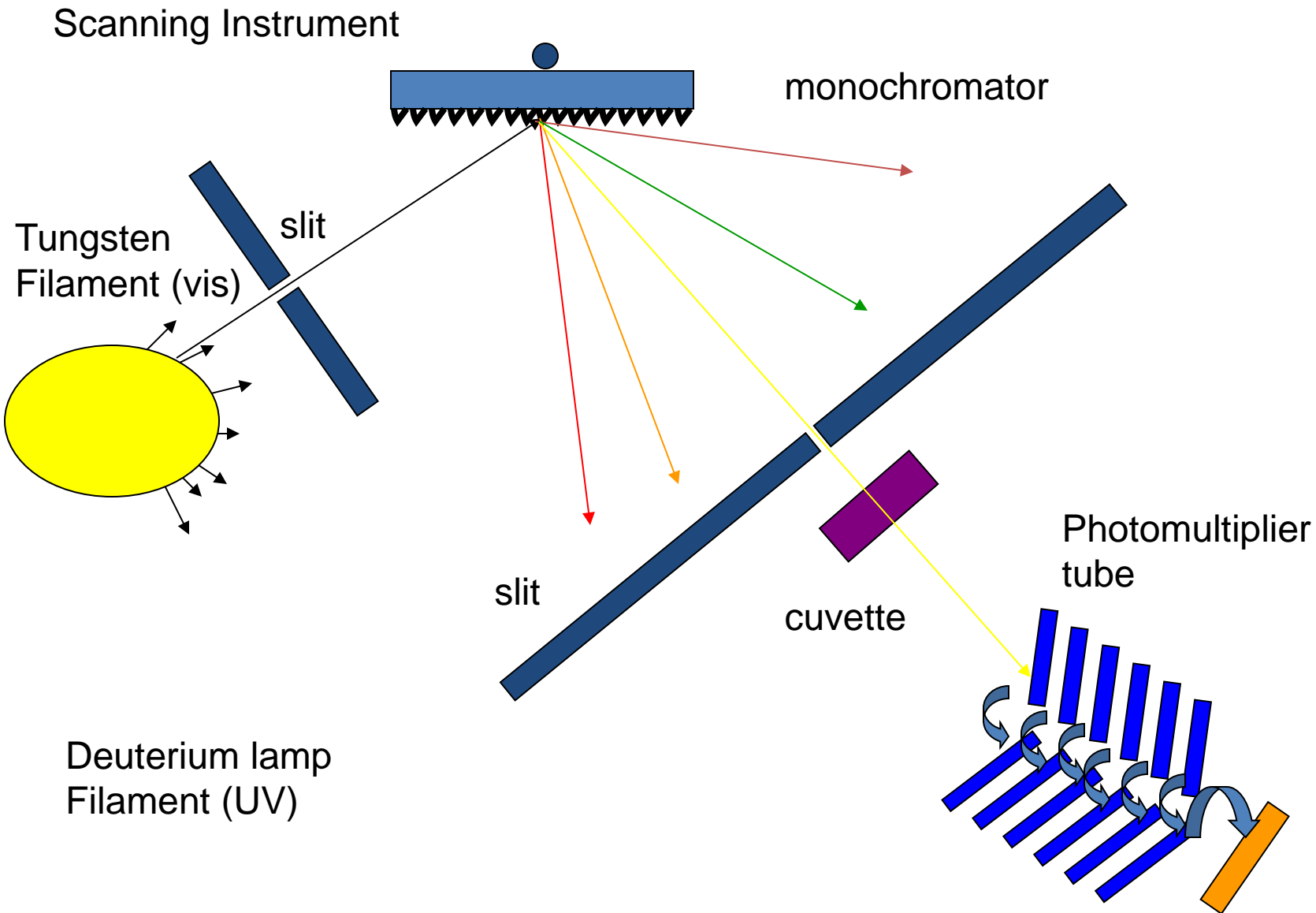
- Violet:** 400 - 420 nm
- Indigo:** 420 - 440 nm
- Blue:** 440 - 490 nm
- Green:** 490 - 570 nm
- Yellow:** 570 - 585 nm
- Orange:** 585 - 620 nm
- Red:** 620 - 780 nm



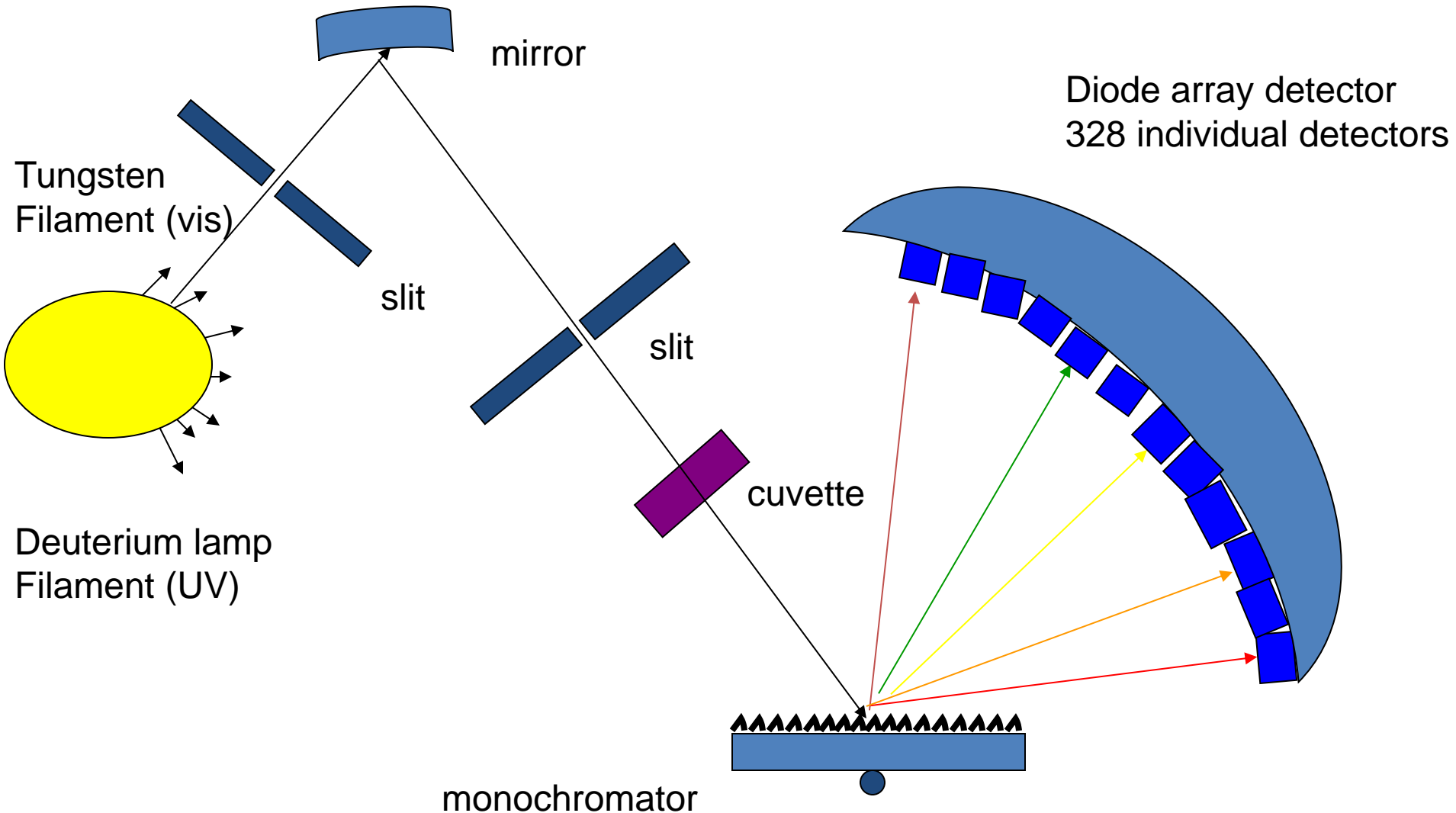
Double Beam UV-Vis Spectrophotometer

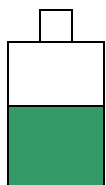


Skenovací UV-VIS spektrometr

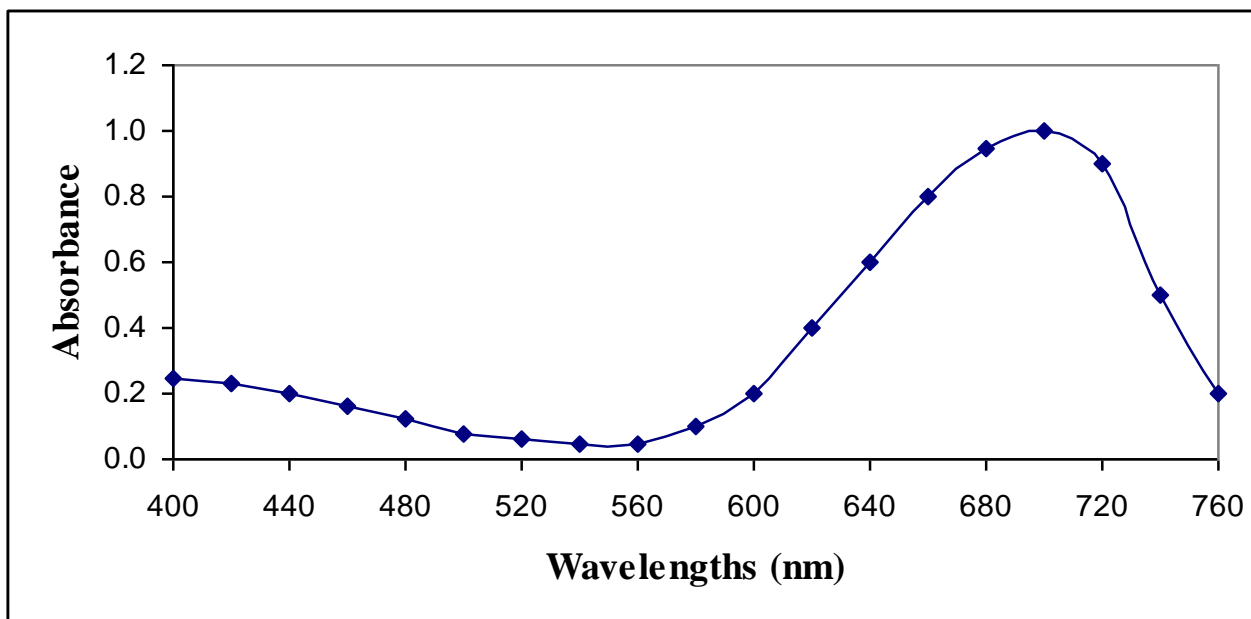
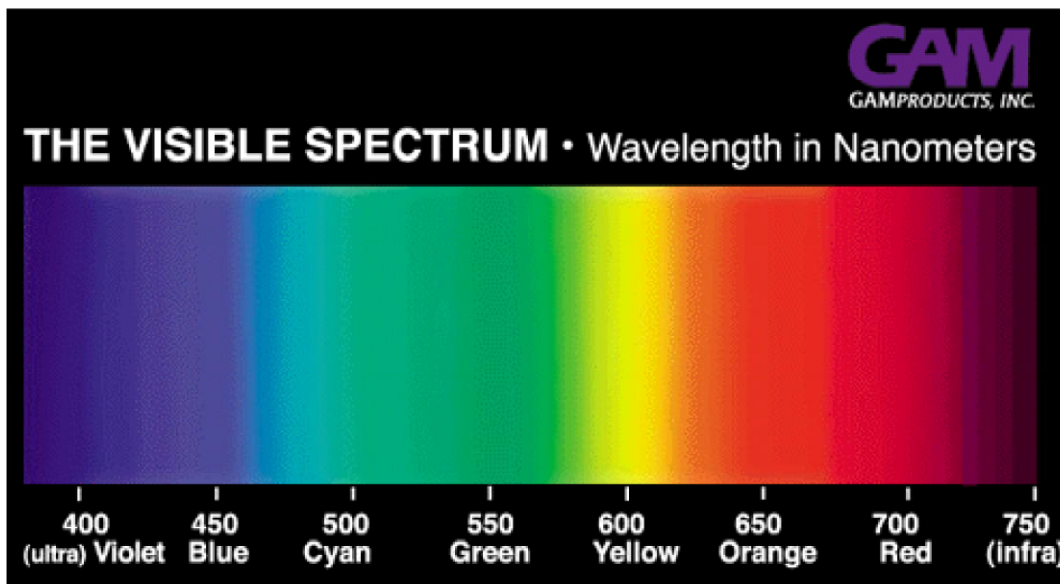


Diode array UV-VIS spektrometr

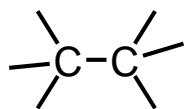




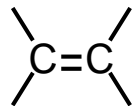
Sample
Solution



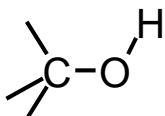
Kvantitativní měření se provádí v maximu absorpční křivky.



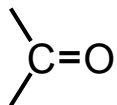
$\sigma \rightarrow \sigma^*$ 135 nm



$\pi \rightarrow \pi^*$ 165 nm



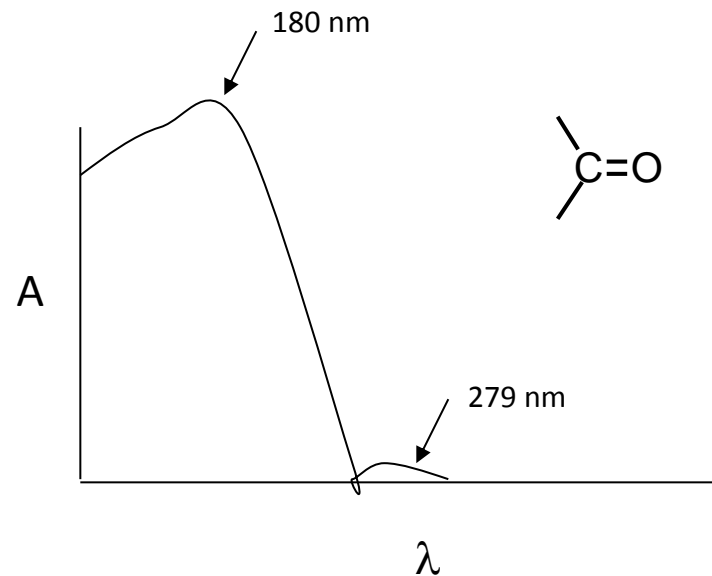
$n \rightarrow \sigma^*$ 183 nm weak



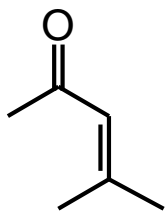
$\pi \rightarrow \pi^*$ 150 nm

$n \rightarrow \sigma^*$ 188 nm

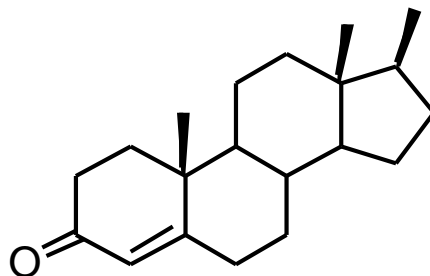
$n \rightarrow \pi^*$ 279 nm weak



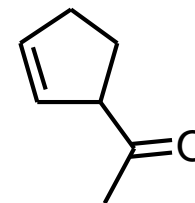
Similar structures have similar UV spectra:



$\lambda_{\max} = 238, 305 \text{ nm}$



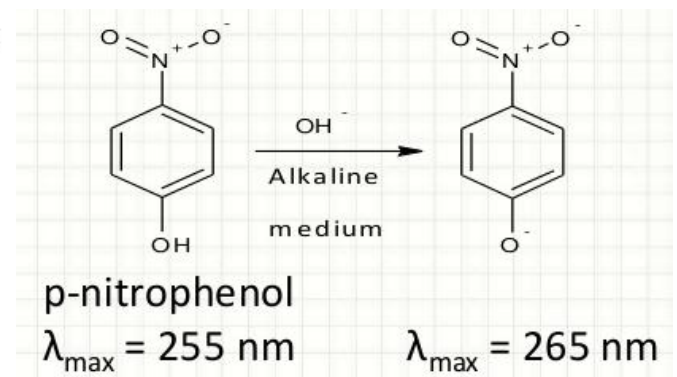
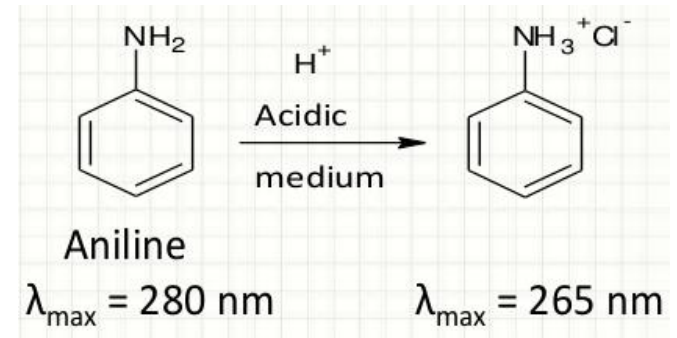
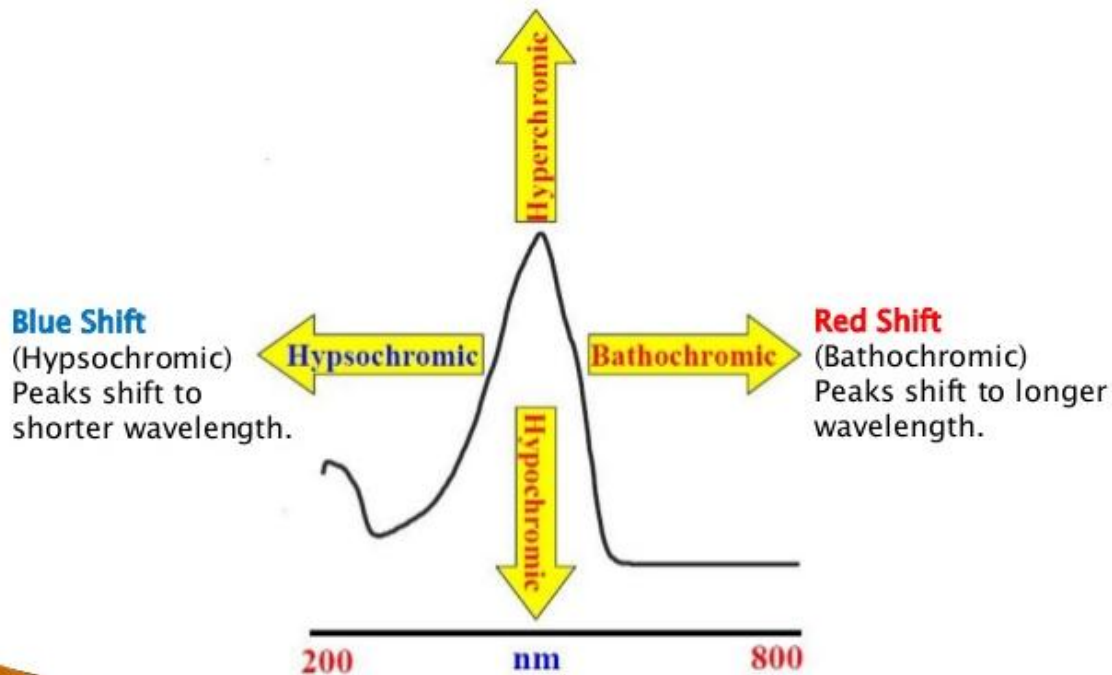
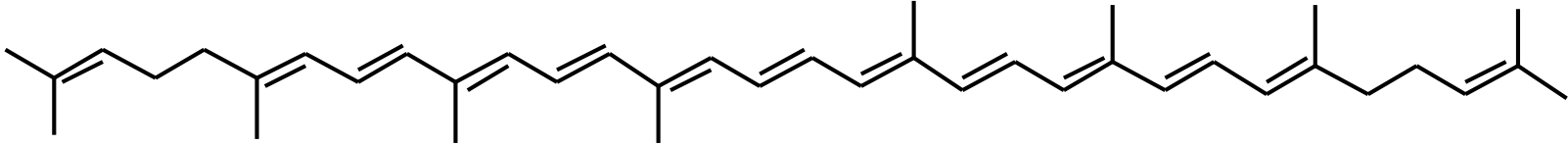
$\lambda_{\max} = 240, 311 \text{ nm}$



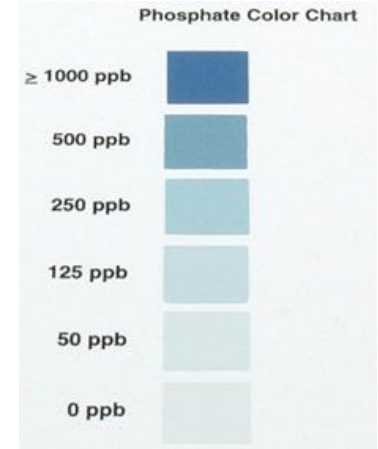
$\lambda_{\max} = 173, 192 \text{ nm}$

Barva souvisí s rozsahem konjugovaného systému

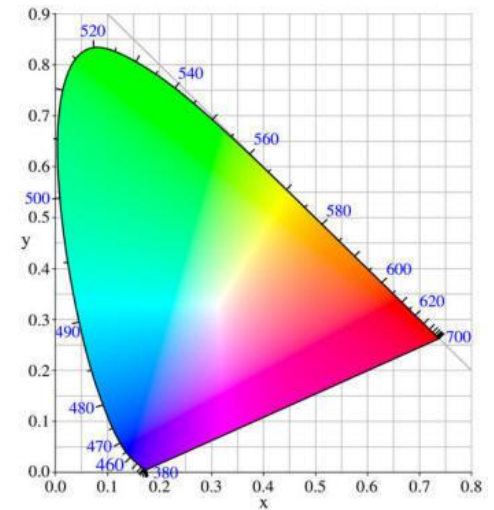
Lycopene:



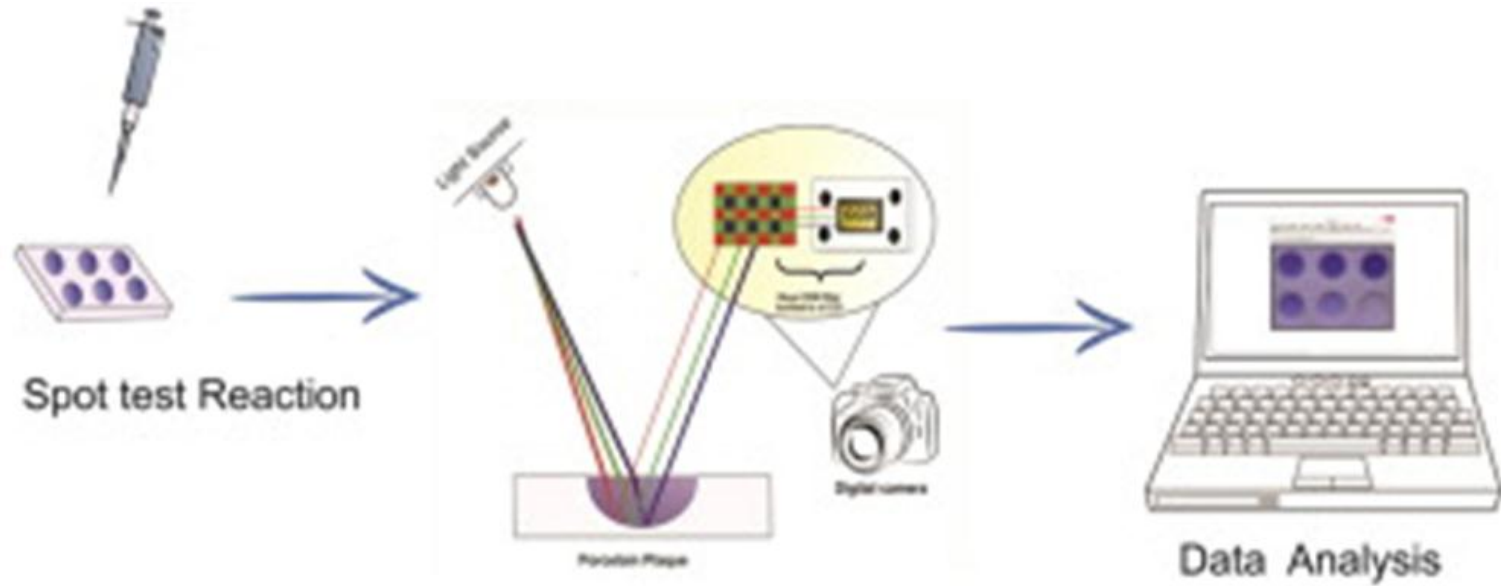
Kolorimetrie



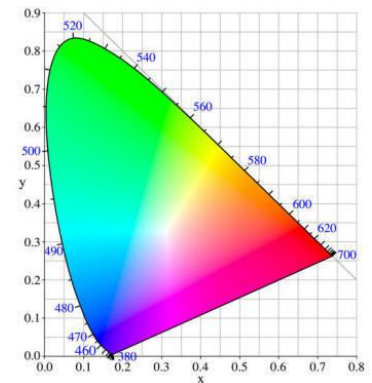
Signal processing



Kolorimetrie



Signal processing



Kolorimetrie

Fosfor

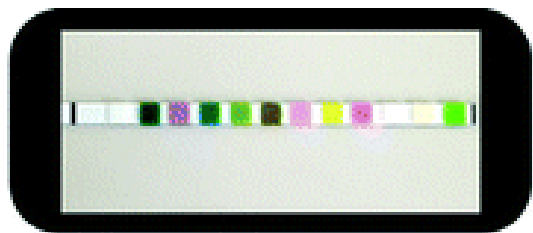
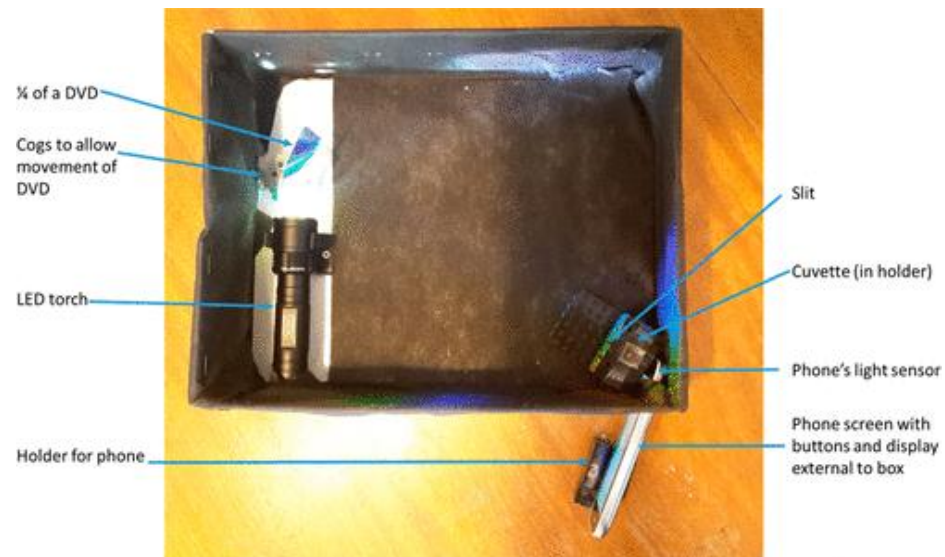
pH

Železo

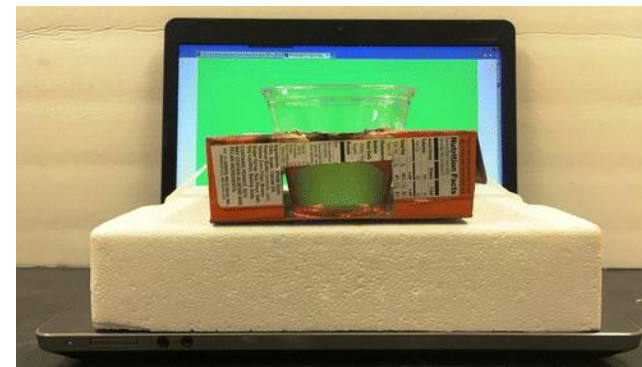
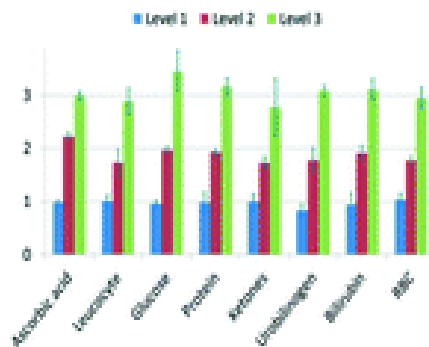
Dusík (amoniakální, nitrátový)



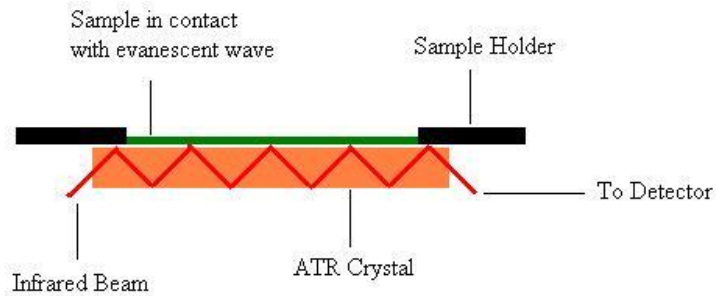
Kolorimetrie - aplikace mobilního telefonu



Name:	Substrate	Product 1	Product 2	Product 3
Reaction (s):	10	10	10	10
Wavelength (nm):	620	620	620	620
pH:	7.0	7.0	7.0	7.0
Quotient:	0.15	0.15	0.15	0.15
Series:	1	2	3	4
Process:	1	2	3	4
Method:	1	2	3	4
ColorManager:	1	2	3	4
Reaction:	1	2	3	4
Brand:	1	2	3	4

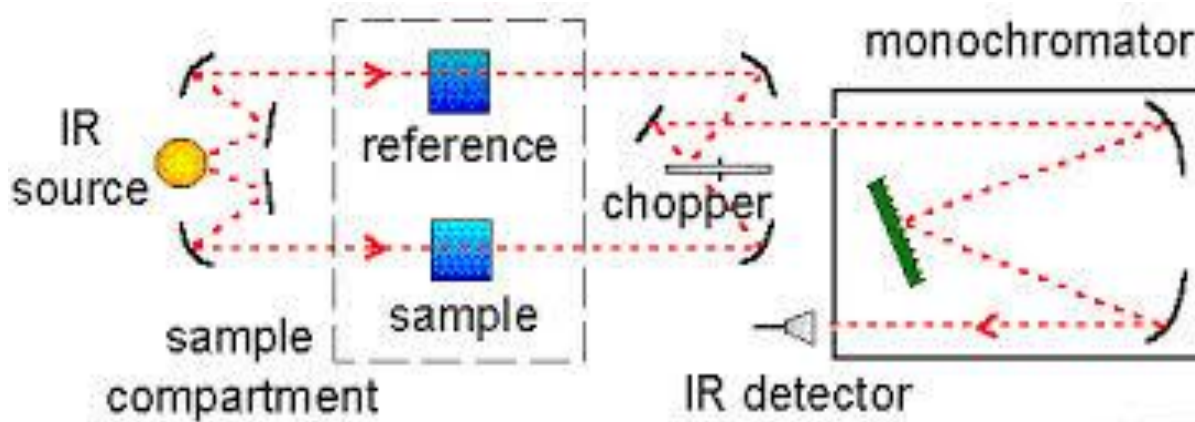


Infračervená spektrometrie



Schematic of a multiple reflection ATR system

ATR
KBr technika



Infračervená spektrometrie (FTIR)

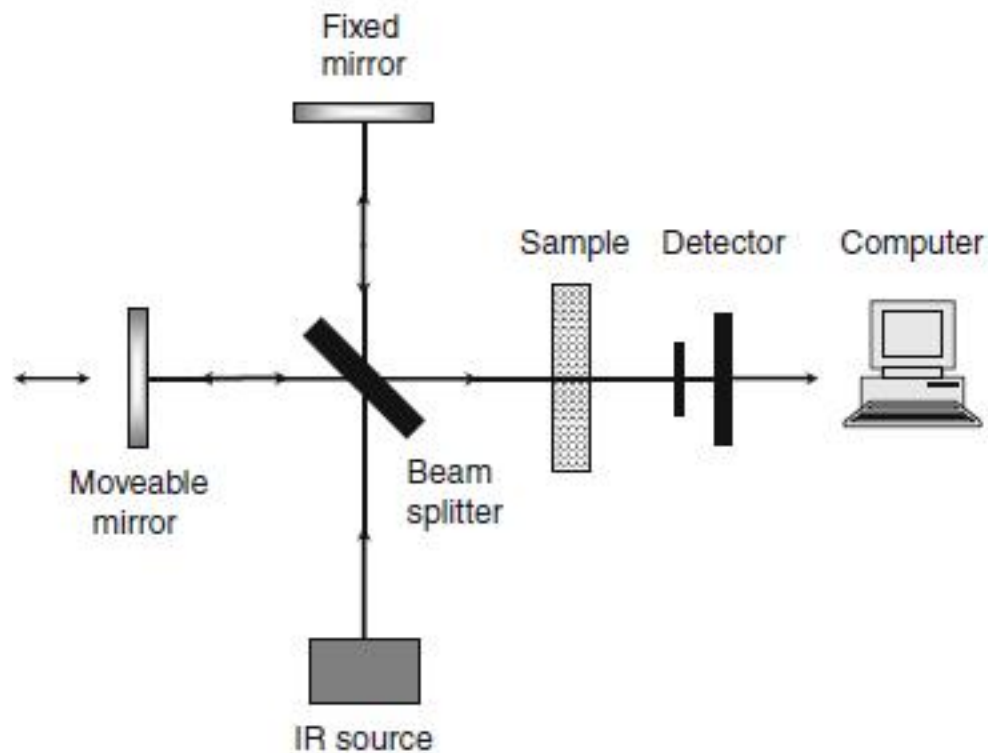
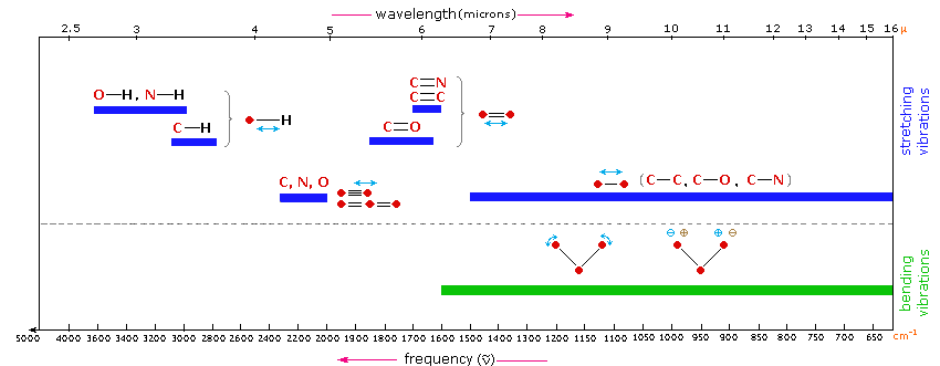
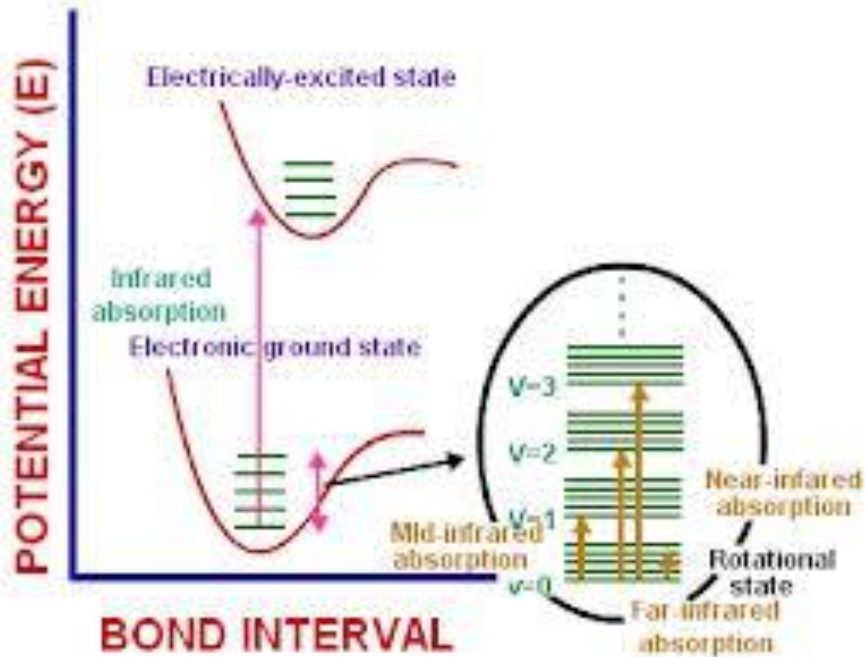
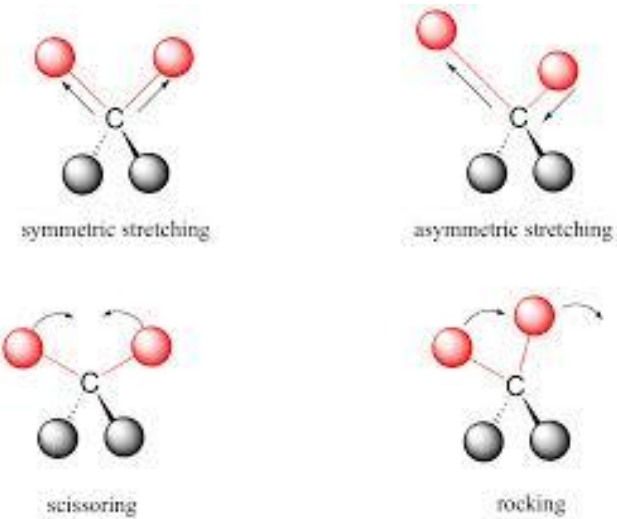
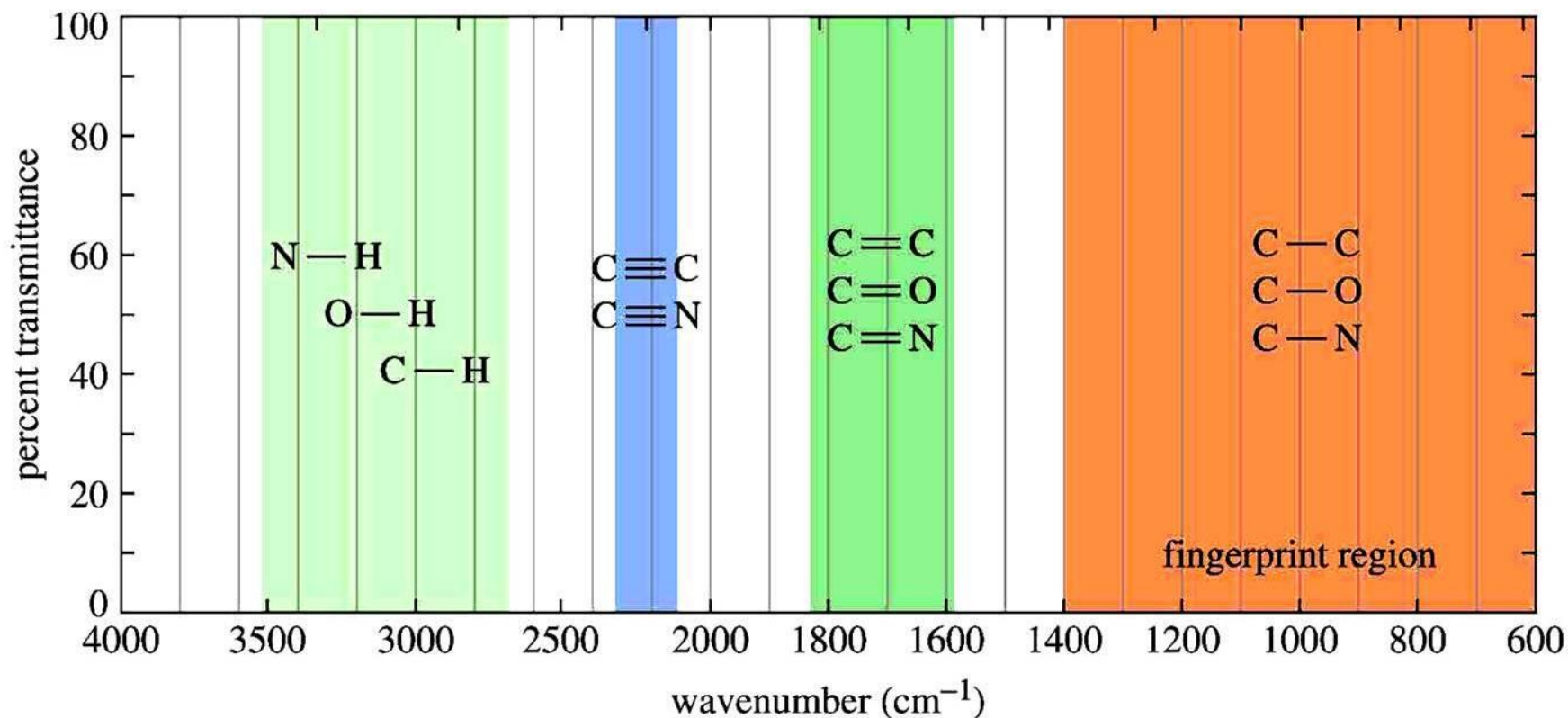


Fig. 35.6 FT-IR spectrometer with interferometer (Reprinted from "Applied Spectroscopy", Jerry Workman, Jr., page 9, Copyright 1998, with permission of Elsevier)

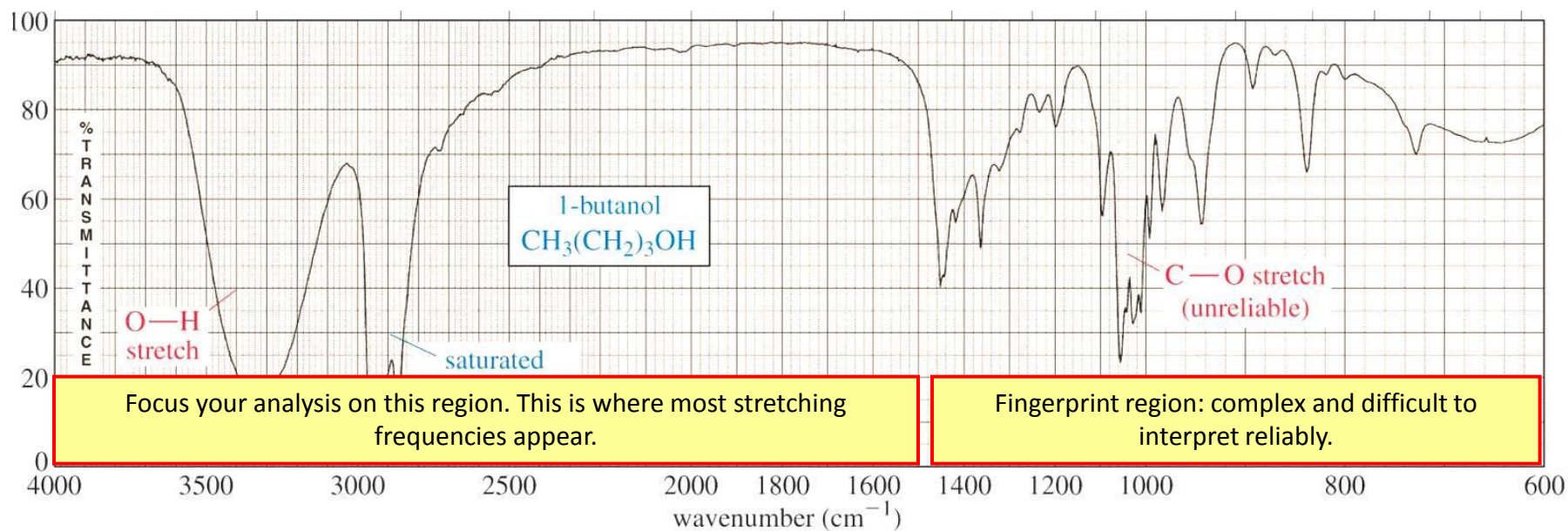
Infračervená spektrometrie (FTIR)



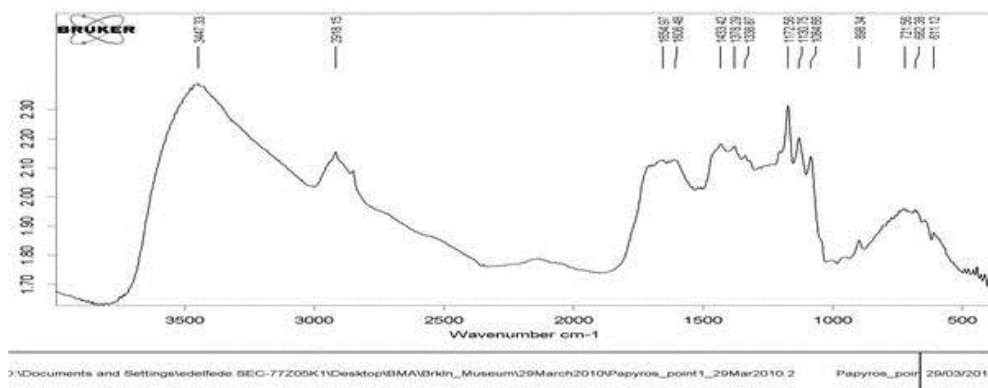
The typical IR absorption range for covalent bonds is **600 - 4000 cm^{-1}** . The graph shows the regions of the spectrum where the following types of bonds normally absorb. For example a sharp band around 2200-2400 cm^{-1} would indicate the possible presence of a C-N or a C-C triple bond.



Although the entire IR spectrum can be used as a fingerprint for the purposes of comparing molecules, the **600 - 1400 cm^{-1}** range is called the **fingerprint region**. This is normally a complex area showing many bands, frequently overlapping each other. This complexity limits its use to that of a fingerprint and should be ignored by beginners when analyzing the spectrum. As a student, you should focus your analysis on the rest of the spectrum, that is the region to the left of 1400 cm^{-1} .



Egyptská kniha mrtvých



↑
Přenosné FTIR zařízení



Fig. 1. The Delhi iron pillar before the construction of the iron grill cage around the stone platform.

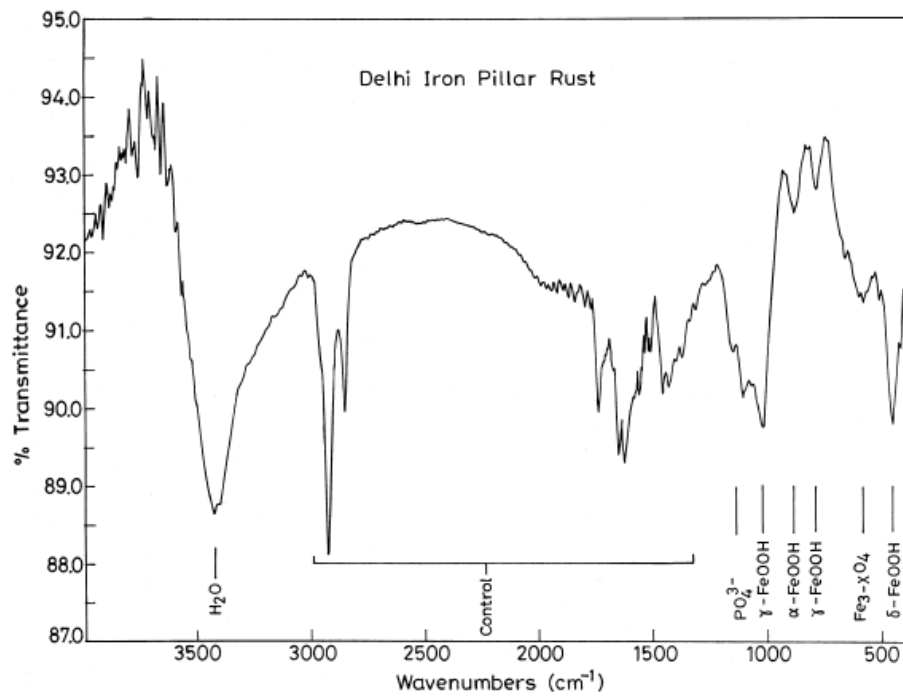


Fig. 5. FTIR spectrum from the DIP rust.

FTIR mikroskopie



Fig. 10.11. Egyptian bronze solid cast statuette of the God Osiris, inlaid with gold and blue glass. The surface has been extensively altered to massive light blue and dark green corrosion, identified as an overall patina of atacamite, with patches of chalconatronite. Frontal view. (For a colored version of this figure, see Plate 10.III.)

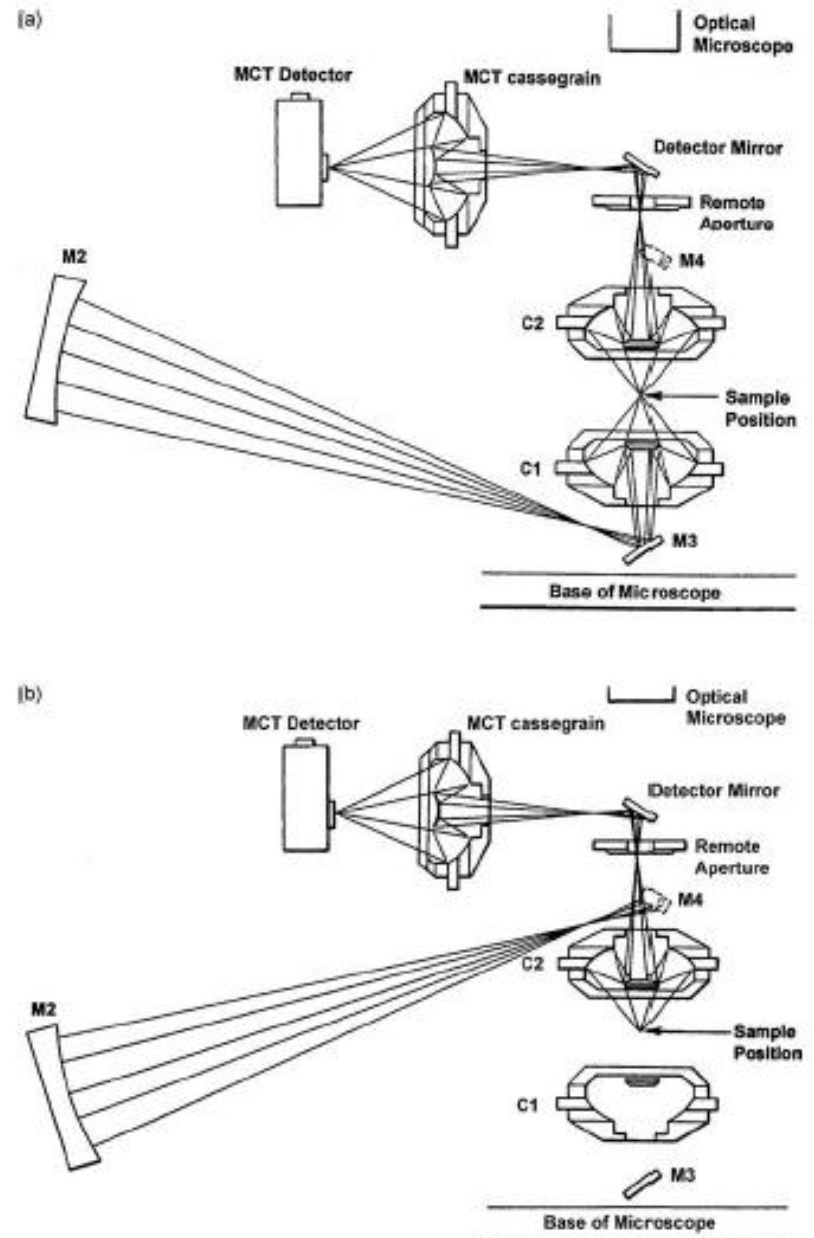


Figure 9.25 Optical paths of FTIR microscope with IR radiation: (a) transmittance; and (b) reflectance. M, mirror; C, Cassegrain lens. (Reproduced by permission of PerkinElmer Inc.)

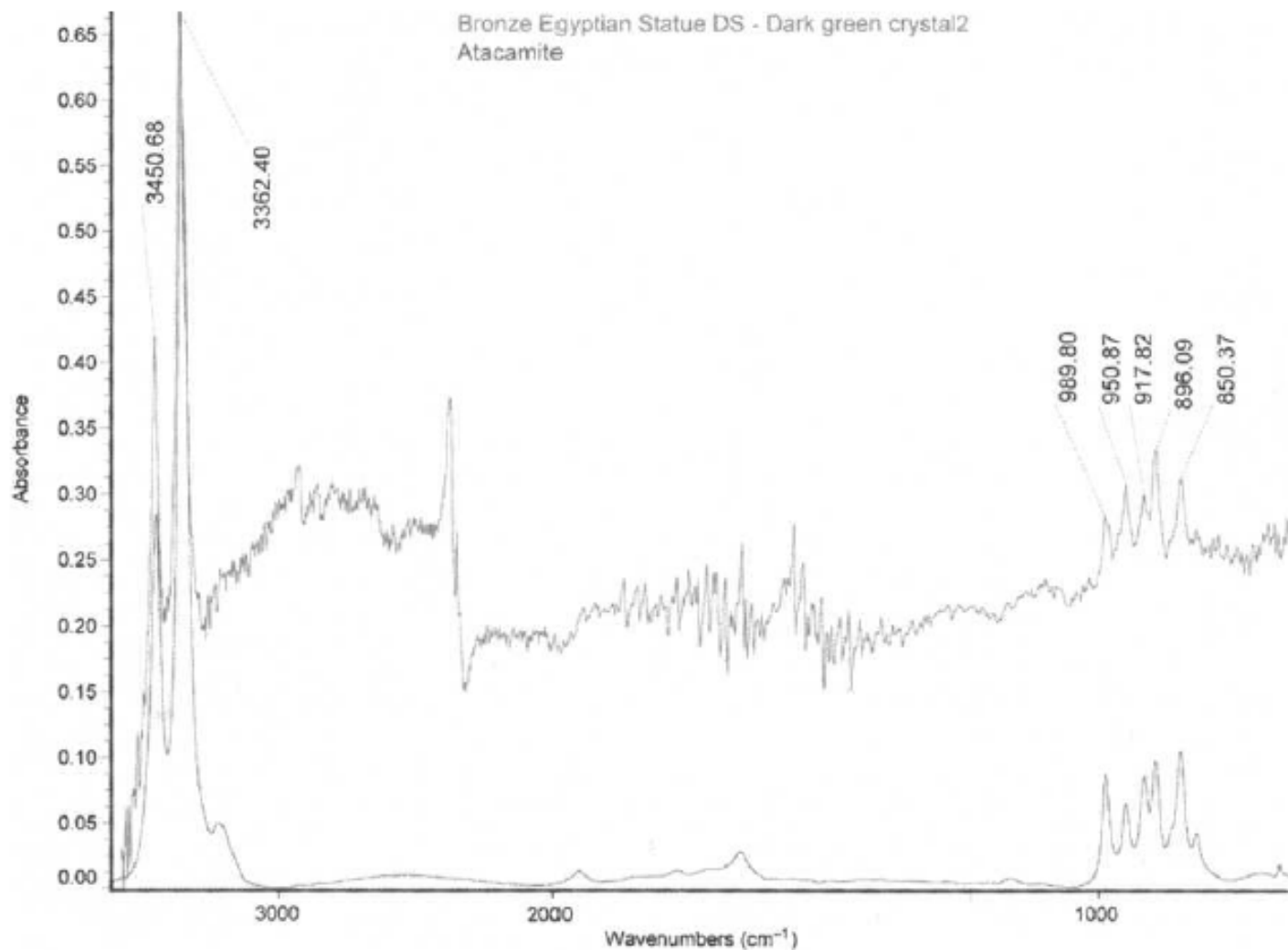


Fig. 10.17. FTIR Spectrum obtained, in situ, from the dark green surface of the Egyptian bronze Osiris shown in Fig. 10.11. The patina was shown to be of atacamite, but the result was only obtained with some difficulty and the chalconatronite patina could not be identified by this technique without sampling.

Infračervená spektrometrie

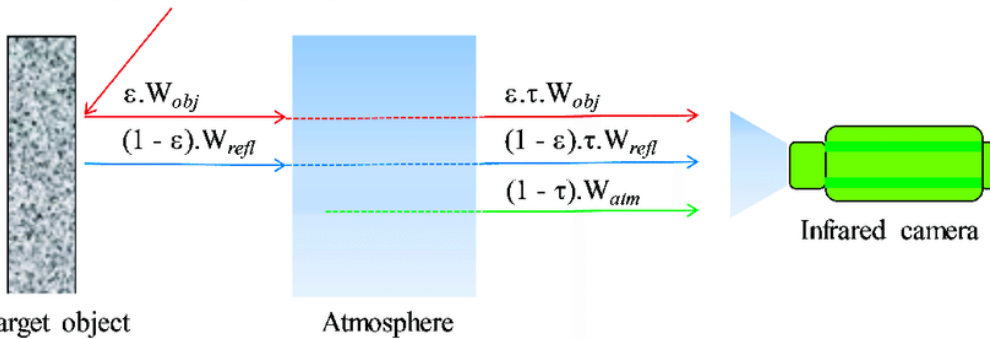
Terénní a mobilní zařízení



Noční vidění a termokamery



Heat source surroundings
(e.g. Sun, halogen lamp...)



Reflektografie

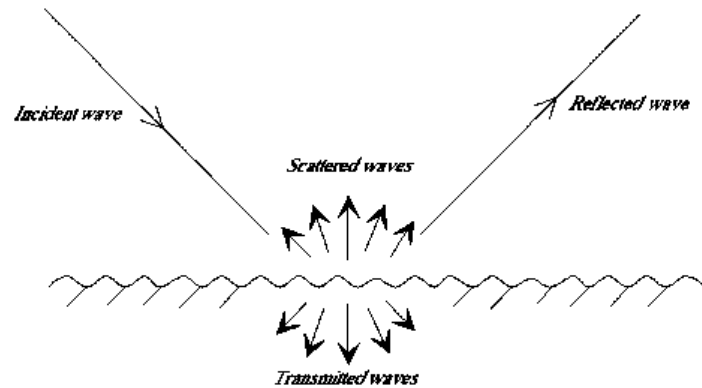


Figure 15. Case of natural environments: sum of specular reflection and diffuse reflection (volume reflection is ignored here).

Aplikace infračervené reflektografie - zviditelnění podkresby



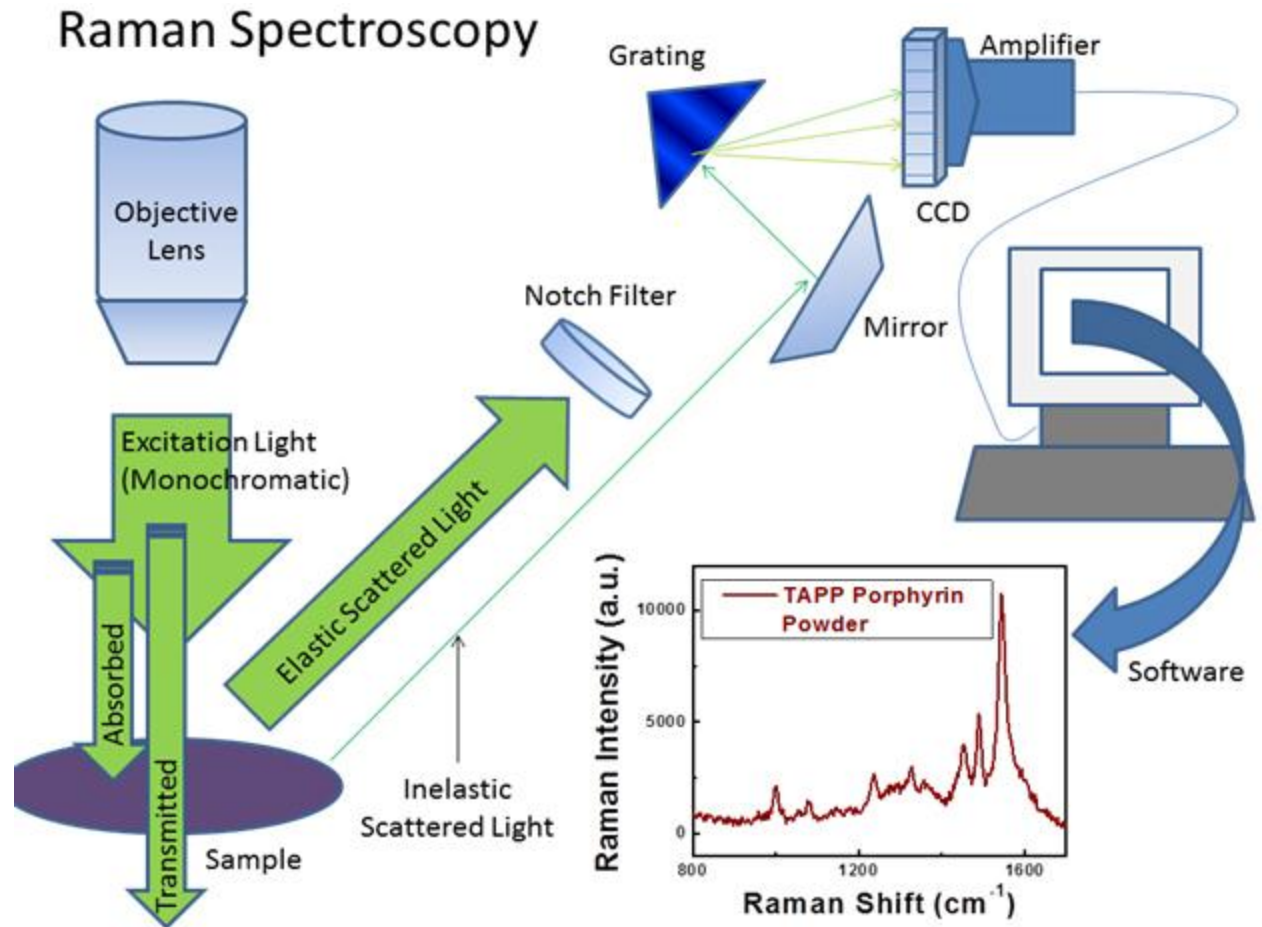
Reflektografie

Aplikace infračervené reflektografie - zviditelnění tetování na mumifikovaných rukou z pohřebiště Semna South, Núbie (dnešní Súdán), stáří cca 2000 let.

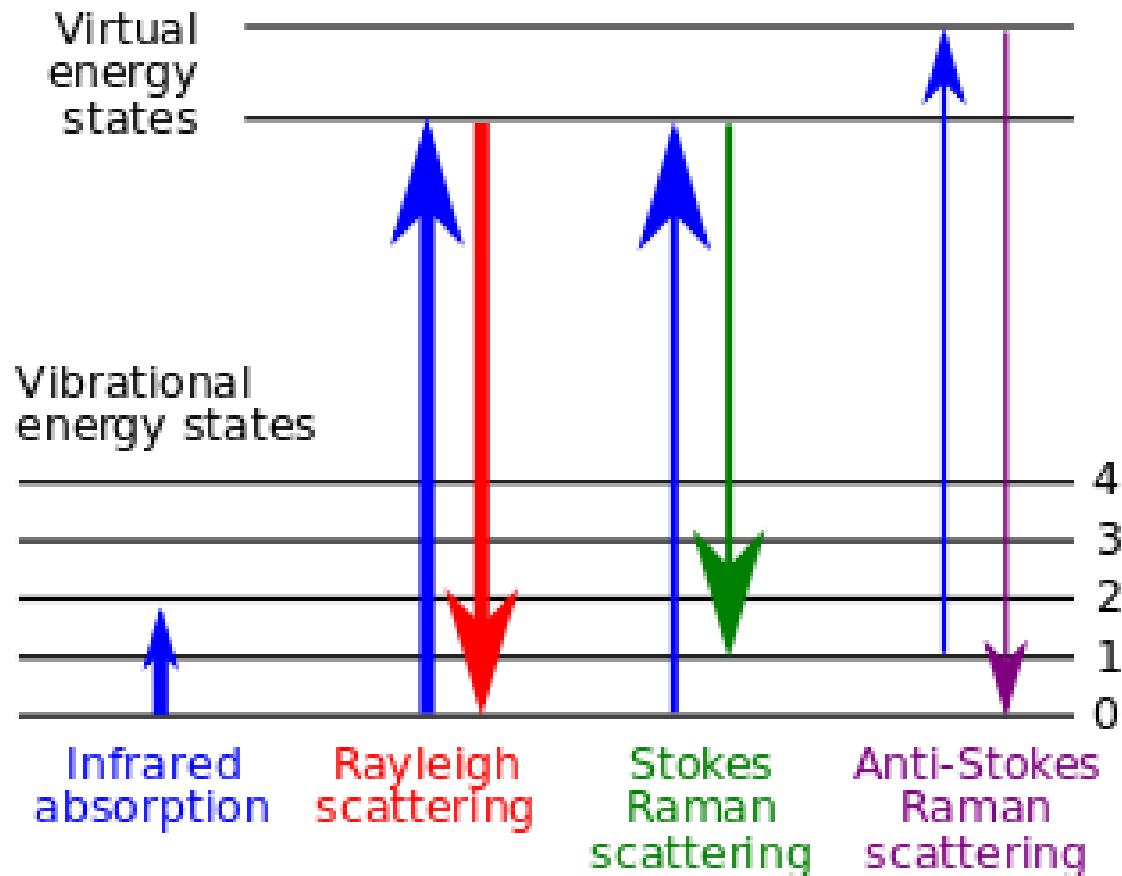


Ramanova spektrometrie

Nd:YAG 1064 nm
He-Ne 632.8 nm

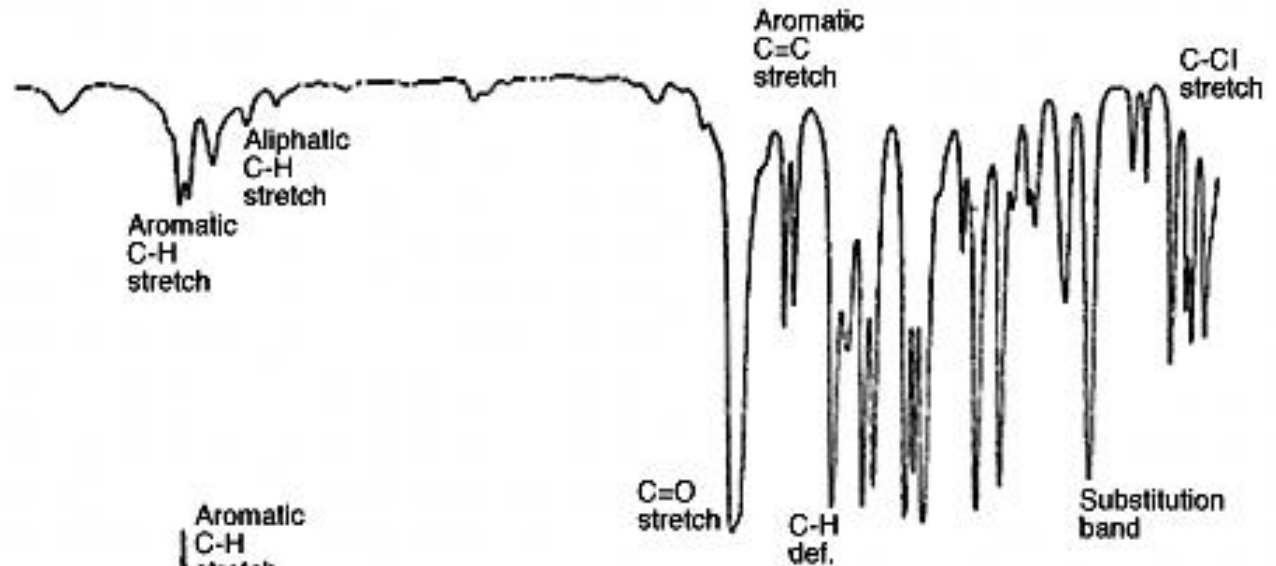


Princip Ramanovy spektrometrie

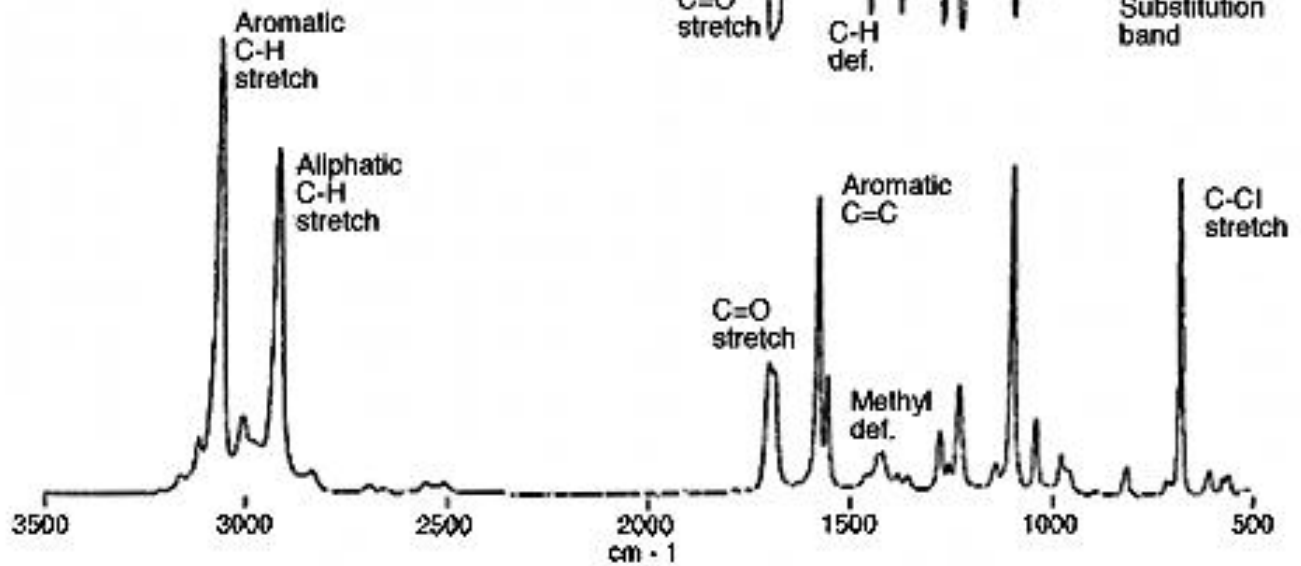


Raman vs. FTIR

FT IR

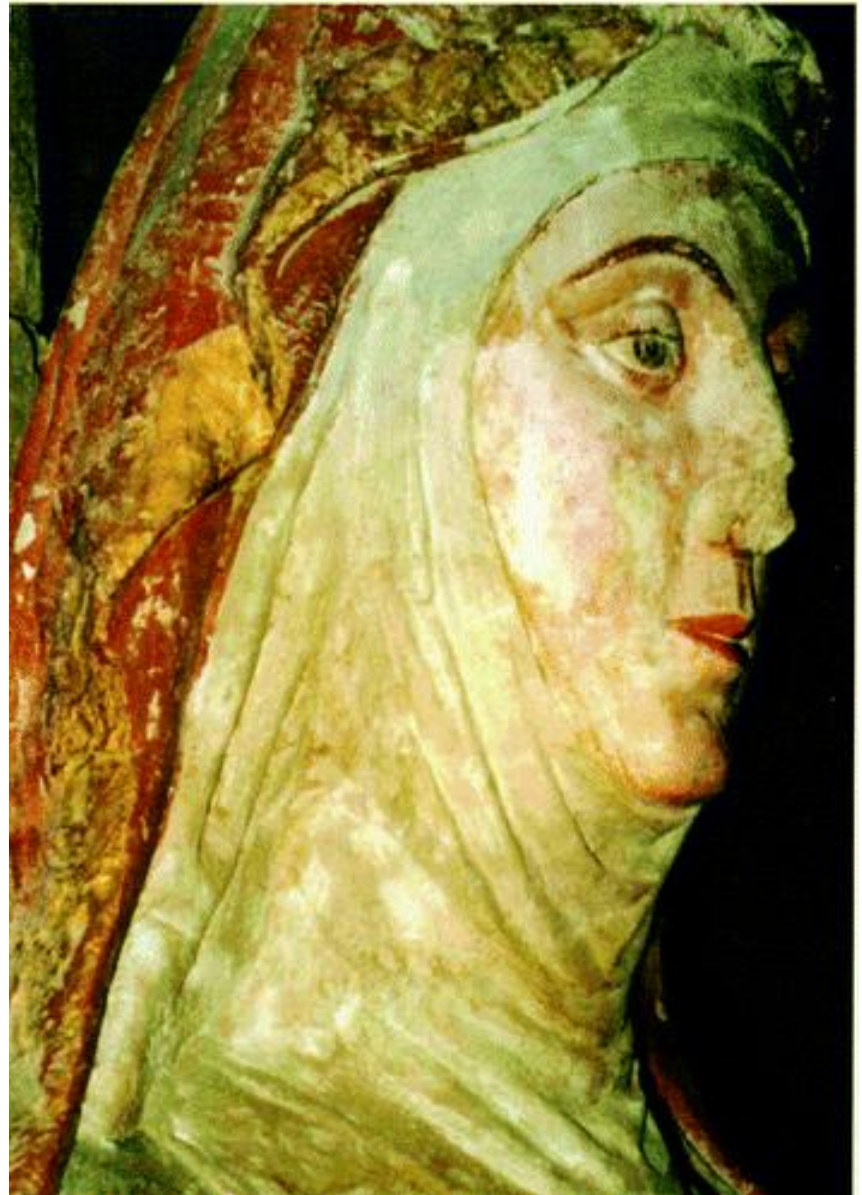


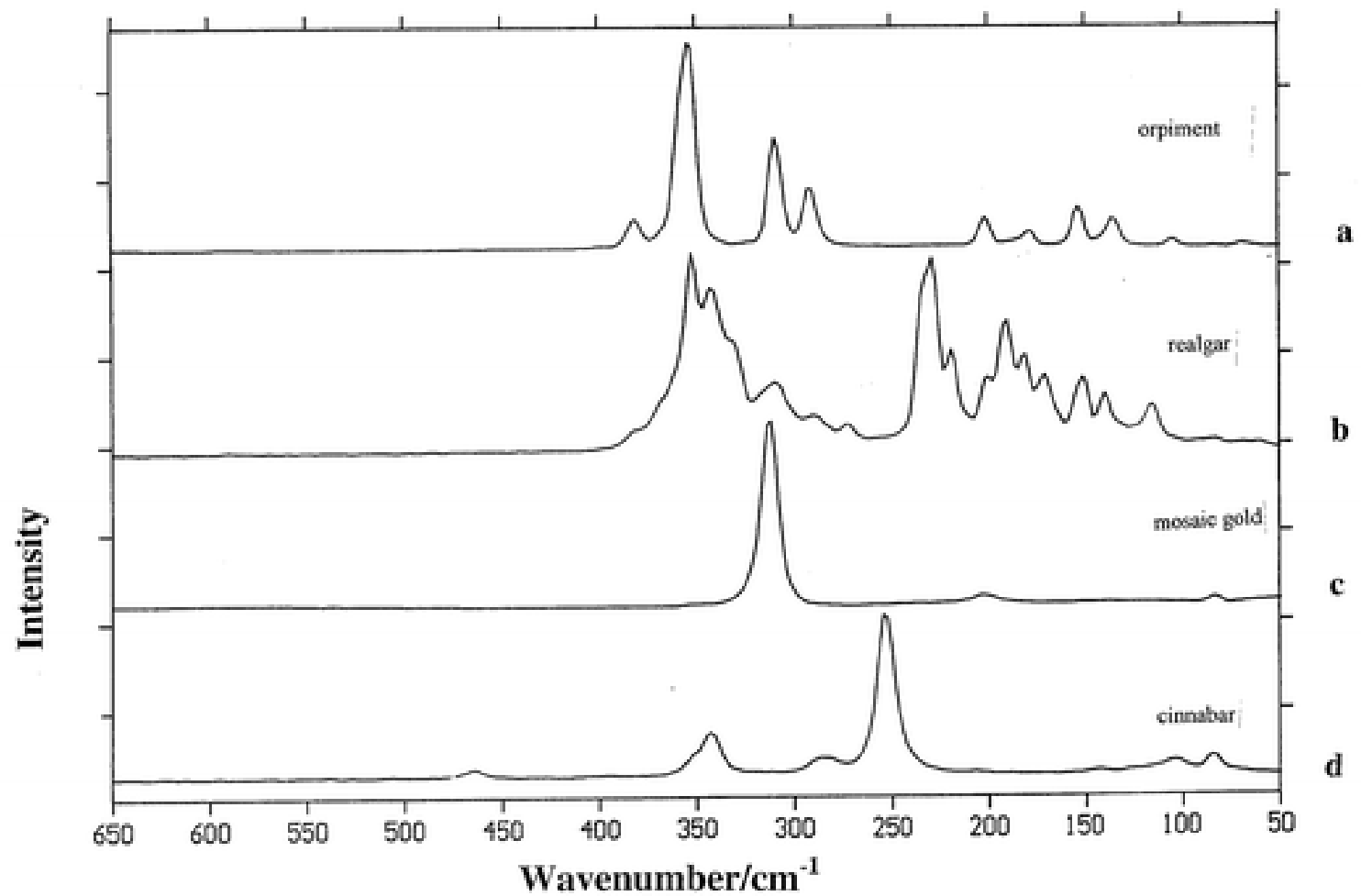
(FT) Raman



Ramanova spektrometrie pigmentů

Polychromovaná socha sv. Anny v Santa
Maria la Real, Sasamon, Španělsko (13.
stol.).





Ramanova spektra auripigmentu (As_2S_3), realgaru (As_4S_4), mozaikového zlata (SnS_2) a rumělky (Hg S).

Oltář ze “San Antolín y San Bernabé”

<i>Pigment</i>	<i>Chemical formula</i>	<i>Raman bands cm^{-1}</i>
Vermilion	HgS	255, 309, 347, 376
Azurite	$2CuCO_3 \cdot Cu(OH)_2$	251, 404, 623, 770, 838, 1098
Malachite	$CuCO_3 \cdot Cu(OH)_2$	153, 168, 179, 223, 272, 352, 435, 516, 538, 722, 755, 1062, 1100, 1372, 1496
Lead White	$PbCO_3$	409, 1054
Lapislazuli	$Na_8[Al_6Si_6O_{24}]S_n$	258, 286, 545, 581, 802, 1097, 1358, 1642
Massicot	PbO	286, 384, 419
Gypsum	$CaSO_4 \cdot 2H_2O$	182, 216, 416, 495, 623, 673, 1009, 1140

Table 1. Chemical formula and Raman band observed (in cm^{-1} , wavenumber) of the identified pigments.

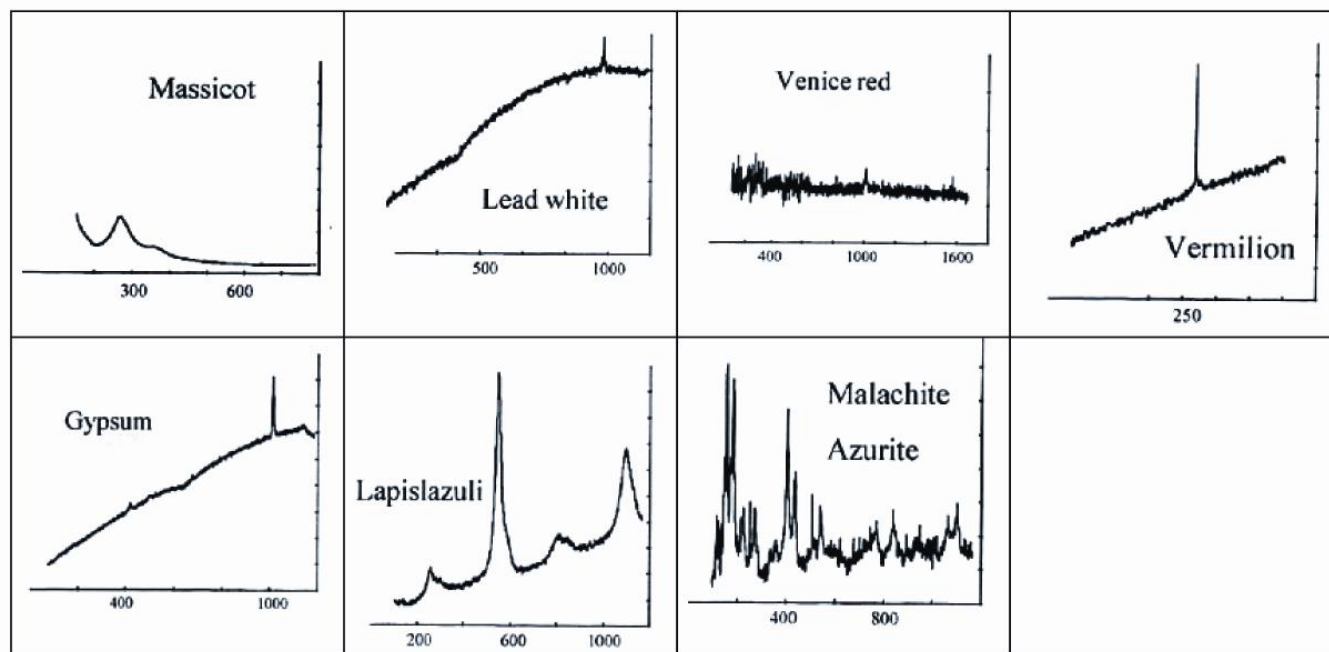
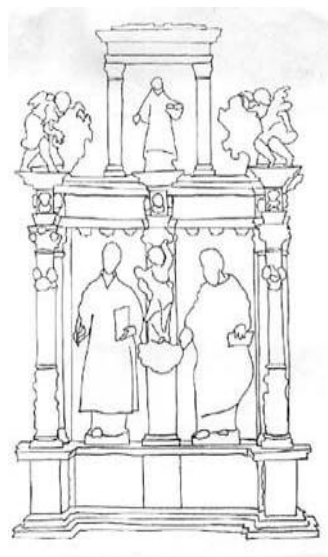


Fig. 5. The Raman spectra of the pictorial materials obtained from the “San Antolín y San Bernabé” altarpiece. The axis are Raman intensity and wavenumber (cm^{-1}).

Rozpoznání imitací

Přírodní barevné korály (karoten)

Barvené korály

Imitace korálů

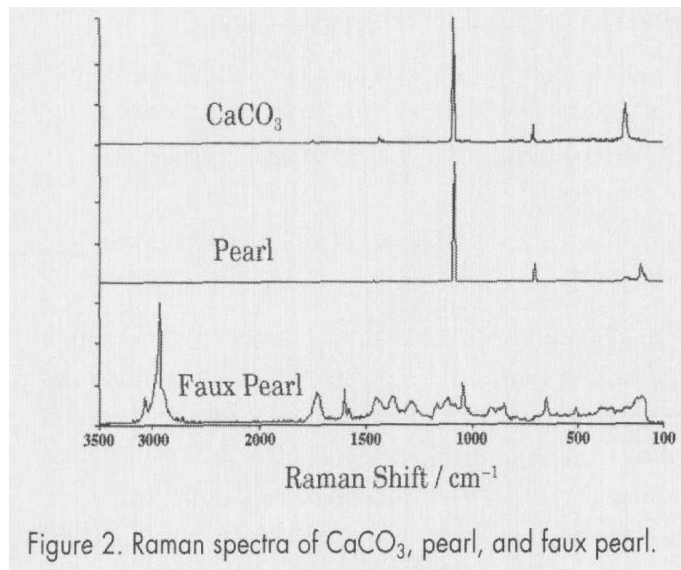
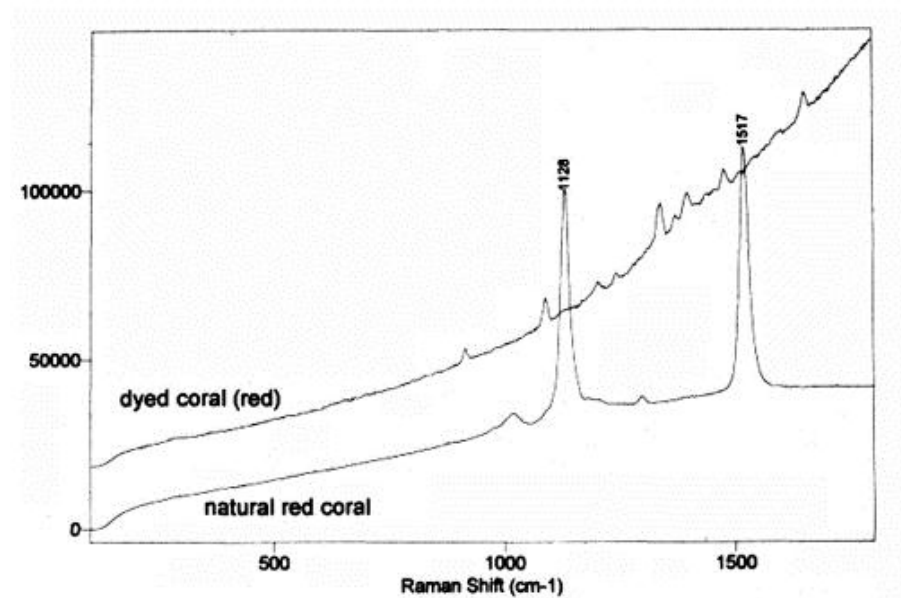


Figure 2. Raman spectra of CaCO₃, pearl, and faux pearl.



Identifikace slonoviny



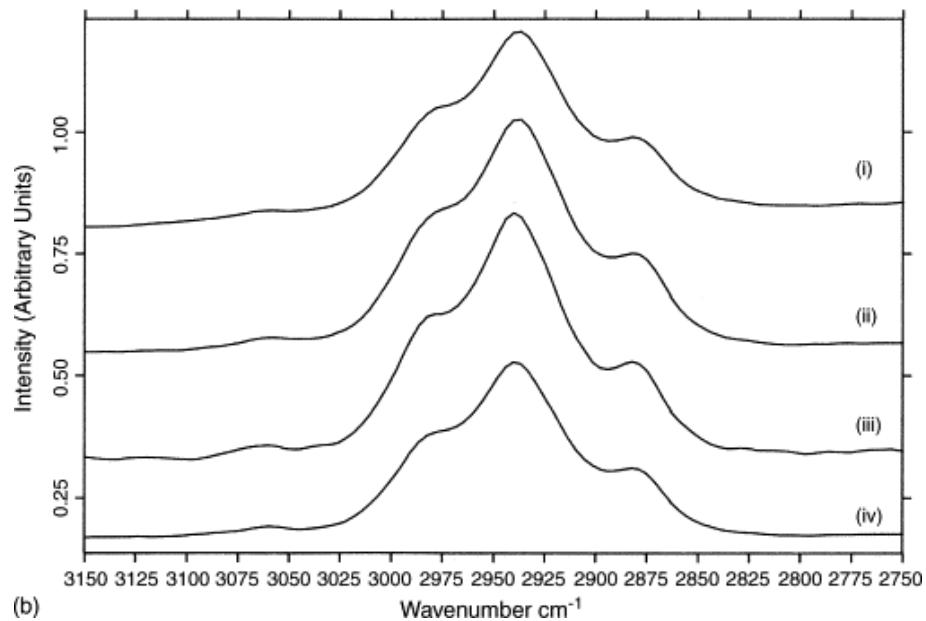
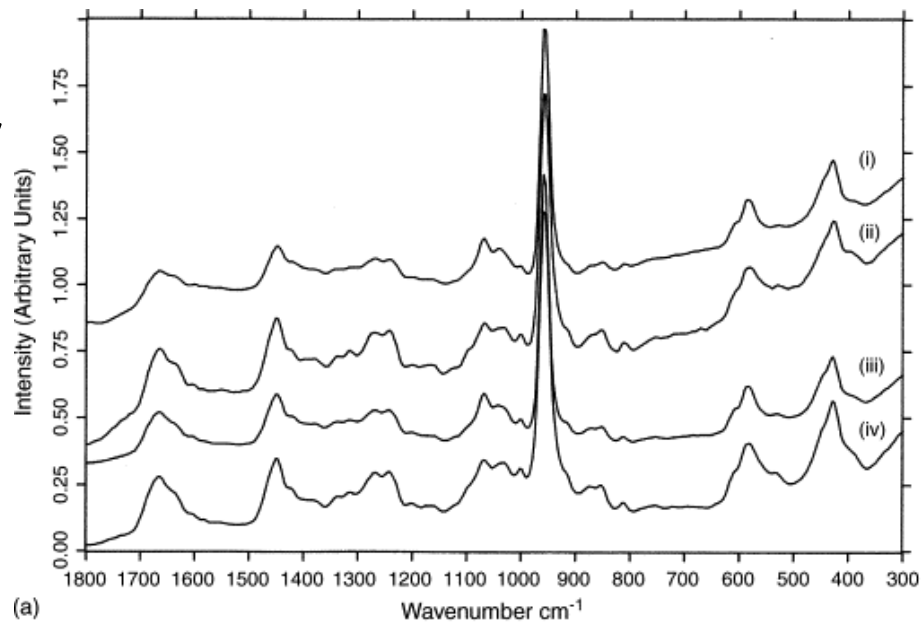
FT-Ramanova spektra:

Římské pečetidlo (i)

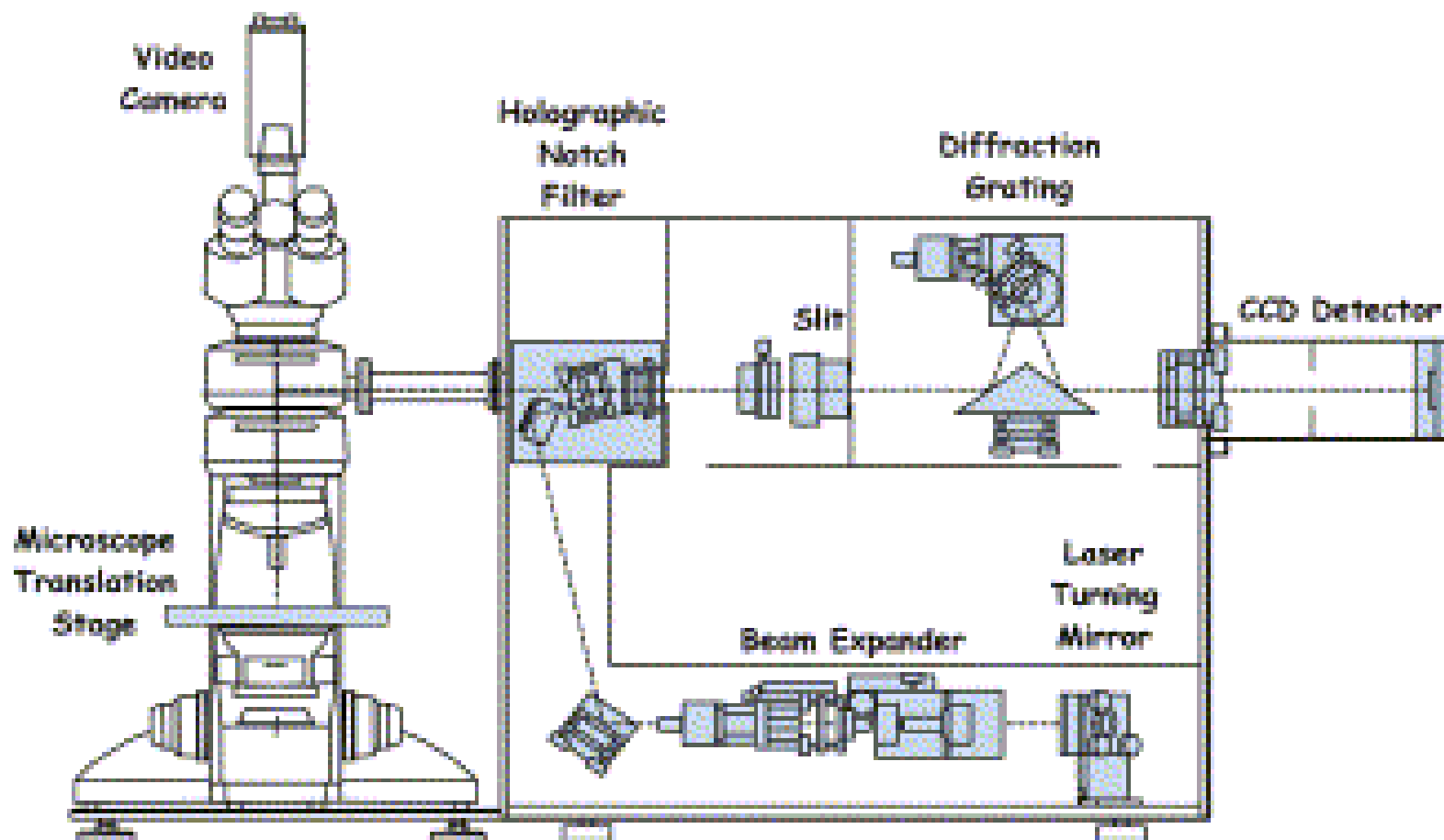
africký slon (ii),

vorvaň (iii)

hroch (iv)

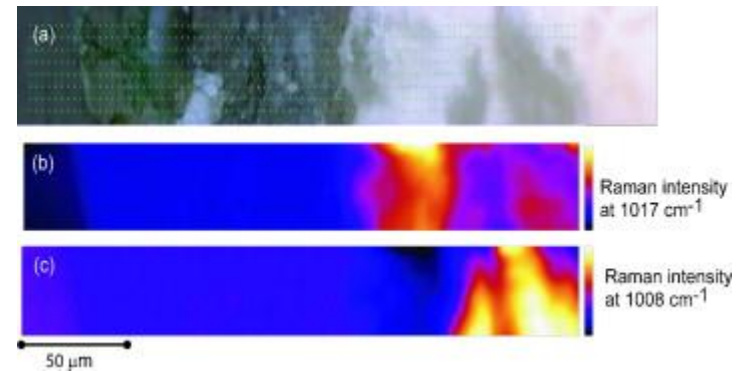
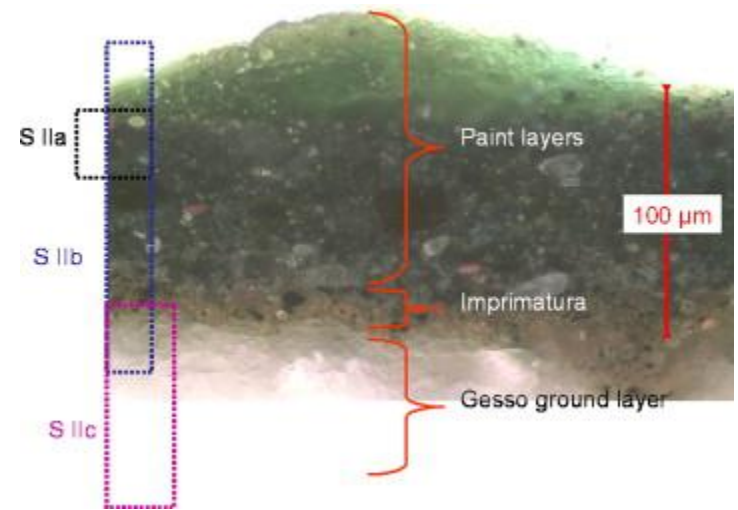


Ramanova mikroskopie



Ramanova mikroskopie maleb

Portrét mladíka (neznámý severoitalský malíř, cca 1515)



Ramanovské mapy vzorku S IIb.
(a) optický obraz, (b) anhydrit, (c) sádrovec (gypsum).

Ramanova mikroskopie

mikrofosilie
v jurských
rohovcích

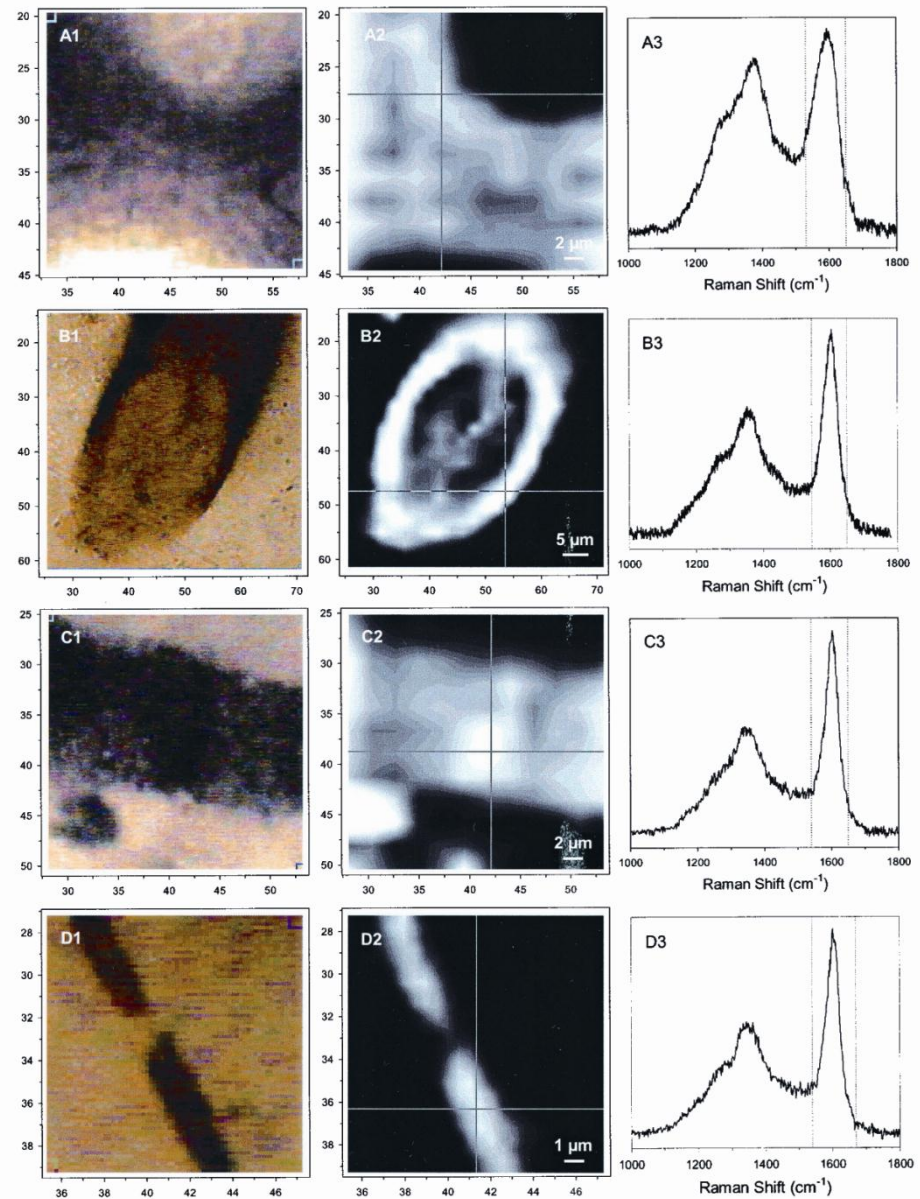
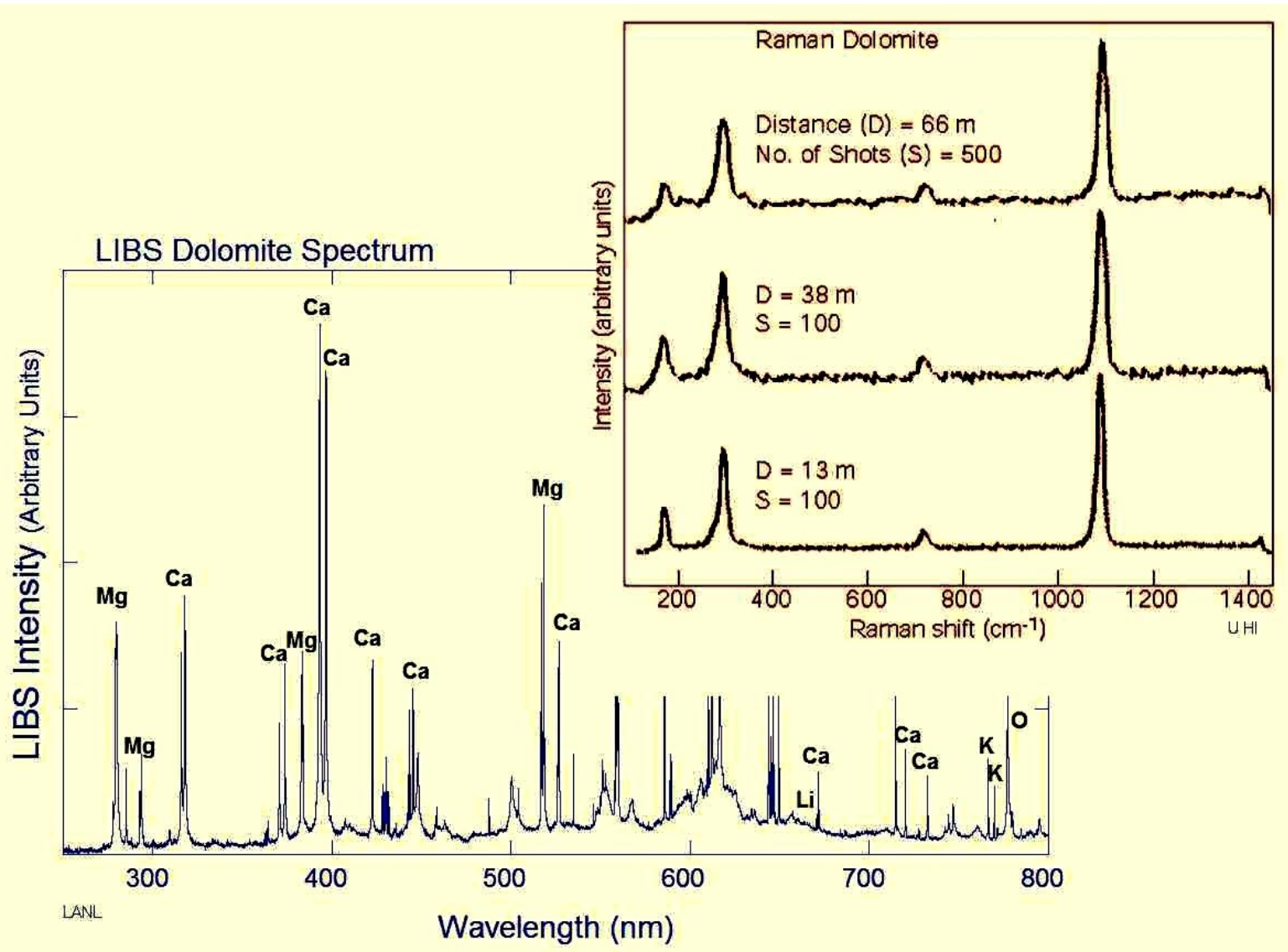


Fig. 1. Optical images (column 1), Raman images (column 2), and spectral bands used for Raman imaging (column 3) of permineralized carbonaceous fossils at or near the upper surfaces of polished chert thin sections: (A) Cell wall in the conductive tissue (lignified xylem) of an aquatic fern *cf. Dennstaedtia* from the essentially unmetamorphosed ~45-Ma-old Clarno Formation of Oregon. (B) Tangential section of the tubular sheath of a *Lyngbya*-like oscillatoriacean cyanobacterium in a conical stromatolite (*Canophyton gaubitzta*) from the subgreenschist facies ~650-Ma-old Chickkan Formation of Kazakhstan. (C) Transverse cell wall of a broad cellular trichome (*Gunflintia grandis*), and (D) a narrow prokaryotic filament (*G. minuta*), in domical stromatolites of the greenschist facies ~2,100-Ma-old Gunflint Formation of Ontario, Canada. Each Raman image was produced by combining several hundred pixel-assigned point spectra ("spexels"), like those shown for each specimen in column 3, acquired over a small square part of the total area analyzed. The resolution of the Raman images is defined by the pixel dimensions of their component spexels; for A–C, 2 μm per pixel, and for D, 0.5 μm per pixel.

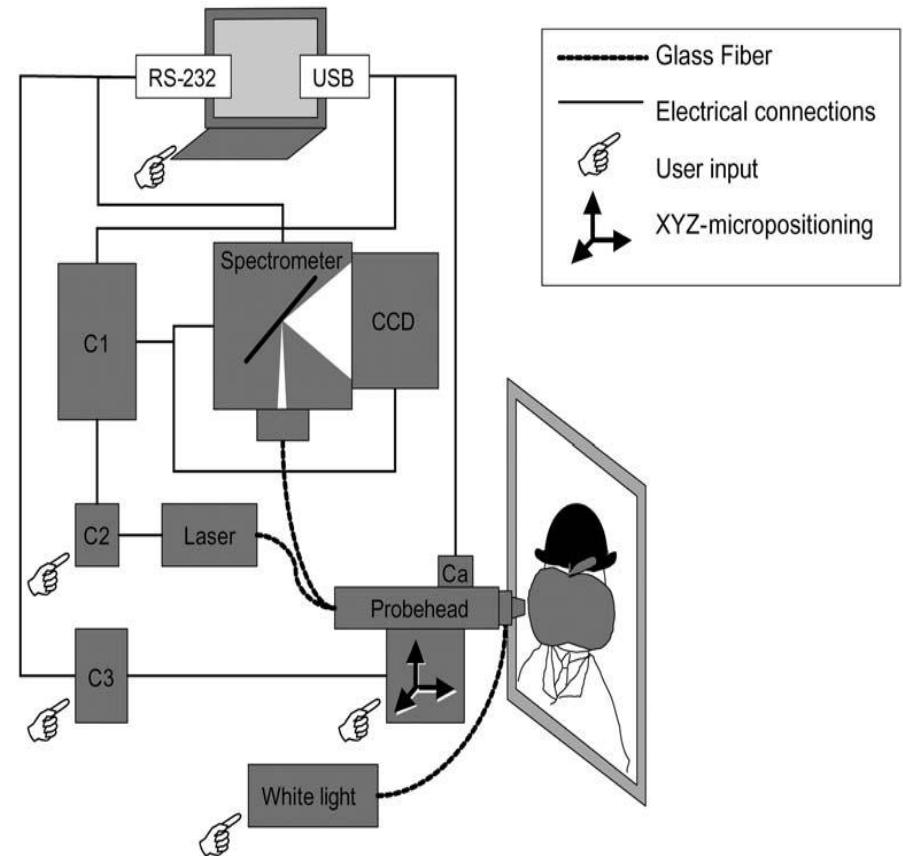
Raman + FTIR mikroskopie



Kombinace Raman + LIBS



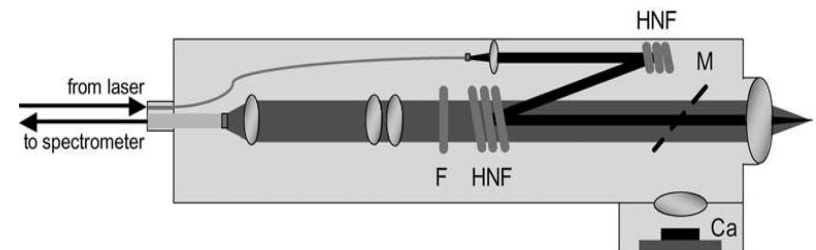
Mobilní zařízení pro Ramanovu spektrometrii



M : 95% propustné zrcadlo pro vizualizaci plochy kamerou (*Ca*).

HNF : holografické filtry odrážející laserový paprsek a propouští ramanovsky posunuté záření (Stokes)

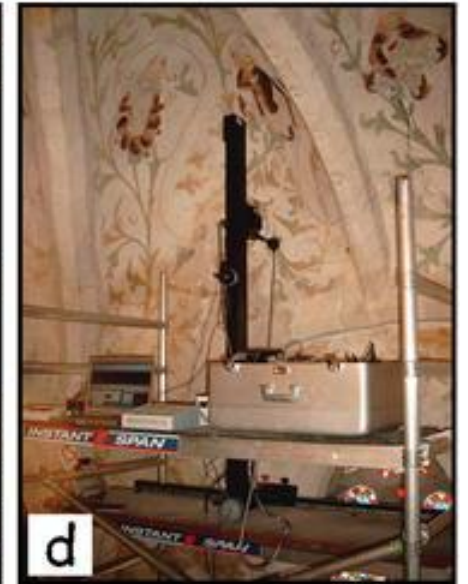
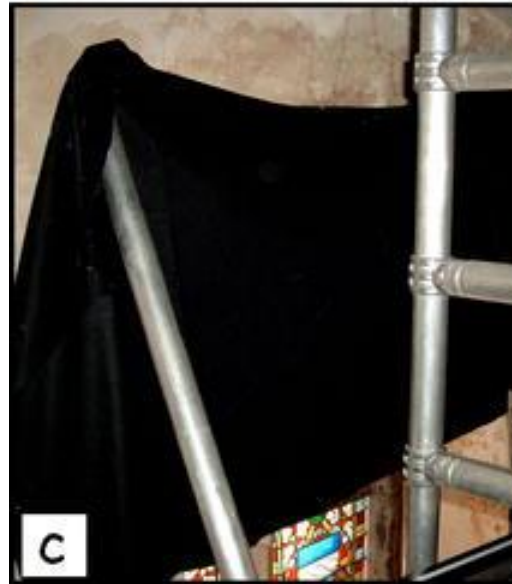
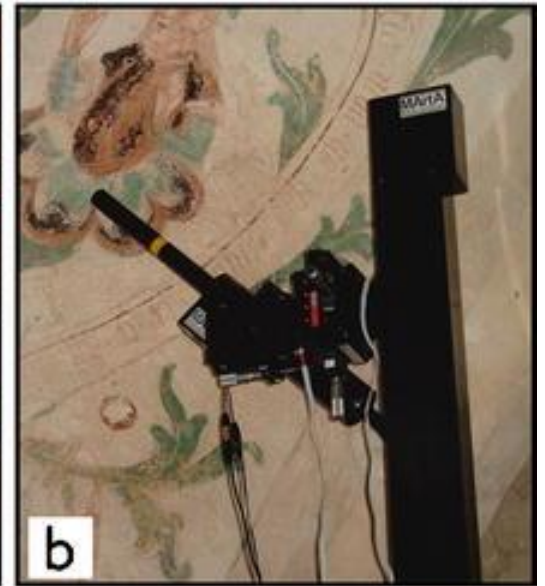
F filtry pro anti-Stokesovskou část spektra



Ramanova spektrometrie

Terénní a mobilní zařízení





Analýza nástěnných maleb (kaple Ponthoz.)

Rentgenová difrakční analýza (XRD)

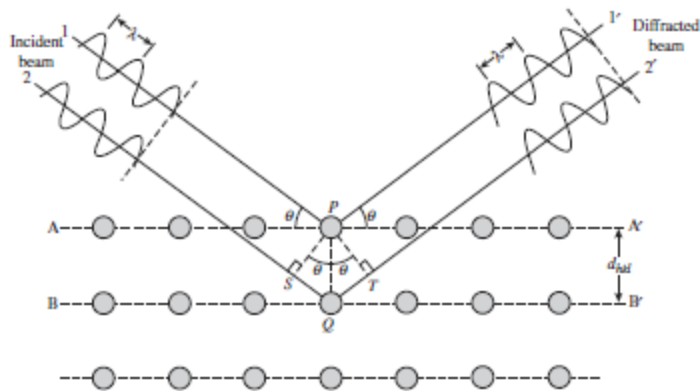
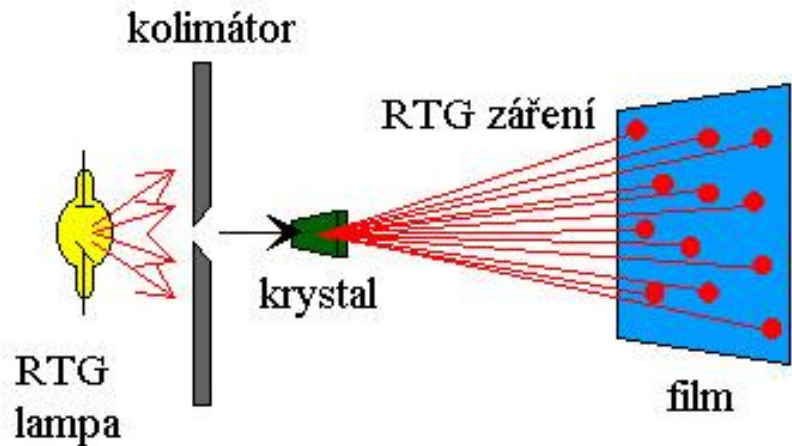


Figure 2.6 Bragg diffraction by crystal planes. The path difference between beams 1 and 2 is $SQ + QT = 2 PQ \sin \theta$. (Reproduced with permission from W.J. Callister Jr., *Materials Science and Engineering: An Introduction*, 7th ed., John Wiley & Sons Inc., New York. © 2006 John Wiley & Sons Inc.)

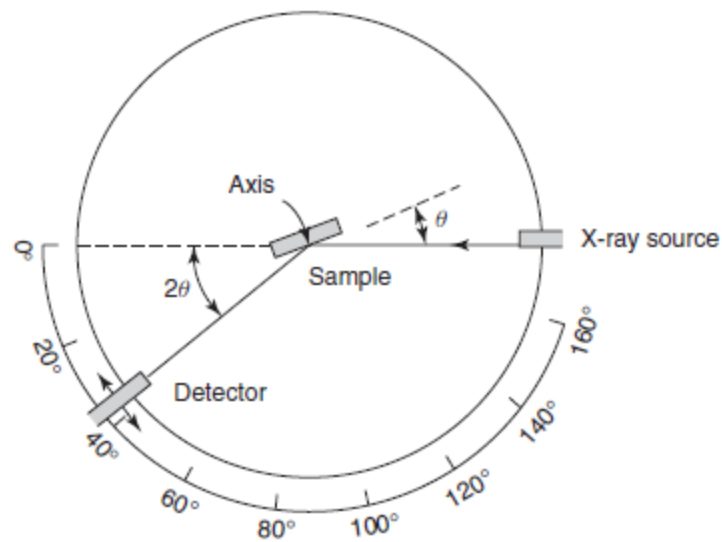


Figure 6.2 Schematic diagram of a XRD diffractometer

Egyptian Osiris: blue corrosion

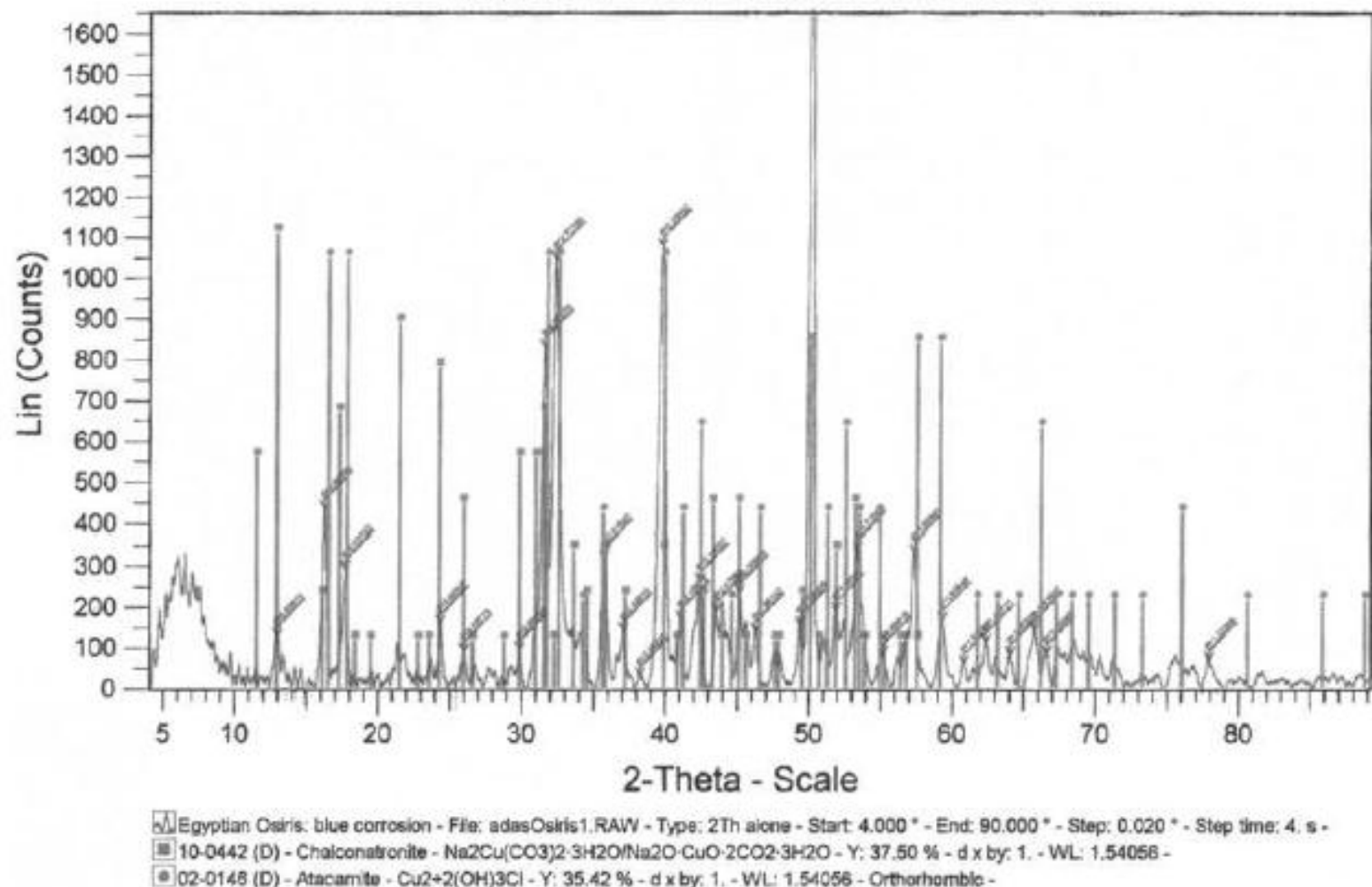


Fig. 10.14. X-ray diffractogram obtained, in situ, for the light blue area of the patina of the Osiris shown in Fig. 10.12, on the back. The principal constituent of this patina is chalconatronite.



Motyka , doba římská, Srbsko

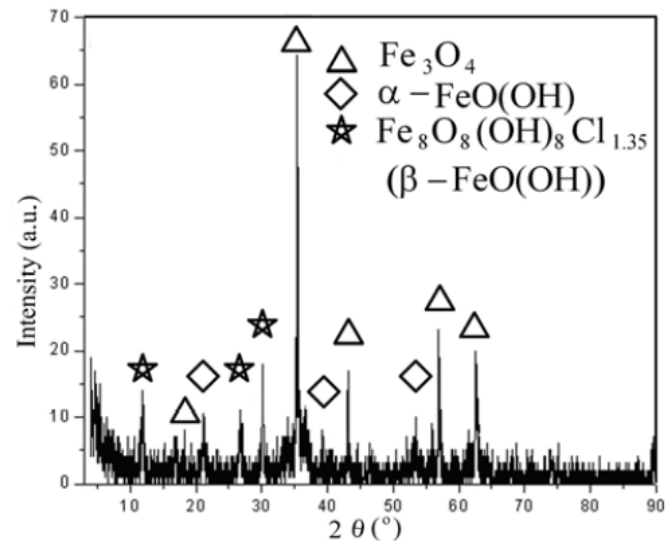


Figure 2. XRD diagram of corrosion products from archaeological find (shovel-spade).



Náhlenice , doba římská, Srbsko

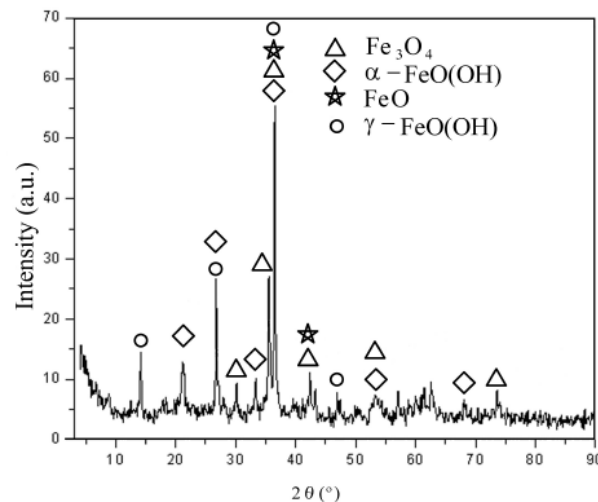
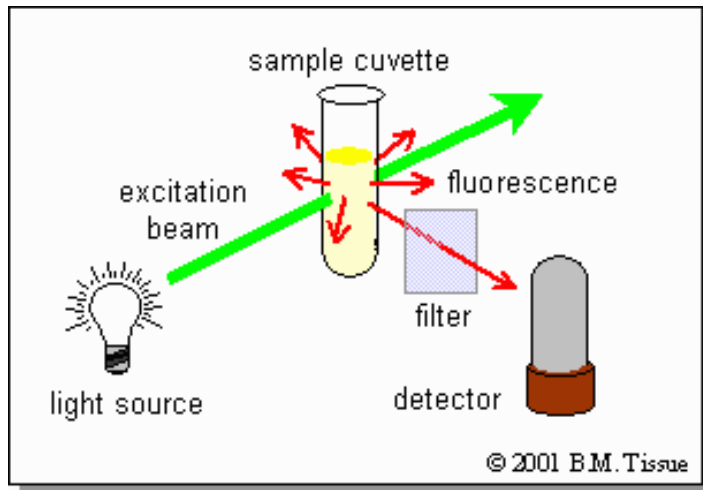
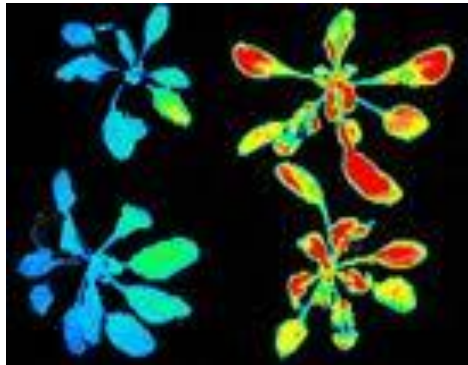
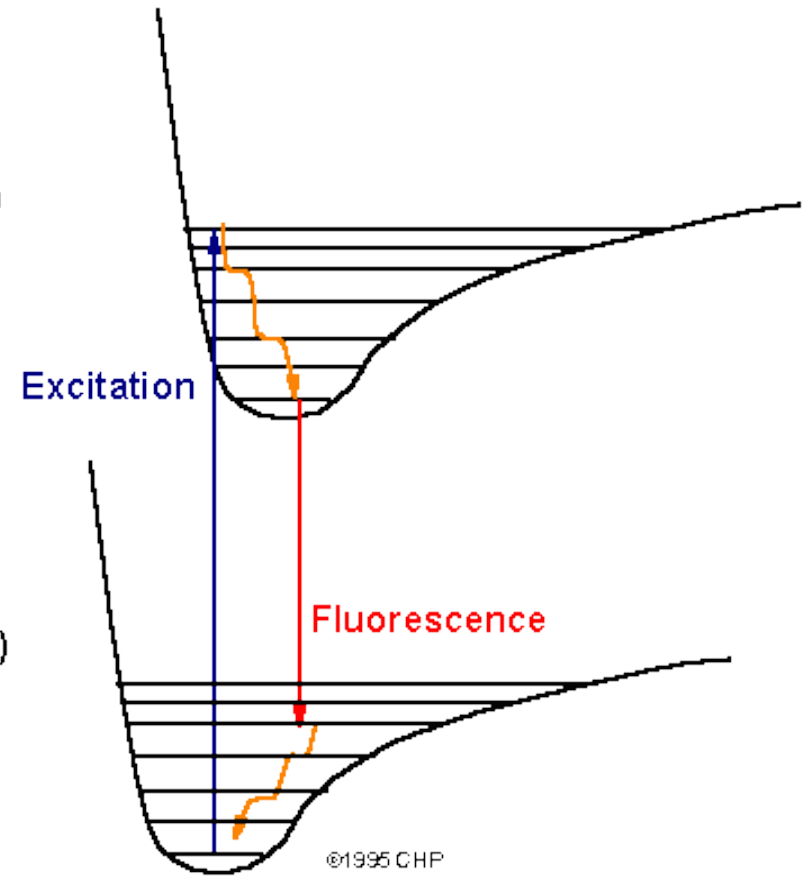


Figure 2. XRD diagram of archaeological find (fibula)

Fluorescence

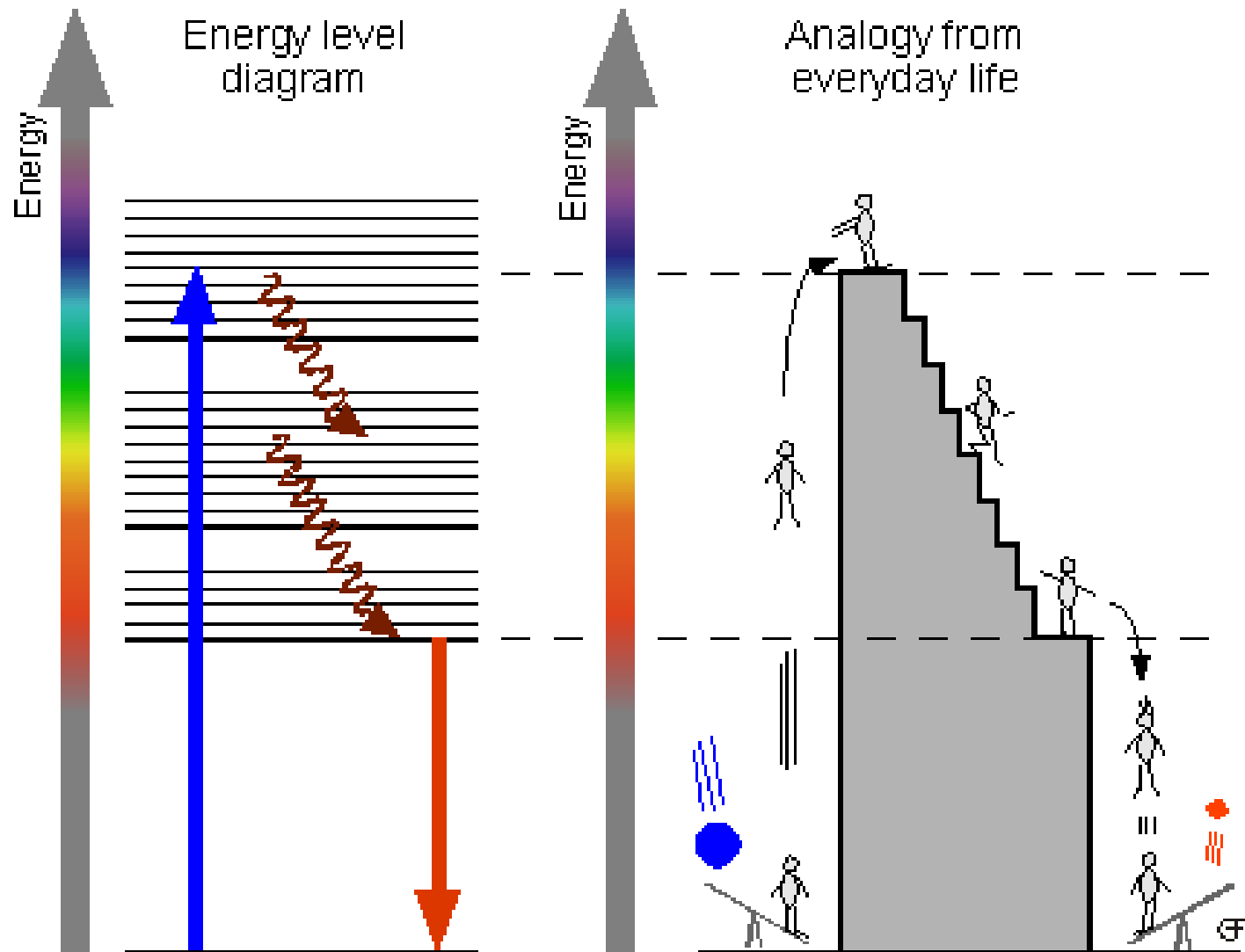


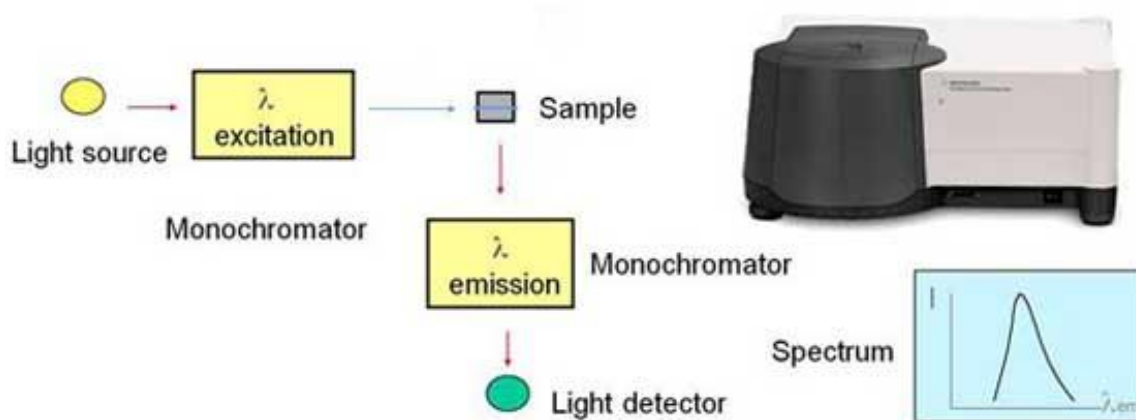
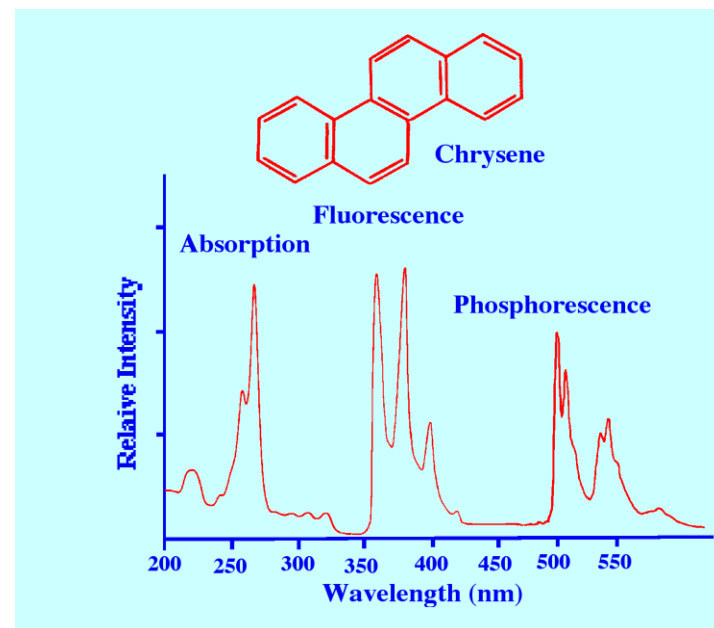
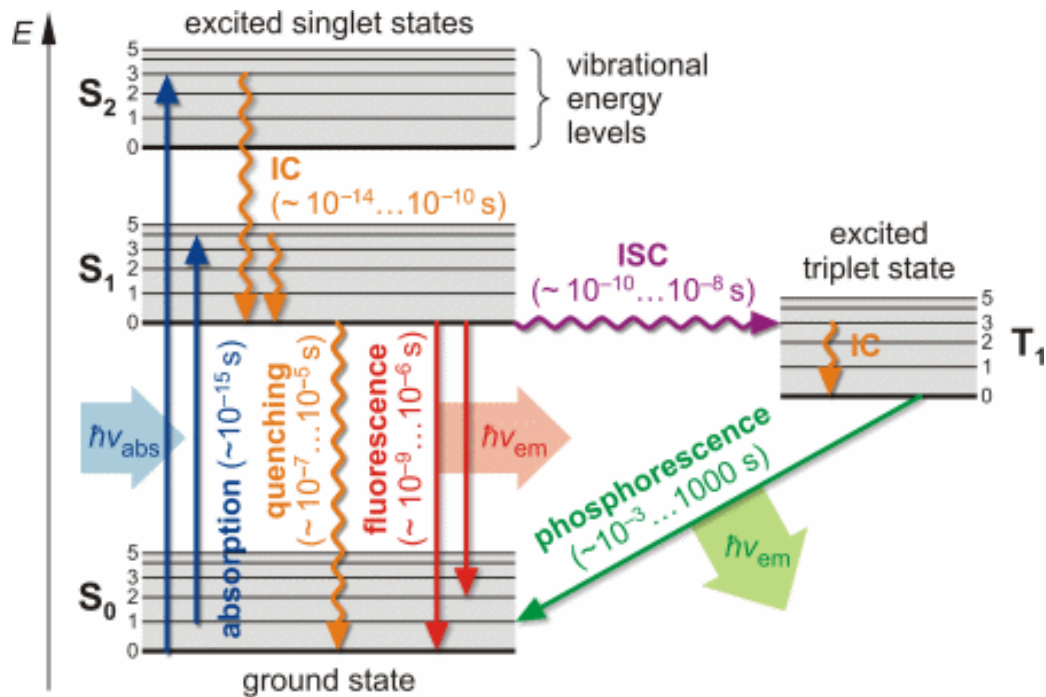
Excited State (S_1)



Absorption, Nonradiative Relaxation and Luminescence

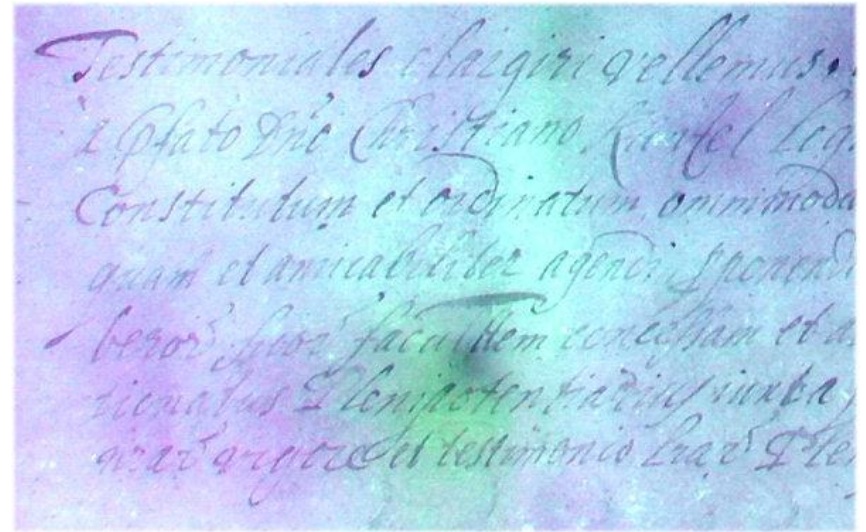
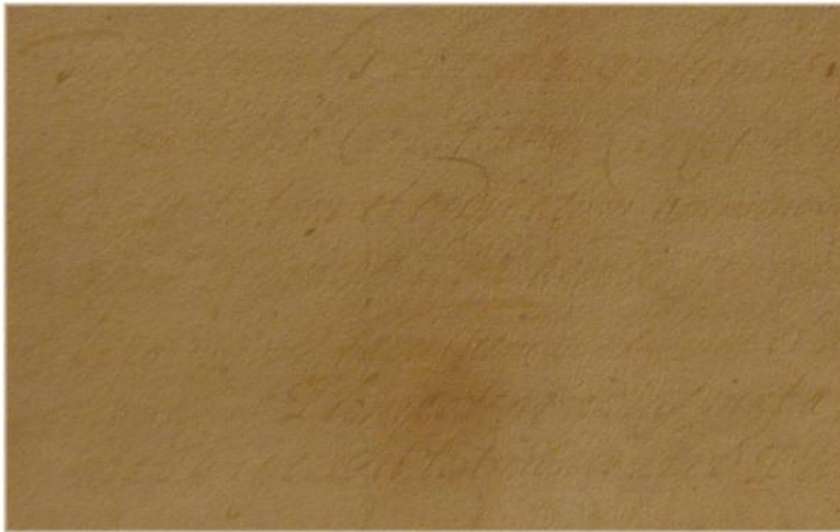
Making **heat** and 1x **red** out of 1x **blue**



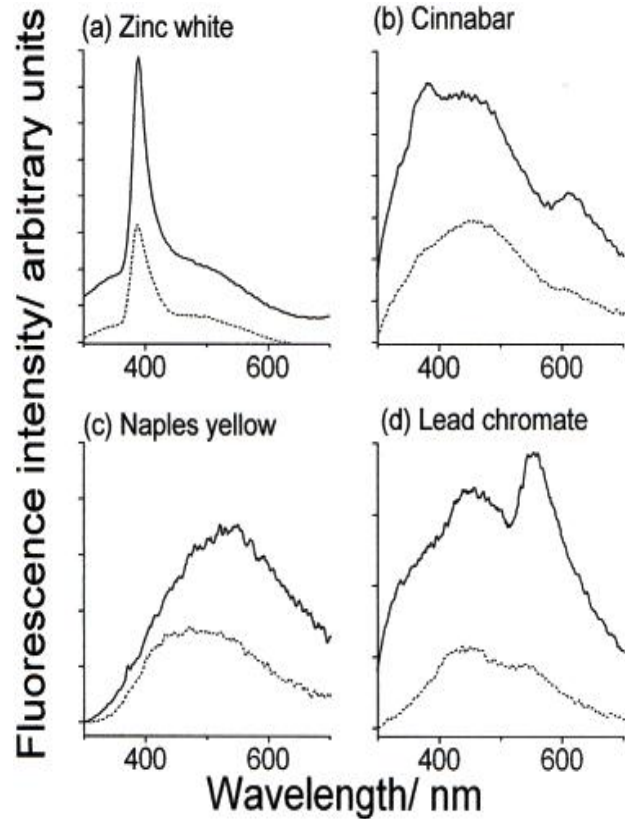


Fluorescence

Aplikace ultrafialové fluorescence - zviditelnění časem degradovaného textu



Pigmenty

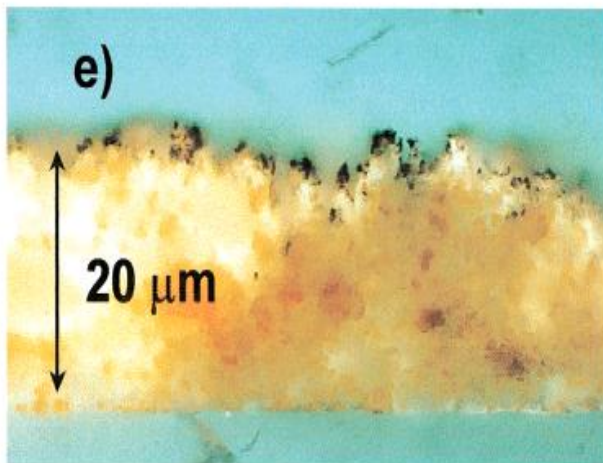


LIF spectra of unvarnished tempera systems taken at a resolution of 1 nm with a laser fluence of 1.2 mJ cm⁻²:

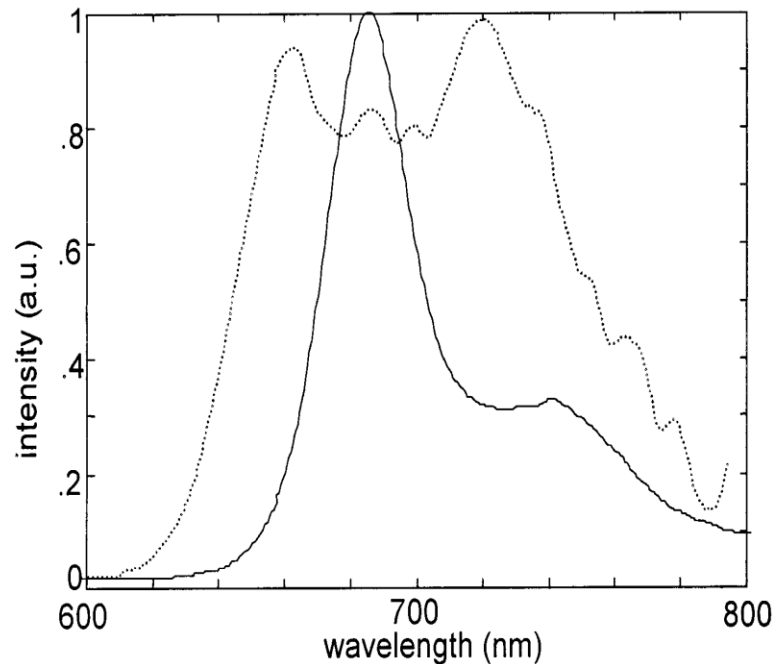
- (a) zinc white,
- (b) cinnabar,
- (c) Naples yellow, and
- (d) lead chromate.

The exciting laser wavelength is 248 nm.

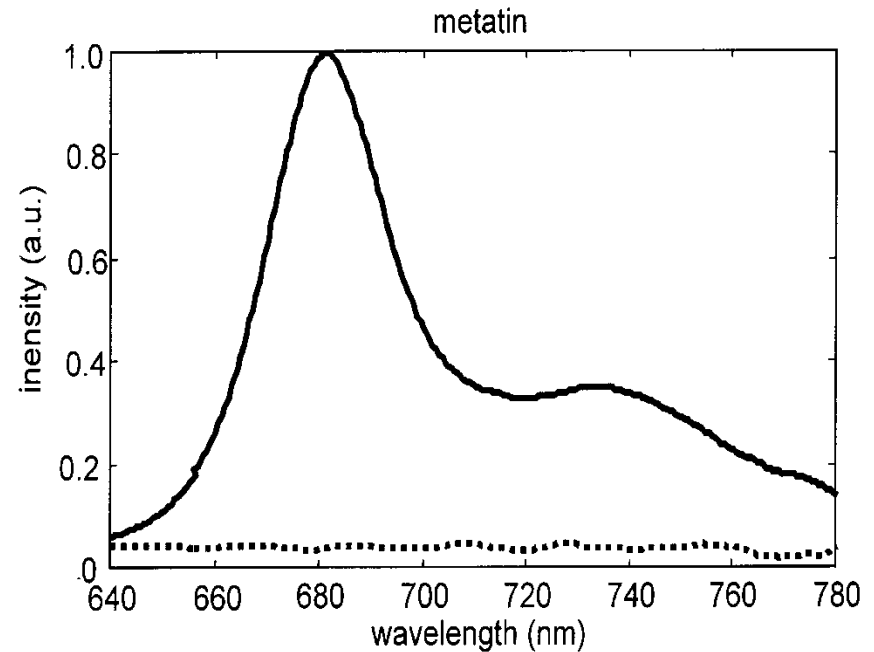
- (e) UV fluorescence image of a cross section of an unvarnished laser-ablated region of a Naples yellow tempera sample. (Magnification is 500).



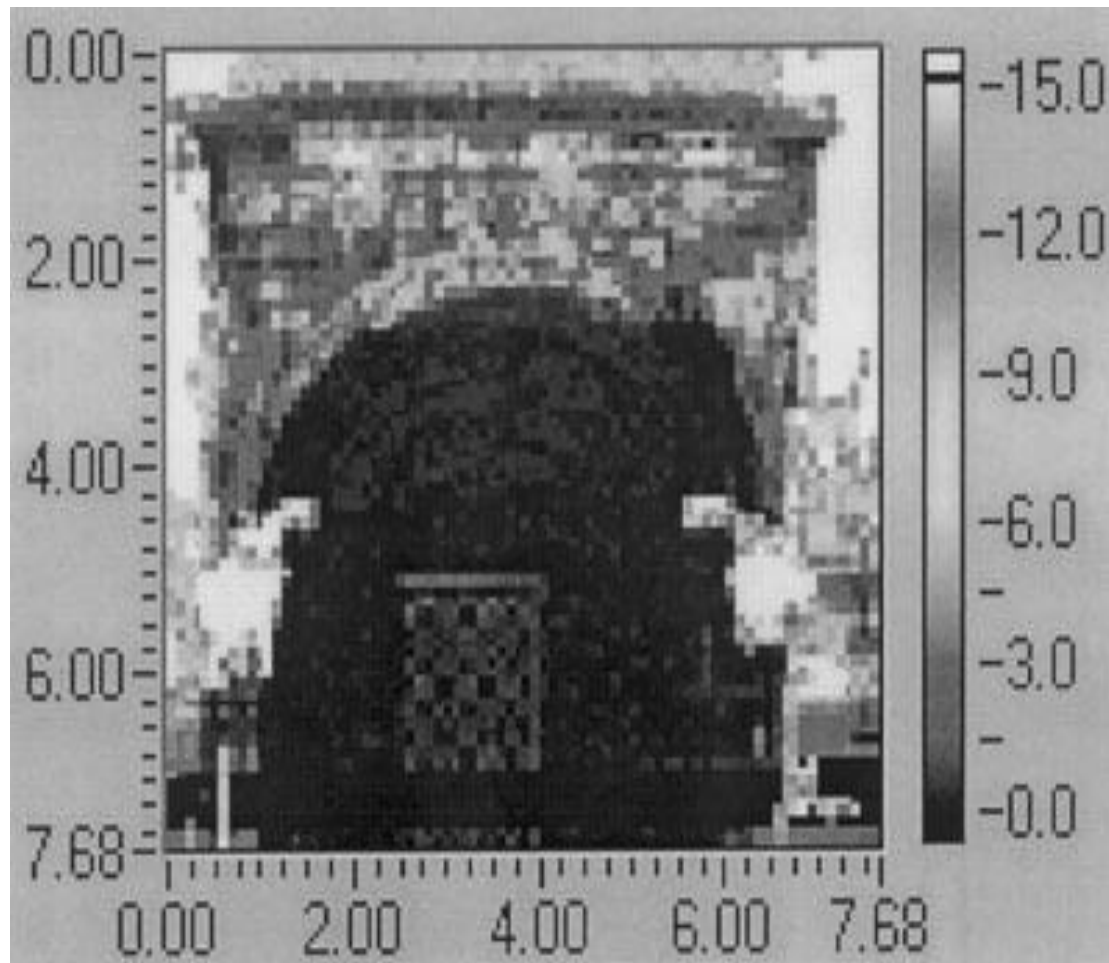
Detekce mikroorganismů



Normalised LIF spectra of green algae (continuous line) and cyanobacteria (dotted line). Excitation 355 nm.

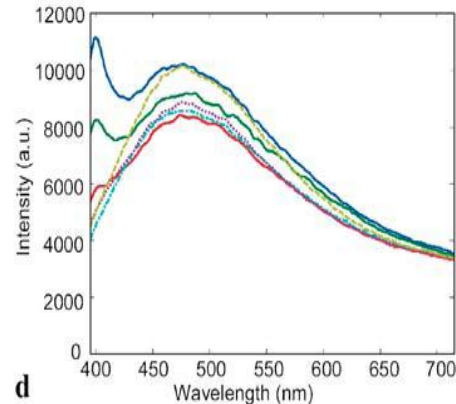
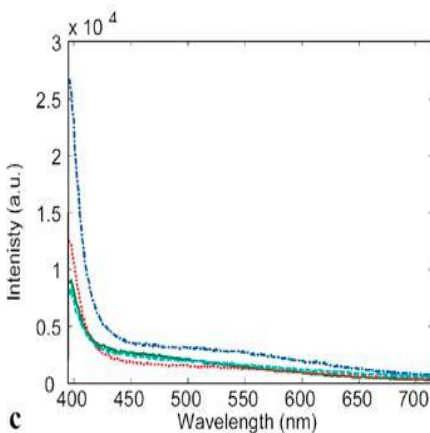
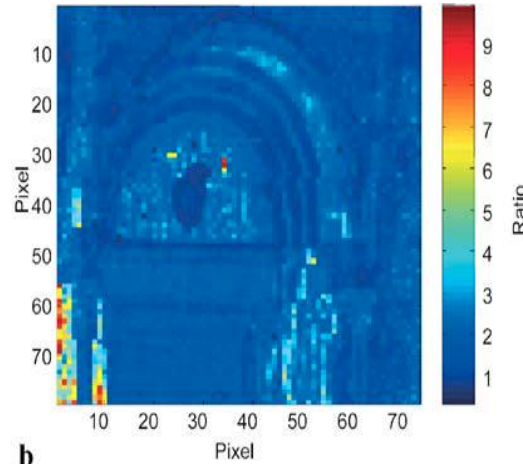
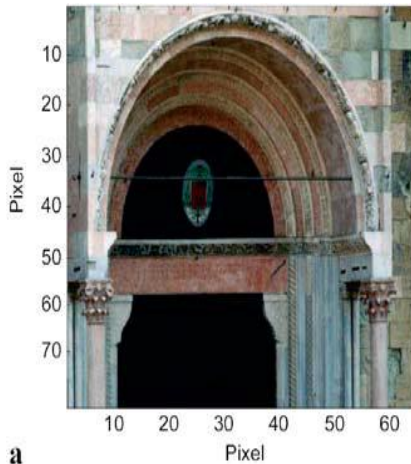


Fluorescence spectra of green algae on a marble substrate. Before a biocidal treatment (continuous line) and after (dotted line). Excitation wavelength 355 nm.



Fluorescence image related to the alga colonisation on the northern portal of **Lund Cathedral**. The intensity of the chlorophyll fluorescence in the band around 685 nm is indicated in grey levels and makes evident the important biodeteriogen colonisation on the stone surface.

Katedrála v Parmě



a a picture of the area investigated;
b the thematic map obtained from the ratio between the integrated area in the range 396 to 408 nm and the integrated area in the range 409 to 450 nm (the *yellow-red areas* in the image indicate areas subject to protective treatment); **c** fluorescence spectra taken from the bottom left area of the protiro and referring to those pixels of the thematic map in **b** where the protective treatment was strongly present (*yellow-red pixels*); and **d** fluorescence spectra taken in the bottom right area of the protiro where the protective treatment is present in a lower degree

Děkuji za pozornost !

